A FEASIBILITY STUDY OF A HYPERSONIC REAL-GAS FACILITY

FINAL REPORT

Submitted To:

Grants Officer
NASA Langley Research Center
Office of Grants and University Affairs
Hampton, VA 23665

Grant # NAG1-721

January 1, 1987 to May 31, 1987

Submitted by:

J. H. Gully Co-principal Investigator
M. D. Driga Co-principal Investigator
W. F. Weldon Co-principal Investigator

(NASA-CR-180423) A FEASIBILITY STUDY OF A HYPERSONIC REAL-GAS FACILITY Final Report (Texas Univ.) 154 p Avail: NTIS HC A08/MF A01 CSCL 14B

N88-10043

Unclas
G3/09 0103727

Center for Electromechanics
The University of Texas at Austin
Balcones Research Center
EME 1.100, Building 133
Austin, TX 78758-4497
(512)471-4496

CONTENTS

CONTENTS--continued

FIGURES

FIGURES--continued

TABLES

INTRODUCTION

Much of the progress made in aerodynamics prior to the space shuttle can be traced directly to design analysis made with blow down, pulse, electric-arc heated gas tunnels or the light-gas gun launcher. This study proposes a different propulsion method using electromagnetic launchers that will accelerate models at a low constant rate to hypervelocity (3 to 11 km/s). Fragile models, with on-board sensors for data acquisition can be used with this launch system.

The data from large (high moment of mass) flying models will provide scaled input for computer models of advanced space transition aircraft. Because the best wind tunnels today cannot simulate speeds higher than about Mach 8 for more than a millionth of a second, reliable data under quasi steady state conditions of interest is difficult to obtain. This new facility will be able to produce long flights (greater than 100 ms) and simulate the heating and atmospheric dissociative effects on air as if an aircraft were flying in the most upper regions of the earth's atmosphere.

During the past decade, supercomputers have gradually moved in to substitute for wind tunnels in a wide range of simulated flight situations. Even though the complexity of the problem limits simulation to only a portion of a wing, or one side of a rudder, this situation is fast changing with the advent of larger and faster computers. The new launch capability provides an opportunity to utilize the supercomputers more effectively. Predicting flight performance by computer is significant, however, testing and correcting the predictions with large, high-mass models in the flight environment closes an important loop. It is because the electric propulsion launch system can be configured as a slow (10,000 gees) launch, that fragile, actual-shape models can be accelerated, in one piece, at extreme angles of attack for flight study through the atmospheric chamber.

The idea of the electric launch is an old concept that has only recently been made possible by advances in high energy pulse power supplies, energy storage systems, and switches that manage the delivery of required energy at very high power levels. Two candidate electromagnetic launch systems which are being recommended for this facility are the railgun and the coaxial induction accelerator (coilgun). The electromagnetic launcher (EML), unlike the light-gas gun, which is sonic limited, has a much higher upper velocity limit. With a railgun the velocity is limited by the depth of current penetration in the rails, with an induction accelerator the frequency and voltage obtained with rotating generators. A launch system with this extended boundary will potentially allow the testing of models in the laboratory that can well exceed the velocities required to represent the flights of future earth-space transition vehicles.

The Center for Electromechanics at the University of Texas at Austin (CEM-UT) has performed a four month feasibility study of a hypersonic real-gas free flight test facility for NASA Langley Research Center (LARC). This study addressed the feasibility of using a high-energy EML to accelerate complex models (lifting and nonlifting) in the hypersonic, real-gas facility. Issues addressed in the report include:

- Design and performance of the accelerator (EML)
- Design and performance of the power supply
- Design and operation of the sabot and payload during acceleration and separation
- Effects of high current, magnetic fields, temperature, and stress on the sabot and payload
- Survivability of payload instrumentation during acceleration, flight, and soft catch

Discussion

Until very recently, aeronautical engineers tested their designs in wind tunnels. The Wright brothers introduced this concept during the development of their second glider. The EML places in the laboratory the unique ability to slowly accelerate very fragile scale models to velocities of interest for the X-30 or National Aerospace Plane (NASP). The nonlinear behavior of the multiple shock two-stage light-gas gun launcher can now be replaced by a steady 10,000 gees EML.

Just as important as the method of launch, is the need for hardened, on-board data acquisition systems, made possible now by developments in smart weapons. These instruments and sensors are designed with, and fabricated by computer. Large amounts of parametric flight data (half a million words) are possible. In the past, in-flight data meant data from full scale prototypes. Flight sensors and recorders can now fit within the model to measure and record the types of data obtained from full scale vehicles, although the flights will necessarily be brief.

The problem associated with electronic reliability in the EML environment is significant, but not insurmountable. Solutions are described in a later section. The ability to instrument a model for complete surface pressure profiling through all velocities is just one new capability.

The Hypersonic Real-Gas Free Flight Test Facility (fig. 1) can be used to precisely and systematically adjust the constants that represent a particular set of flight requirements. This is important because a vehicle entering the atmosphere at just under escape velocity, possesses 32,000 BTU/lb of energy. This energy is transformed, through the mechanism of gas-dynamic drag, into thermal energy in the air around the plane, a fraction of which enters the vehicle as heat. This fraction depends on the characteristics of boundary-layer flow, which is determined by the shape, surface conditions, and Reynolds number. All of these numbers can be determined fairly quickly during the flight of accurate models.

In the energy conversion equation, it is important to manage this given amount of energy in such a way that it becomes a part of the flight plan. If heat could be dissipated during a long glide, this would minimize structural weight, heat protection, operational restraints, and cost of the aircraft. The external shape of

DIAGRAM OF PROPOSED HYPERSONIC FREE-FLIGHT FACILITY

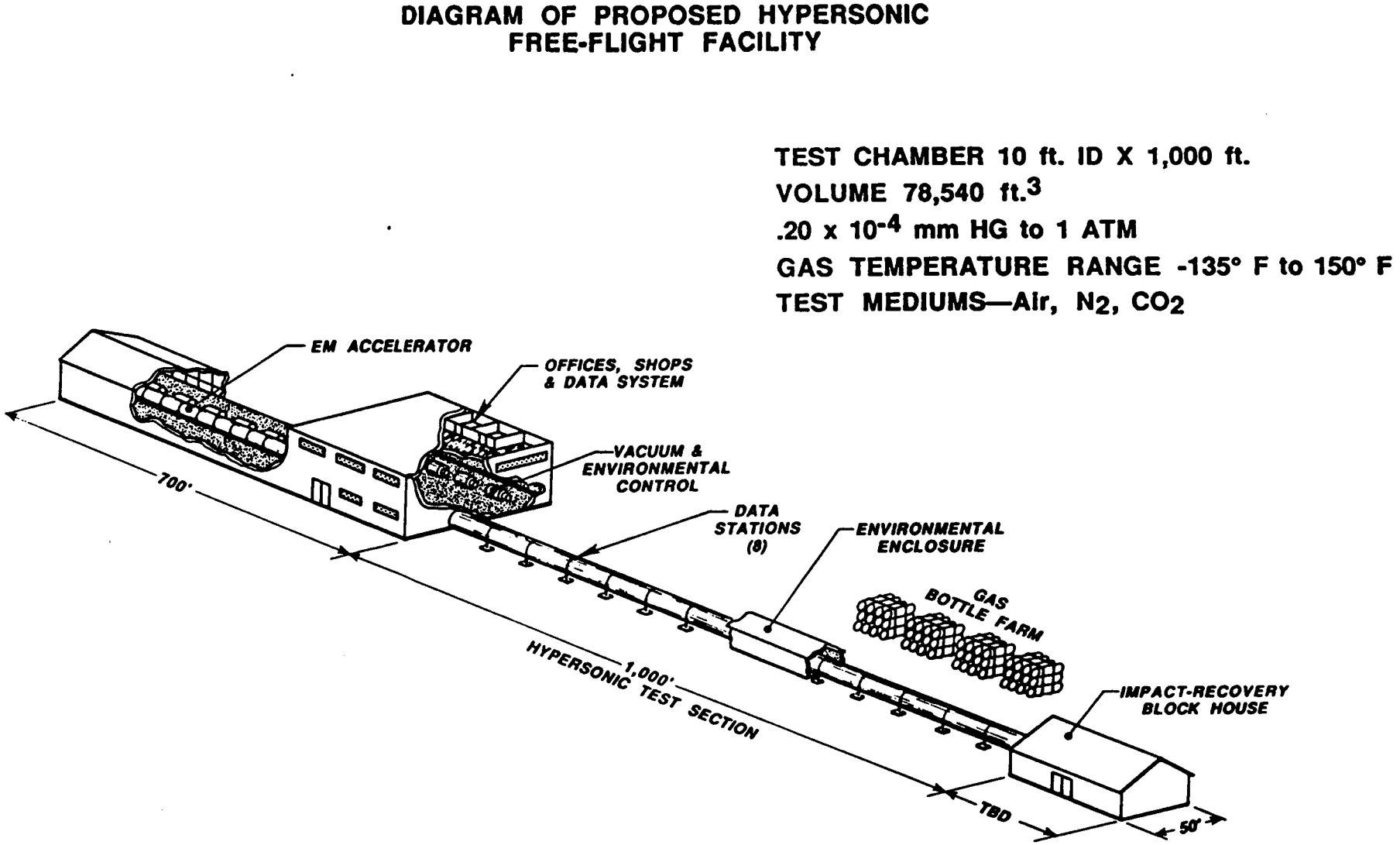

Figure 1. Diagram of proposed hypersonic free-flight facility

an aircraft will be determined by requirements for the hypersonic glide, so the subsonic handling and landing characteristics may be much worse than an F-4, which by some standards is uncontrollable. Solutions for flight stability problems can be developed in the flight facility. There is also a relationship between aerodynamic shapes, heat input, and structural material characteristics. If the Hypersonic Real-Gas Free Flight Test Facility were built, these and other issues could be studied experimentally and the results used to adjust computer simulations of full scale devices.

HIGH ENERGY LAUNCHER FOR BALLISTIC RANGE

Introduction

The proposed hypersonic real-gas free flight test facility is intended as a test sight for studying flight behavior of space vehicle models in actual re-entry conditions (i.e. real velocities, atmospheres, and pressures). In the proposed system, models are to be accelerated by an EML at acceleration levels of up to 10,000 gees. The models would carry instrumentation for temperature and pressure and range in length from 0.1 to 0.6 m, and in mass from 5 to 10 kg. Velocities of interest range from 2 to 6 km/s. Simulated altitudes of the test range are from sea level to 120 km, and test atmospheres can be air, nitrogen, or carbon dioxide.

For this application, EMLs have two strong attributes. First, because the models are electrically propelled, acceleration profiles can be tailored for each experiment as desired. For example, the models can be accelerated at a constant, increasing or decreasing rate. Although the proposed system has a nominal upper limit on acceleration of 10,000 gees, the system can be designed to operate at far higher levels of performance when needed. Future experiments could very well require these higher accelerations to achieve velocities above 11 km/s. Second, EMLs can be recycled quickly to allow a launch every hour. A launch facility with this capability could support the experimental development for a number of projects, possibly on a world basis.

Energy calculations for this launch study used a 40% overhead factor for sabot. This will permit a 10 kg model launch with a 4 kg driven sabot. The launch energy can be calculated as follows:

$$E = \frac{MV^2}{2} = \frac{14(6000)^2}{2} = 252 \text{ MJ Total Energy}$$

where

E = energy
M = mass
V = velocity

Technology to launch such energetic payloads has been demonstrated on a smaller scale, and with support from the Department of Defense (DoD), demonstrations will be made at the 9 MJ kinetic energy level. The proposed hypervelocity test facility will certainly represent a unique and highly versatile, world class aeronautical design and test facility.

Launch Concepts And Theory

Two candidates for the EML are the railgun and coilgun (coaxial induction accelerator). Railguns accelerate projectiles by virtue of very high current through an armature (solid or plasma) attached to the projectile (fig. 2). The current flowing in the rails produces a magnetic field between the rails which acts on the armature, carrying the same current normal to the field. The armature experiences a force parallel to the rails as a result of the interaction of the current in the armature and the magnetic field between the rails.

An electromagnetic induction launcher consists of a system of stator coils which when connected to a multi-phase alternating power source, produces a traveling field which accelerates an armature carrying currents induced by the traveling field (induction accelerator) or carries a stored current supplied from a starter source (fig. 3). The fact that the armature has no electrical contact with the stator and rides on the traveling magnetic wave, makes induction accelerators very attractive for the free flight facility. Regardless of the type EML chosen for the final design, the launcher must be at least 188 m long to satisfy the maximum acceleration cap of 10,000 gees.

This length suggests the launcher, if a railgun, should be of the distributed energy storage type (DES). Distributed energy storage guns use discrete energy storage and switching components at numerous locations along the rails. These stores are controlled by actively sensing projectile in-bore velocity and position and discharging the stores accordingly. Distributed energy storage guns have two major advantages, where rail length is a factor. First, switching in stored energy in discrete locations along the rail minimizes resistive losses that breech-only fed guns need to overcome. Second, pulse shaping of the current waveform is possible, making the acceleration profile easier to control.

If a coilgun is used as an EML, it can be of the passive, switchless inductive type developed by CEM-UT. This type EML has coaxial coils around the launcher that induce eddy currents in the sabot, which is accelerated by traveling, accelerating magnetic waves, that pull and push on the sabot. This is the linear, topological equivalent to the wound rotor induction motor. No electrical contacts are required on the shuttle, and its velocity is controlled by the electromagnetic wave which increases in frequency at the end of the launch and the slip between shuttle and stator fields. The shuttle, in turn, transmits the accelerating force on the payload by mechanical connection.

Railguns are powered by homopolar generators (HPGs)/inductor systems, compensated pulse alternators (compulsators), or capacitors. Coilguns can be powered by rising frequency generators (RFGs), polyphase synchronous surge generators, or from the utility grid, if high power and enough real estate is available.

Either EML type allows modular design. Distributed energy storage railguns are by their nature repeated subassemblies of energy store/switching/railgun. Similarly, coilguns are made up of discrete coils and tube structures, mechanically aligned, and joined. This modularity is very important in accommodating the varying range of mission requirements.

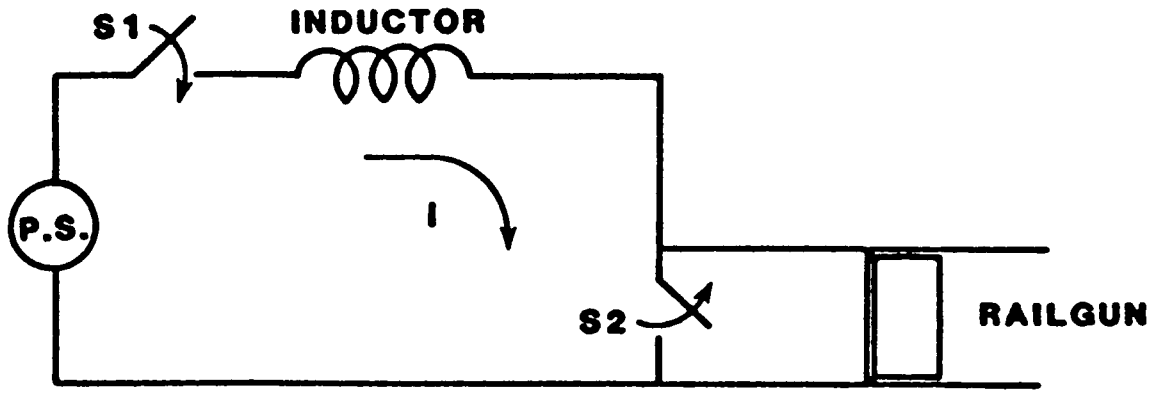

Figure 2. Operation of three component power supply

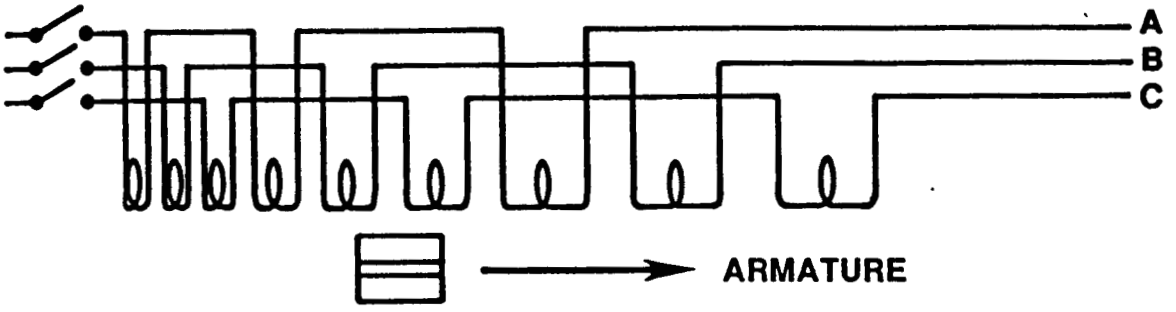

Figure 3. Principle of coaxial accelerator

COAXIAL ACCELERATOR

Introduction

A preliminary design performed at CEM-UT has led to a passive, iron-free, modular coaxial accelerator (188 m long), capable of launching a load of 14 kg at 6 km/s at a constant acceleration of 10,000 gees. Provisions have been made so that the same accelerator can also launch the 14 kg load at 11 km/s, at a constant acceleration of 32,800 gees, by changing a few connections only, and by increasing the number and size of electrical machines used as pulsed power supplies for the system.

The armature (sabot) is excited by induced currents which interact with the traveling (accelerating) magnetic wave produced by the varying pitch, three-phase stator coils. Essentially the armature "rides" the magnetic wave and is subjected to a constant propelling force (and consequently constant acceleration) distributed as a body force inside the aluminum armature. During the entire cycle of operation there is no electrical contact between the armature and the coaxial accelerator.

The power supplies are low impedance compulsators invented at CEM-UT in 1978. Their parameter range fits the characteristics of the compulsator which CEM-UT is under contract from the U.S. Army/DARPA, contract number DAAA-21-86-C-0281, entitled, "Repetitive 9 MJ Electromagnetic Gun Weapon System." However, electrical synchronous machines of current designs (manufactured by companies such as General Electric, Allis-Chalmers, Westinghouse, A.S.E.A., etc...) can be compensated and mechanically and electrically upgraded, to serve as power supplies for the coaxial launcher in the high energy pulsed mode.

Several features have been devised to increase the efficiency of the system. One was to induce an initial current in the precooled armature (sabot) using a starter coil, substantially reducing the "slip" necessary in order to maintain the secondary current at the necessary value. Another was to divide the stator barrel into several distinct frequency zones, each being energized by a separate alternator at the appropriate time, and each being electrically distinct, while magnetically all segments form a continuous accelerating magnetic field wave. Both of these features substantially improve the efficiency of the system.

An even higher efficiency can be obtained--in the future--by developing a new CEM-UT concept, the rising frequency generator (RFG) capable of producing and delivering an increasing-frequency train of pulses to the accelerator. A discussion of this machine is presented in Appendix A.

While not included in the requirements for the coaxial launcher, an electromagnetic braking system for the sabot (traveling shuttle) may be appended, being built as a segment of the barrel similar to the others. The connections of two stator phases are reversed causing the traveling magnetic wave to reverse its direction, resulting in deceleration of the sabot.

Finally, the conflicting requirements of a weak structure inherent to stranding and transposing the conductors for the windings of the coaxial accelerator and the

electric generators, together with the necessity for a mechanically and structurally strong overall system have been resolved by the folded plate transposed conductor, a CEM-UT invention. The conductor built according to this invention has high packing factor, retains good mechanical properties and is fully compatible with the frequency range and the fabrication procedures used for the coaxial accelerators.

System Description

The system, shown in fig. 4 is comprised of a modular coaxial accelerator, each module being energized by its own pulsed electrical machine. The 14-kg projectile (sabot and payload) is accelerated, at a constant acceleration of 10,000 gees, to an exit velocity of 6 km/s by the traveling magnetic wave produced by the currents in the three phase stator. An additional requirement was to launch a similar projectile (14 kg) to almost double the velocity (11 km/s). Table 1 presents different options in which the second requirement can be accommodated.

The last design option was chosen, such that the same accelerator is used to launch the 14 kg load at 11 km/s. Due to the modular construction of the barrel, only a small number of connections must be changed. In addition, the number of power supplies, their size, and frequency ratings will be increased.

The three main components of the system are: the launcher, the pulsed electrical machines representing the power supply, and the projectile.

a. The launcher has an ideal length of 188 m and an actual length of 192 m excluding the "starter coil" which is 1.2 m long and an end coil 6 m long--the total length approaching 200 m. The standard unit coil, which forms the base for the modular construction is 0.15 m long.

   For the 6 km/s variant, the accelerator is divided into four electrically independent, but magnetically series connected segments. Each part is 48 m long and has 14, 8, 7, and 7 segments respectively, each segment having a different pole pitch in order to match the power supply instantaneous frequency with the velocity of the armature passing through the respective segment.

b. The power supply is configured of four compulsators storing 179, 211, 242 and 274 MJ. While the projectile is passing through the segment, only half of the stored energy is used. The frequency and voltage of the alternators drops to 70% of the initial value (for instance in the last stage the frequency drops from 480 to 340 Hz). The current per elementary turn is maintained constant at 477 kA, the impedance dropping at the same rate as the voltage and frequency. The initial voltage of the machines varies from 8.73 kV for the first generator to 29.9 kV for the fourth one. If instead a parallel connection is used with four paths in parallel, the

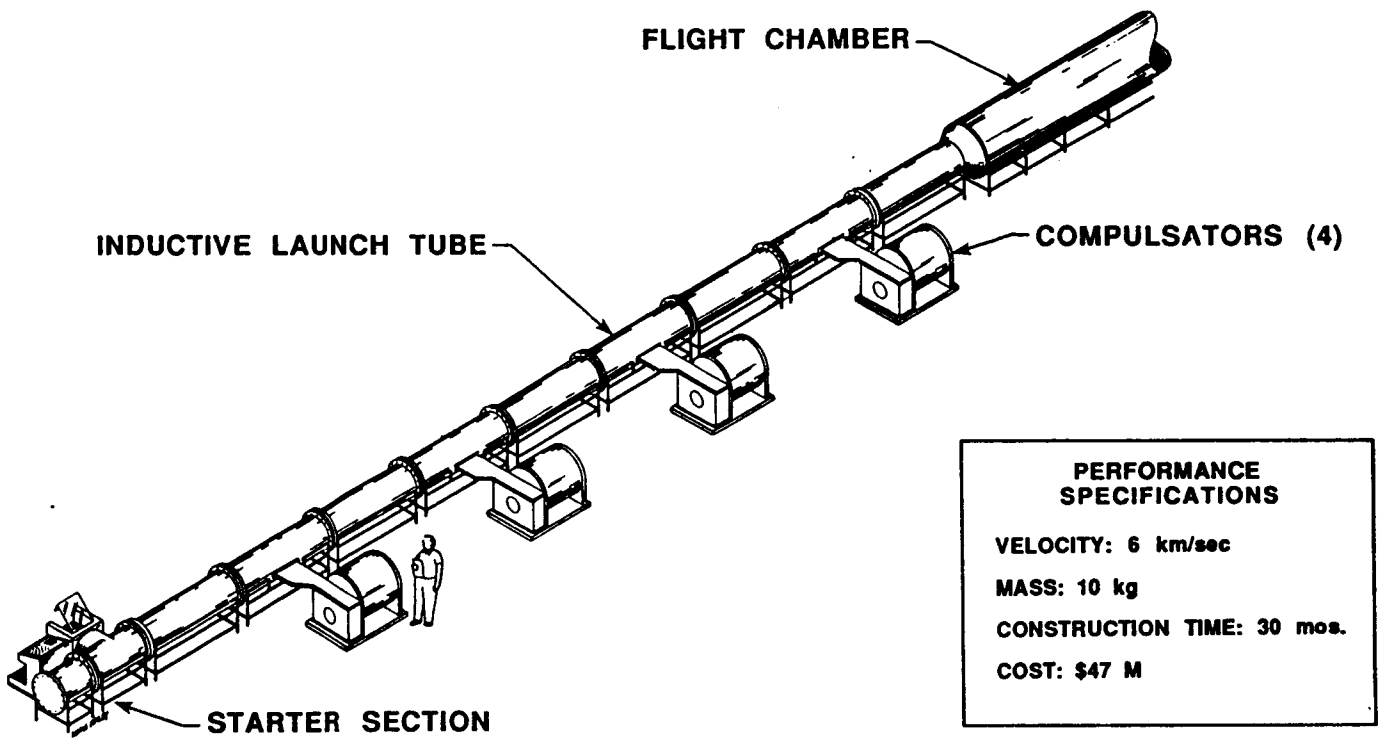

Figure 4. Induction accelerator

Table 1. Operating envelope

Exit velocity (km/s)	Projectile mass (kg)	Acceleration A (gees)	Launch length (m)	Launch time (ms)
6	14	10,000	188	61.2
11	14	10,000	620	112
11	14	18,333	336	61.2
11	14	32,800	188	34.4

initial voltage becomes 2.18 and 7.48 kV for the first and the last of the compensated alternaters while the current increases to 1.9 MA, constant for all the generators.

The above values for the currents and voltages are rms and per phase.

Figure 5 gives the diagram of the frequency and voltage variation for each compensated alternator in the discharge time for each of the four parts of the launcher. At the bottom of the diagram the energy stored by each compulsator is given.

c. The armature is a thin aluminum shell with an OD of 0.457 m and a length of 0.3 m. In the course of design, two values for the thickness were considered, 0.3 and 0.4 cm, respectively. Provisions are made to initially cool the armature at liquid nitrogen temperature. A starter coil will induce an initial current in the armature, thus maintaining the "slip" and the corresponding losses at a reasonable value. The nominal value for the armature (secondary) current is 1.49×10^6 A for the 6 km/s launcher and 2.91×10^6 A for the 11 km/s launcher variant.

System Analysis

Main Parameters

This section presents the preliminary analysis and design of a coaxial accelerator and the corresponding power supply required to electromagnetically accelerate a mass of 14 kg to 6 km/s. At this exit velocity, the kinetic energy of the projectile is:

$$W_p = \frac{1}{2}MV^2 = \frac{1}{2}(14)(6{,}000)^2 = 252 \times 10^6 \text{J}$$

For constant acceleration of 10,000 gees = 98,100 m/s^2 the ideal length of the launcher is:

$$S = \frac{V^2}{2a} = \frac{(6{,}000)^2}{98{,}100} = 183.5 \text{ m}$$

Connections between segments of the stator winding increase this length to 188 m. Additional starting coils and final segment extends the length to 196 m.

The launch time is:

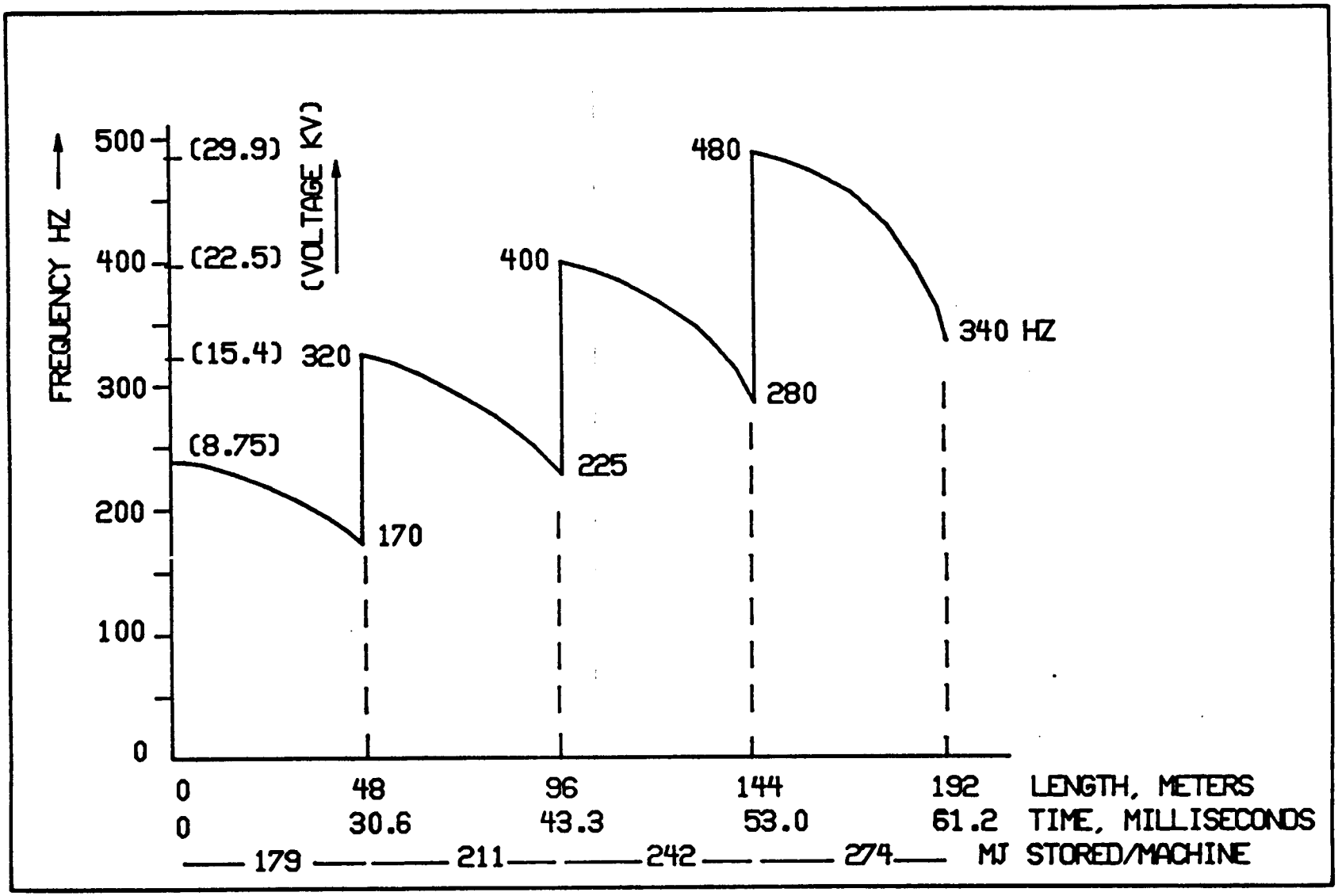

Figure 5. Frequency variation during discharge for compensated pulsed alternators

$$t = \frac{V}{a} = \frac{6,000}{98,000} = 61.16 \times 10^{-3} s$$

The average axial force acting on the projectile, in the direction of motion is:

$$F = Ma = 1.373 \times 10^{6} N$$

A variant of the system uses the same coaxial launcher (barrel) by changing a few connections to launch a 14 kg projectile at 11 km/s. In this case the kinetic energy of the projectile at the end of the launch is:

$$W_p^1 = \frac{1}{2}MV'^2 = \frac{1}{2}(14)(11,000)^2 = 847 \times 10^{6} J$$

The acceleration is:

$$a' = \frac{V'^2}{2s} = \frac{(11,000)^2}{2 \times 1.88} = 3.218 \times 10^{5} \frac{m}{s^2} = 32.8 \text{ kGee}$$

The force acting on the projectile is:

$$F^1 = Ma^1 = 14 \times 3.218 \times 10^{5} = 14.505 \times 10^{6} N$$

and the launch time is:

$$t^1 = \frac{V^1}{a^1} = \frac{11,000}{321,800} = 34.18 \times 10^{-3} s$$

Launcher Configurations

A section through a preliminary version of a coaxial accelerator design is presented in figure 6. The stator coils (primary) are disposed circumferentially along the launcher bore.

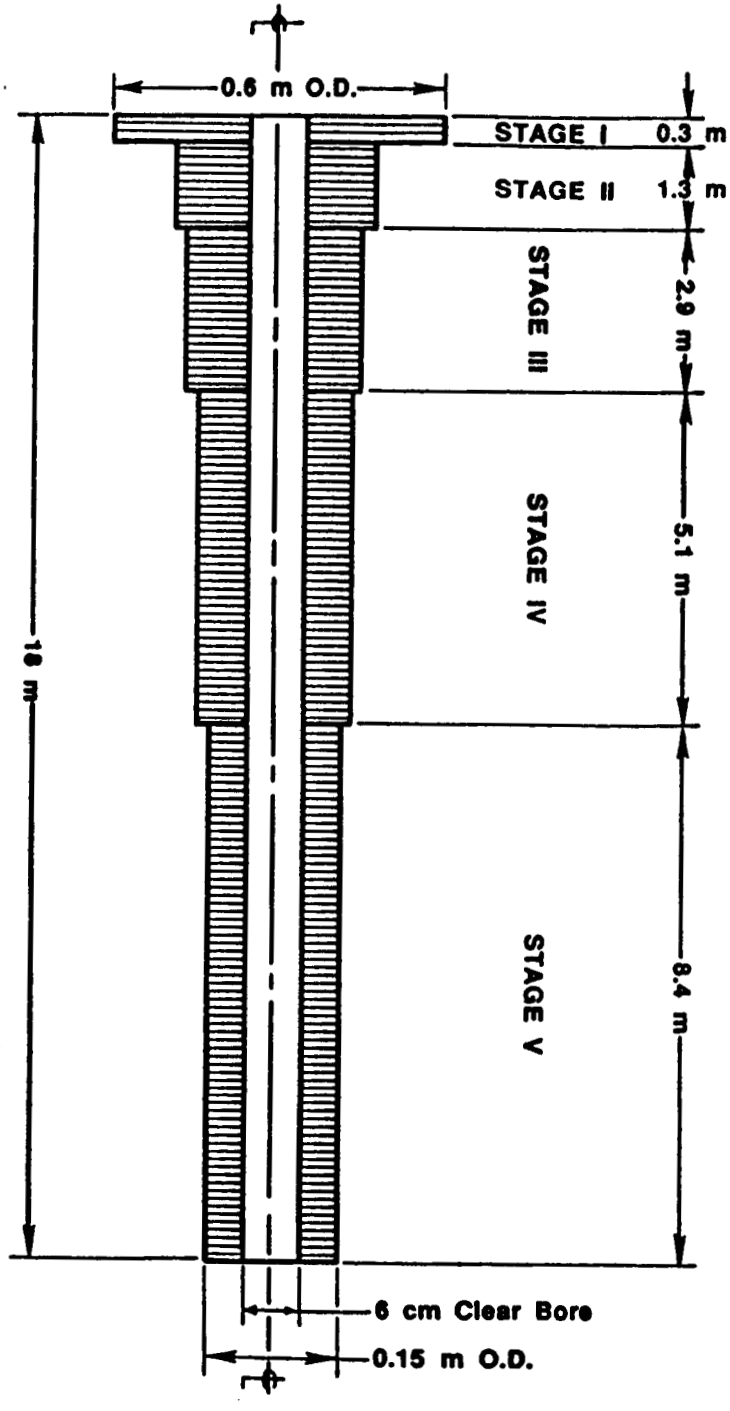

Figure 6. An earlier version of a coaxial launcher

The large dimensions of the stator coils in the initial stages of the accelerator are explained by the need to induce the entire secondary current in the early moments of the launching. A substantial reduction in the size of these coils is achieved by using a "starter segment" whose role is to induce the secondary current in the projectile just before launching.

Then, the stator winding becomes uniform, of equal thickness along the barrel, and can be made from identical, standard coils (fig. 7a). A third variant of stator winding presenting manufacturing advantages is shown in figure 7b. Later in this report, a more detailed discussion of the stator design will be presented.

The armature of the induction launcher is actually the aluminum sabot of the projectile. It has the same outer diameter and length for both 6 and 11 km/s design variants; only the thickness being different--0.3 and 0.4 cm respectively. The armature is initially cooled at liquid nitrogen temperature.

Electromechanical Considerations

Figure 8 presents schematically the stator winding and the corresponding magnetic flux plot for a tubular, linear induction motor. The stator winding is assumed to have a constant polar pitch τ.

In the typical 3-phase winding of a conventional induction motor, the 3-phase system of currents energizing the stator produce a traveling rotating wave progressing with a speed:

$$\eta_s = \frac{120f}{p}$$

where

n_s = rpm of the field wave
f = the frequency of the excitation current
p = number of poles

In the tubular linear induction motor (fig. 8) the velocity of the magnetic field traveling down the launcher is:

$$V_s = 2\tau f$$

where

V_s = traveling field velocity (m/s)
τ = polar pitch (m)

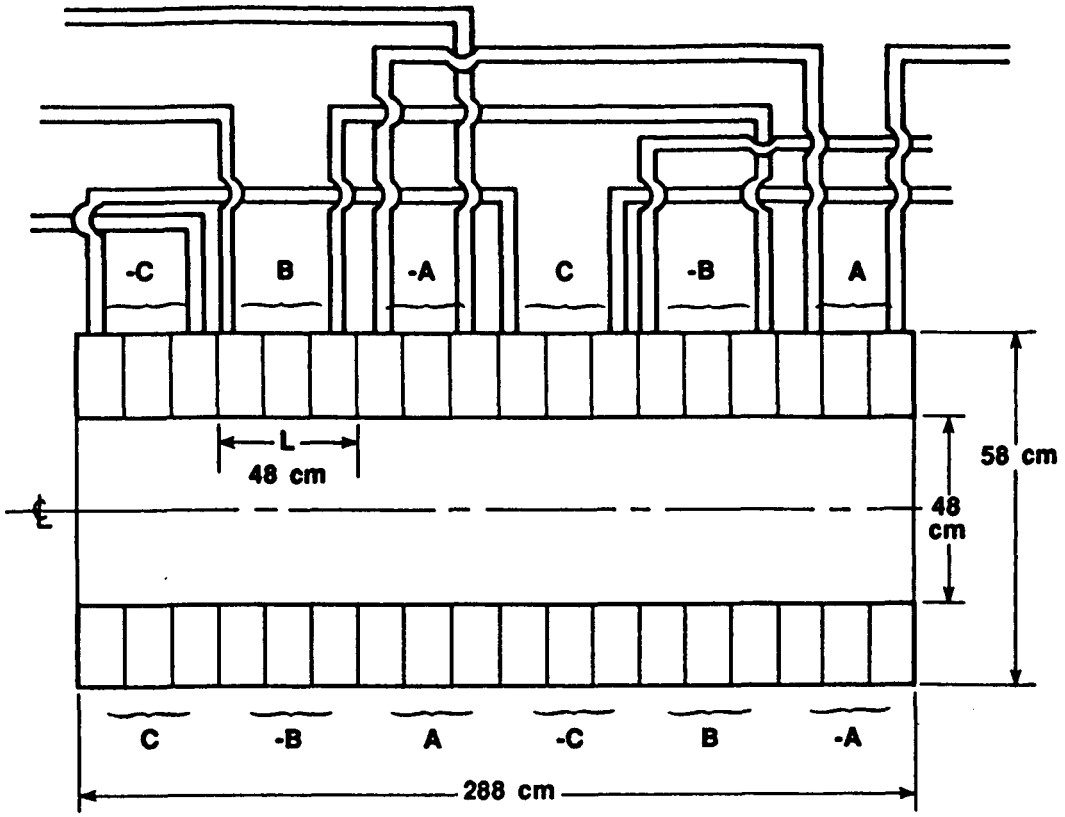

a) normal, successive phase coil design

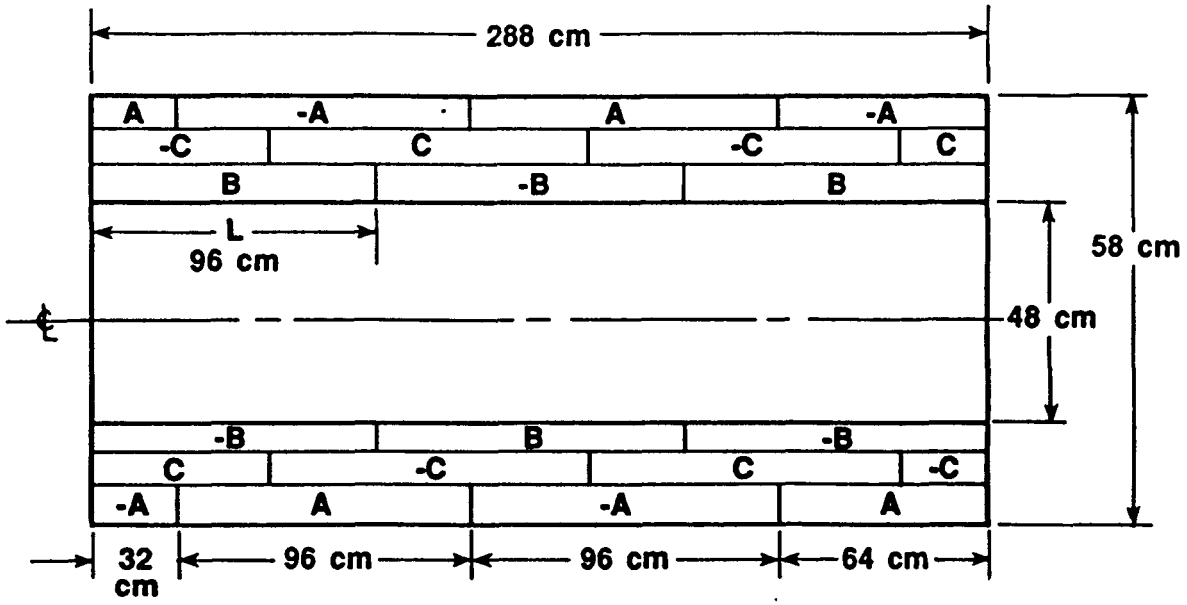

b) layered phase design

Figure 7. Segment of stator winding of a coaxial launcher with identical coils

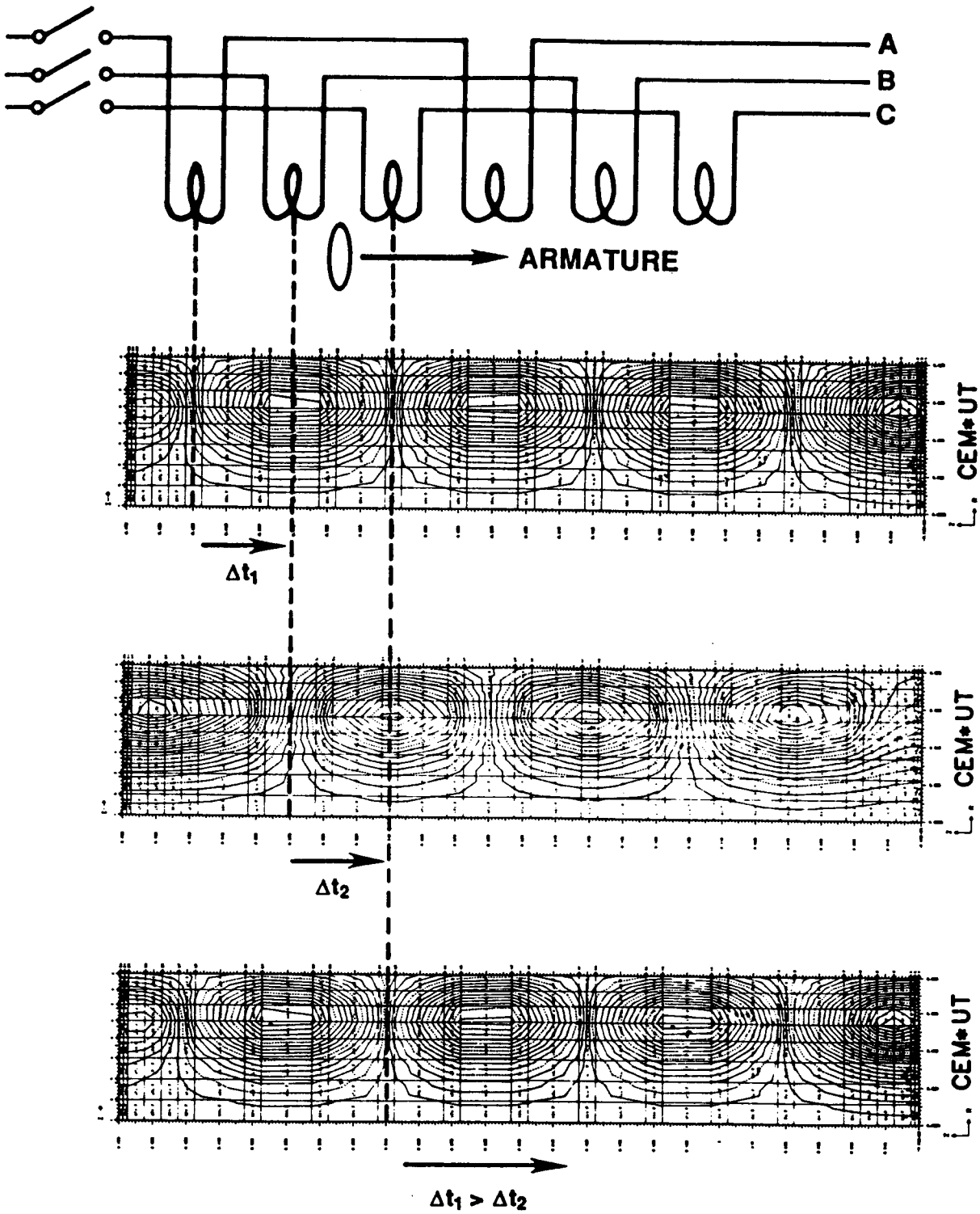

Figure 8. Schematic of stator phases and resulting flux plot for tubular, linear motor

f = frequency of the excitation currents (H_2)

The velocity, V, can be controlled along the launcher barrel by varying either frequency, f, or the polar pitch, τ, or both. The need for controlling the velocity of the traveling magnetic wave in order to obtain an accelerating field wave arises from efficiency considerations.

From the theory of the conventional induction motor it is known that the efficiency for starting operation (expressed in energy terms) is less than 50%. For each unit of energy stored kinetically in the rotor, a great amount is dissipated in the Joule heating of the rotor by slip losses.

In exactly the same manner, a projectile accelerated from rest by a constant velocity traveling field will be subject to the same slip losses, which amount to W_{PJ}, for the entire launch period:

$$W_{PJ} = \int_o^t F_p s V_{TF}\, dt = m_p V_{TF} \int_o^t s \frac{dv}{dt} dt$$

Changing the integration limits,

$$W_{PJ} = m_p V_{TF} \int_o^{V_{TF}} (1 - \frac{v}{V_{TF}}) dv$$

where

F_p = force applied to projectile (N)
m_p = projectile mass (kg)
V_{TF} = speed of traveling field (m/s)
v = instantaneous speed of projectile (m/s)

and $$s = \frac{V_{TF} - v}{V_{TF}} \times 100 = \text{slip (percent)}$$

Accelerating from rest to the speed of the traveling field and neglecting friction losses gives a minimum energy loss, of:

$$W_{PJ} = m_p V_s \left[V - \frac{u^2}{2V_{TF}} \right]_o^{V_{TF}} = \frac{1}{2} m_p V_{TF}^2 .$$

Actually the projectile does not reach the speed of traveling field (fig. 9a) and the energy loss is given by:

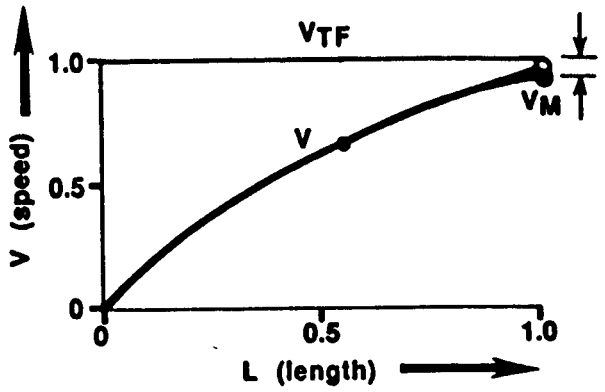

a) Traveling field speed and projectile speed for single stage acceleration

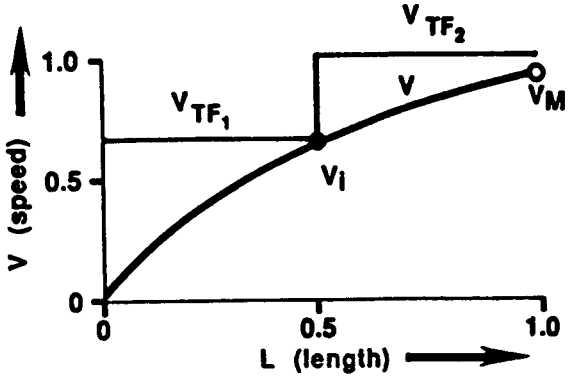

b) Two stage acceleration

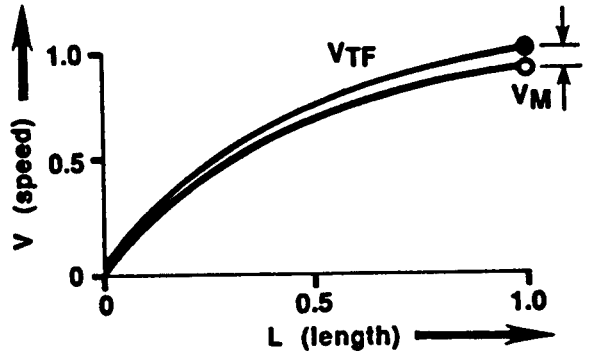

c) Acceleration using continuous pole-pitch variations or continuous frequency variation

Figure 9.

$$W_{PJ1} = \int_0^{V_M} m_p(V_{TF} - v)dv = m_p(V_{TF} \cdot V_M - \frac{V_M^2}{2})$$

where

V_M = projectile output velocity (at the muzzle of the launcher)

For a two staged system (fig. 9b) comprising two traveling field speeds, the energy loss decreases considerably:

$$W_{PJ2} = \int_0^{V_i} m_p(V_{TF1} - v)dv + \int_{V_i}^{V_M} m_p(V_{TF2} - v)dv$$

If the intermediary speed $V_i = \frac{V_M}{2}$ and $V_{TF2} = 2V_{TF1}$

$$W_{PJ2} = \frac{m_p V_M}{2}(\frac{3}{2} V_{TF2} - V_M)$$

The number of stages can be further increased, improving the energy efficiency and reducing to a minimum the Joule loss in the projectile, (fig. 9c). At the limit this corresponds to a continuous increase in the pole pitch (fig. 10) or a continuous change in the currents producing a traveling field (fig. 8). The accelerating traveling field will ideally be followed closely by the projectile keeping the slip (and consequently, the losses) at constant low values.

Power Supplies

The manner of obtaining an accelerating field is to continuously vary the supply frequency. This way, the armature is accelerated down an essentially constant pitch stator winding, (fig. 8) the driving frequency increasing with armature velocity. Of course, this is just the opposite of what happens in an alternator or compulsator as inertially stored energy is extracted. Additionally, as the speed voltage of the accelerator rises, it is desirable for the voltage of the generator to rise as well. For this project a combination of the two technical solutions proposed above is chosen--a pole pitch variation combined with a change in the power supply frequency.

However, the frequency of the power supplies will be increased step-wise (fig. 4) (in four steps for the 6 km/s variant, in ten steps for 11 km/s variant). Inside one particular step, the constancy of the acceleration for the traveling wave is achieved by a pole pitch variation (fig. 11). As it becomes clear from inspection

FOLDOUT FRAME

FOLDOUT FRAME

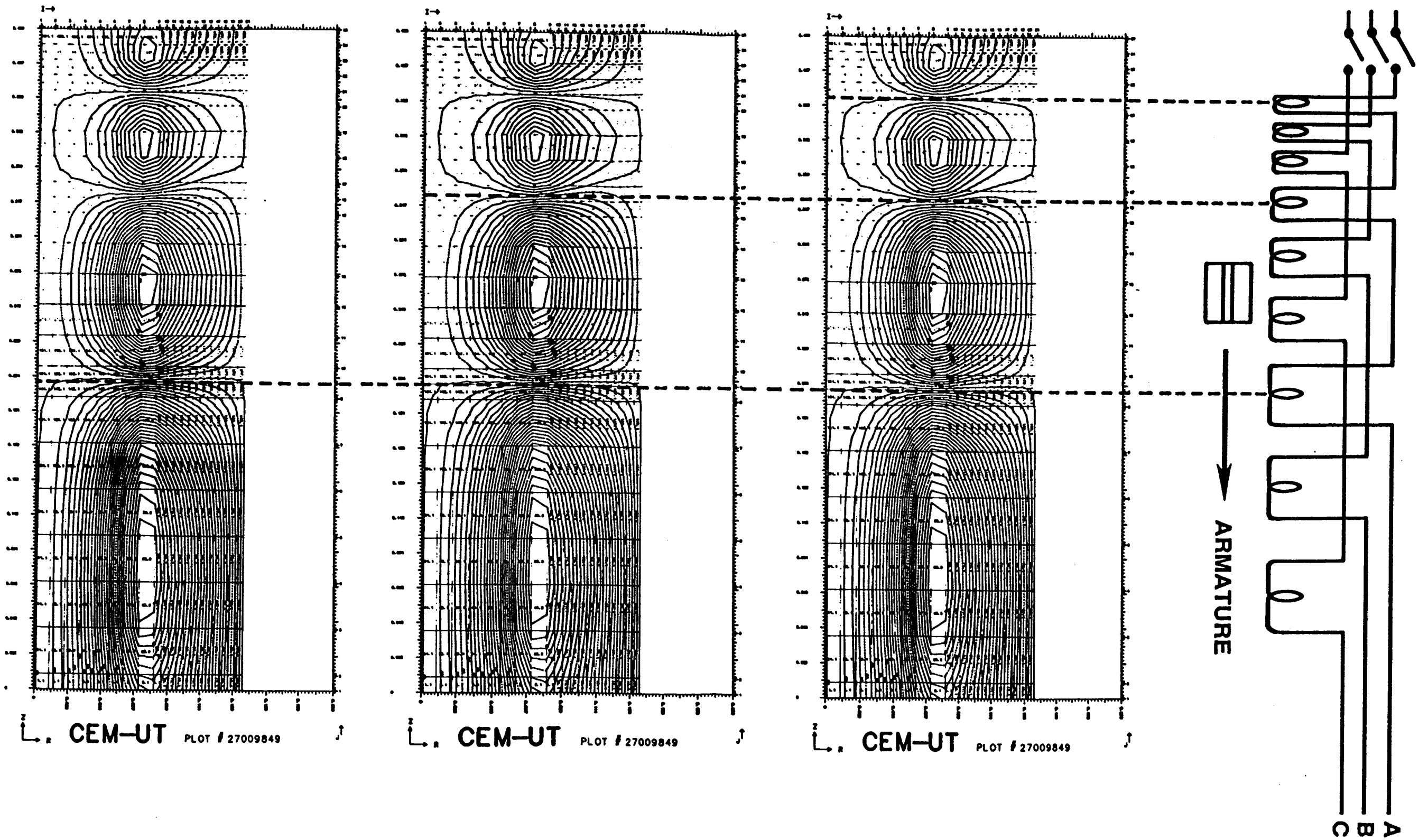

Figure 10. Flux plot of an accelerated traveling field $\tau_1 < \tau_2 < \tau_3$ (increasing pole pitch)

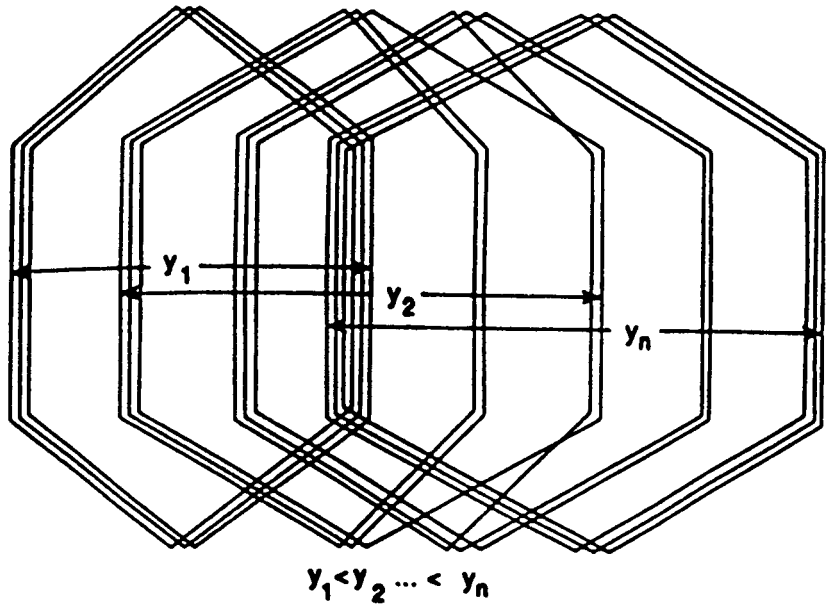

Figure 11. Variable pitch (graded) winding

of figure 4, an additional increase of the polar pitch is necessary, to compensate for the speed and frequency drop due to the machine discharge. The compensated pulsed alternators proposed for such a task are low internal impedance generators capable of high discharge currents and high discharge torque, similar in kind to the self excited passively compensated pulse alternator, which CEM-UT is contracted to fabricate for the U.S. Army. Large electrical synchronous machines of current designs manufactured by established companies, may also be compensated and electrically and mechanically upgraded to serve as pulsed power supplies for the coaxial launcher.

In the future, the RFG, a CEM-UT concept, is proposed to meet the power supply requirements of the coaxial accelerator. This device, which is in the initial development stage, can utilize the electrical generating configuration of an alternator, low impedance alternator, or compulsator, single or multiphase. It consists of a rotor and a stator having a moment of inertia many times higher than the rotor (a naturally occurring situation which can be tailored by design) both of which are initially rotating in the same direction, the stator rotational speed being somewhat higher. The electrical frequency of the output, of course, is a function of the differential speed, $\omega_s - \omega_r$, as is the generated voltage. As power is generated, equal and opposite torques will be applied to the rotor and stator, and the rotor will change speed faster (slow down) due to its lower inertia. As the rotor slows, the difference between rotor and stator speed increases, increasing frequency and output voltage and achieving the desired affect.

By matching the generator voltage, frequency, rotor and stator inertias, and initial velocities to the requirements of the coaxial accelerator, an integrated power supply/accelerator system can be designed. An important part of this integration is done by mounting the pulse generator excitation source on the same shaft as the pulse generator thus forming a "cascade" of electrical machines essential to obtain the proper electromechanical energy conversion.

A variant of this RFG concept involves using a stationary stator with a rotating magnetic field produced by a multiphased ac excitation current.

Electromagnetic Principles

Eliminating the use of iron for the magnetic circuit permits an increase in electrical machine performance, especially for pulsed operation. For induction accelerators this means the analytical tools of equivalent circuits and the theory and methodology of design related to such tools must undergo significant modifications.

The equivalent circuit variants (figs. 12a and b) consider series or parallel connections and take into account both parts of the accelerator--the projectile filled segment and the rest of the barrel, which is many times longer.

The first section of the equivalent circuit corresponds to the length of the projectile (neglecting all the edge effects), the second takes into account the rest of the barrel ($L - \ell$) where, in addition to the energy loss in the stator, only reactive power is consumed.

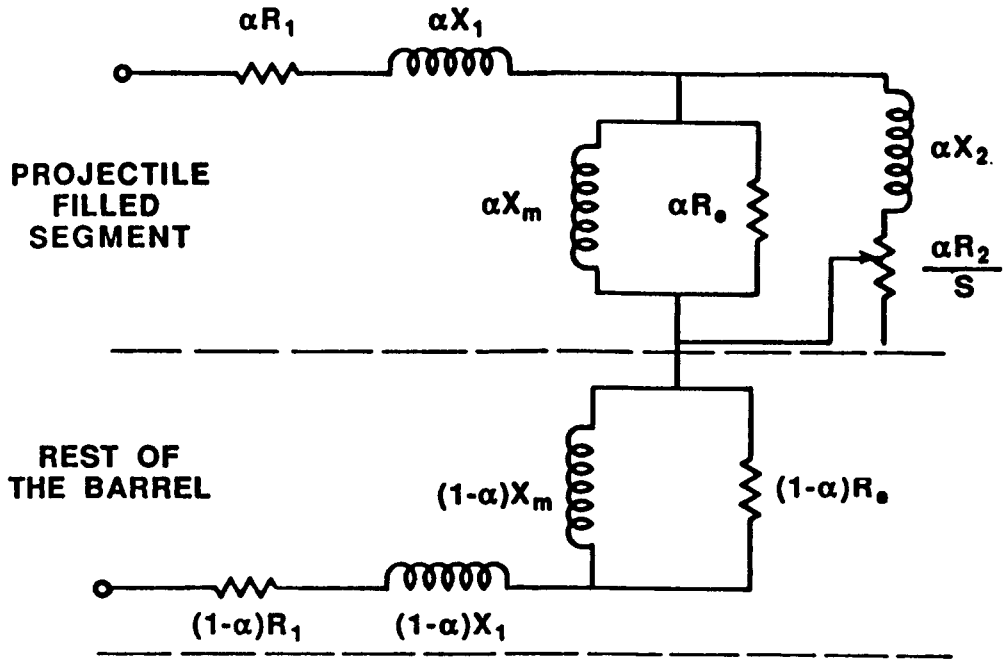

a) series connection

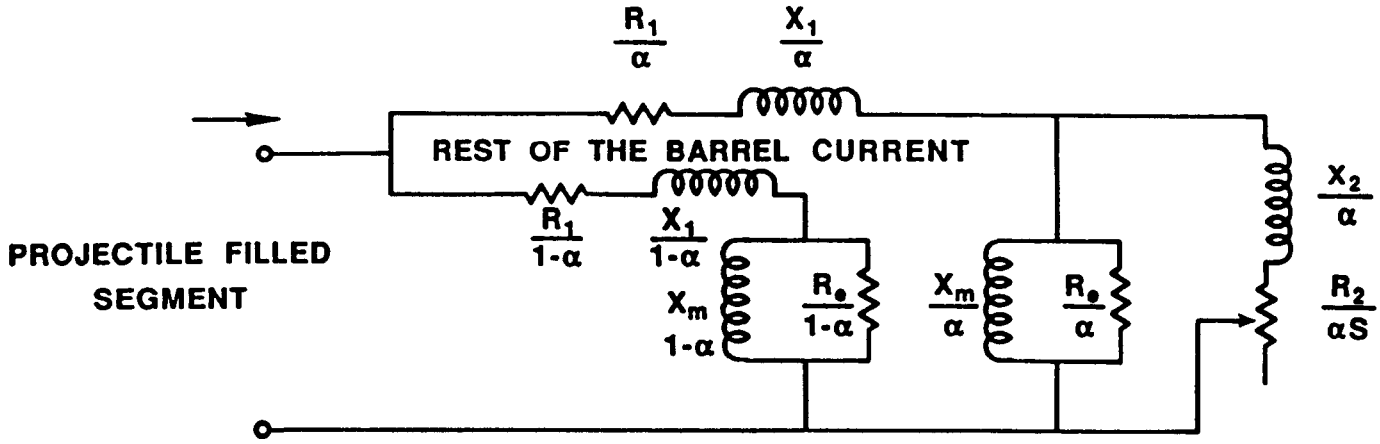

b) parallel connection

Figure 12. Equivalent circuits for induction accelerator

Using a similar treatment as in classical theory of linear induction motors [1,2], in the short secondary variant, the accelerating force is:

$$F = \frac{(I_2^2 R_2 \cdot X_m^2)(\frac{\ell}{L})}{V_s s\left[(\frac{R_2}{s})^2 + X_m^2\right]}$$

Optimizing the system for a maximum force-to-loss ratio, assuming a constant stator resistance, R_1, the value of the product between the force and the speed of the traveling field, FV_s per unit stator loss results:

$$\frac{FV_s}{R_1 I_1^2} = \frac{\frac{\ell}{L} s (\frac{R_2}{R_1})\left[1 + (\frac{Xm}{R_1})^2\right]}{(\frac{L-\ell}{L})\left[(\frac{R_2}{R_1} + s)^2 + (\frac{R_2}{X_m})^2\right] + \frac{\ell}{L}\left[s^2 + (\frac{R_2}{X_m})^2\right]\left[1 + (\frac{X_m}{R_1})^2\right]}$$

which can be optimized further by considering $R_2 X_m$ as a variable.

where

R_1 and R_2 = resistances of the primary and secondary circuits
X_m = manetizing reactance
s = slip
I_1 = stator current

Onuki and Laithwaite [3] propose an optimization looking for the minimum stator length with the additional requirement of a permissible heat loss based on Euler-Lagrange's equations:

$$\frac{\partial}{\partial v_s}\left\{\frac{m_p V}{2FR_2(\frac{1}{x_1} + \frac{1}{x_m})V_{TF}} \frac{(v_s - v)}{(v_s - v)^2 + \left[R_2 (\frac{1}{x_1} + \frac{1}{x_m})V_{TF}\right]^2}\right\}$$

$$+ \lambda \frac{\partial m_p (v_s - v)}{\partial v_s} = 0$$

where λ = Lagrange multipliers

imposing the constraints mentioned above.

It has been shown that efficiency considerations exclude the use of an induction accelerator with uniform properties per unit length of stator. A continuously varying pitch, a continuously increasing supply frequency during the launch, or a combination of both requires changes in the use of the equivalent circuit as a tool for modeling of the machine properties. For a computer-based design, a time marching procedure, continuously changing the parameters of the equivalent circuit as the projectile advances through the barrel was used. Such an iterative procedure takes into account the influence of the transient processes produced by switching the symmetric system of voltages into the accelerator, and also the influence of parameter variations, (supply frequency, reactances, polar pitch, resistance change due to field diffusion and temperature rise) [4,5].

The design was done segment by segment (for the stator winding) using TEXMAP, a finite element electromagnetic code developed at CEM-UT. The speed of the projectile at any instant, and at any point along the barrel is a function of the J x B forces and the speed history since the beginning of the launch, such that a recursive procedure is used for each segment of the machine, in a "space" marching algorithm.

Figures 13a and b shows the projectile in an asymmetric position in the traveling magnetic field, without using the starting coil at two moments in time. The difference in the magnetic flux configuration is due to the field diffusion into the projectile. Another analytical tool used for evaluating the performance of the coaxial accelerator is the phasor diagram (fig. 14).

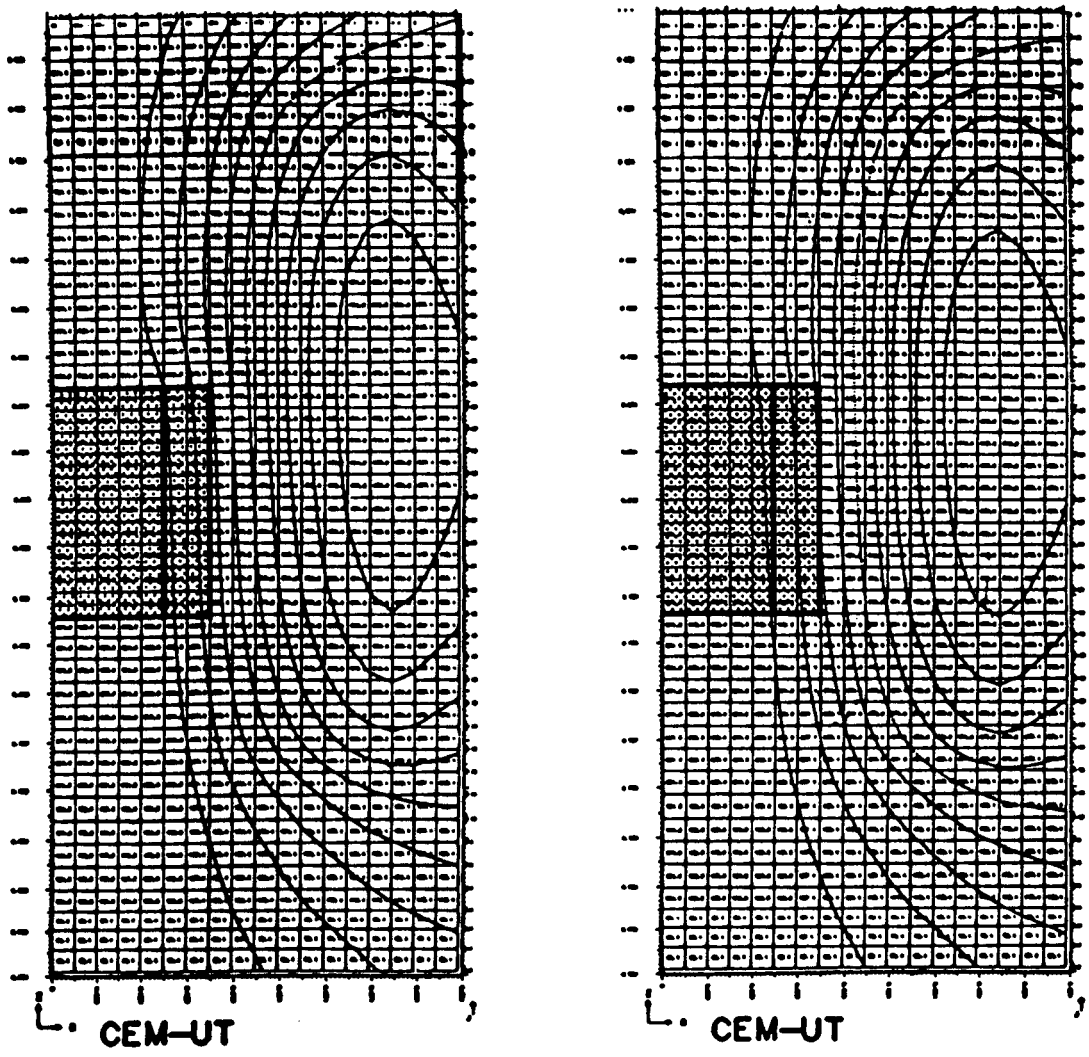

Figure 13. Magnetic field diffusion in the projectile at the moments (a) t = 4 ms and (b) = 10ms

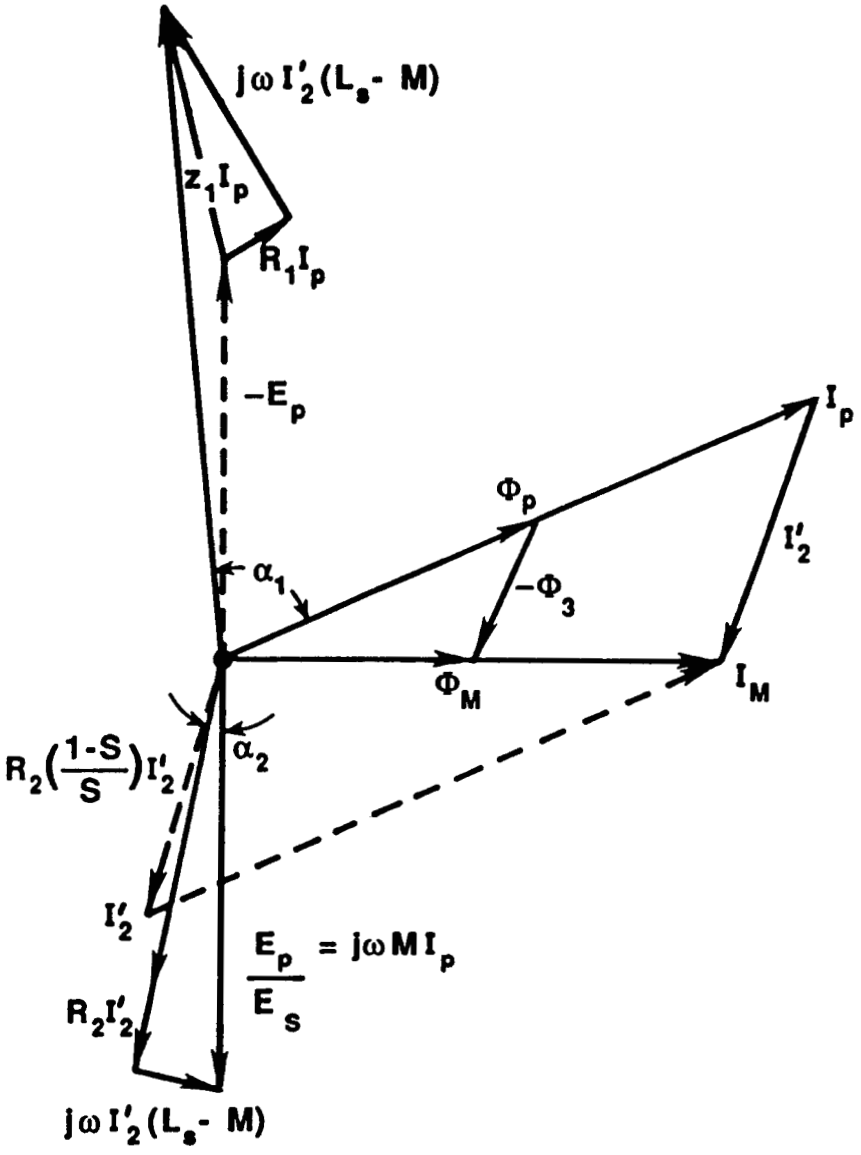

Figure 14. Phasorial diagram for the coaxial accelerator (stator segment containing the projectile)

STATOR WINDING DESIGN

The stator winding is a three phase tubular winding producing a traveling wave of magnetic flux along the barrel when energized. Usually one phase of the stator winding is made of a series of alternatively polarized coils spaced apart at a distance equal to the polar pitch and producing alone a standing magnetic flux wave, which pulsates in time with the frequency of the sinusoidal current flowing through the winding. The succession and relative disposition of all three phases is shown in figure 7a which illustrates a segment of one of the barrel windings. Each phase coil has an even number of turns, half of direct, half of inverse polarity. The coils of all three phases produce by superposition, the traveling field wave. The elementary standard coil used, in series and parallel combination, to manufacture each of the segments of the stator barrel winding is shown in figure 15. The dimensions include the insulation (turn-to-turn and phase-to-phase) and the transposition and stranding.

The one serious disadvantage of the standard configuration winding with the interphase connections, is that they form an additional outside structure, which the voluminous, and since the connections require the same cross-sectional area as the winding itself the design of the bus structure is important. Also the projectile, following the traveling wave is subjected continuously to phase-to-phase electric potentials. Because of these drawbacks, the winding selected for the present design is a layered, distributed winding shown in figure 7b reproduced for convenience as figure 16.

Each layer (inner, middle, and outer) carries only one phase, and the total magnetomotive force (mmf) is obtained by superposition and by the choice of the phase angle between different layers. For a given segment of length L, the sum of different mmfs is:

$$\text{mmf} = \overline{B} - 1/3\overline{C} - 1/3\overline{A}$$

The condition for a symmetric polyphase system of mmf is:

$$\overline{A} + \overline{B} + \overline{C} = 0, \text{ at any moment}$$

then

$$\overline{B} = -\overline{C} - \overline{A}$$

or, substituting in the original relation for the winding segment of length L:

$$\overline{B} - 1/3(\overline{C} + \overline{A}) = \overline{B} + 1/3\overline{B} = 4/3\overline{B}$$

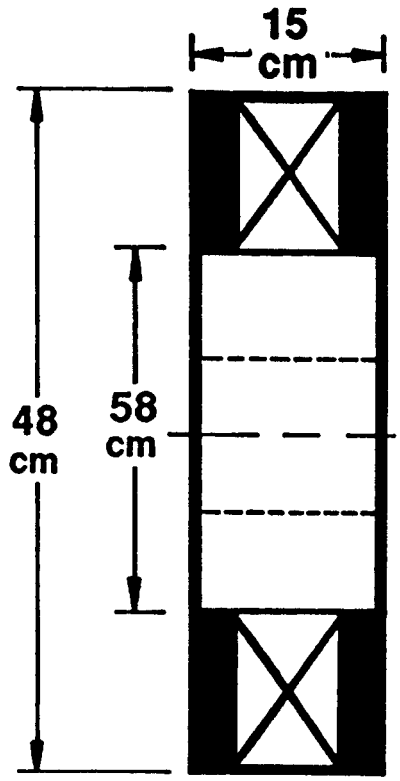

Figure 15. Elementary coil (one turn) for standard winding

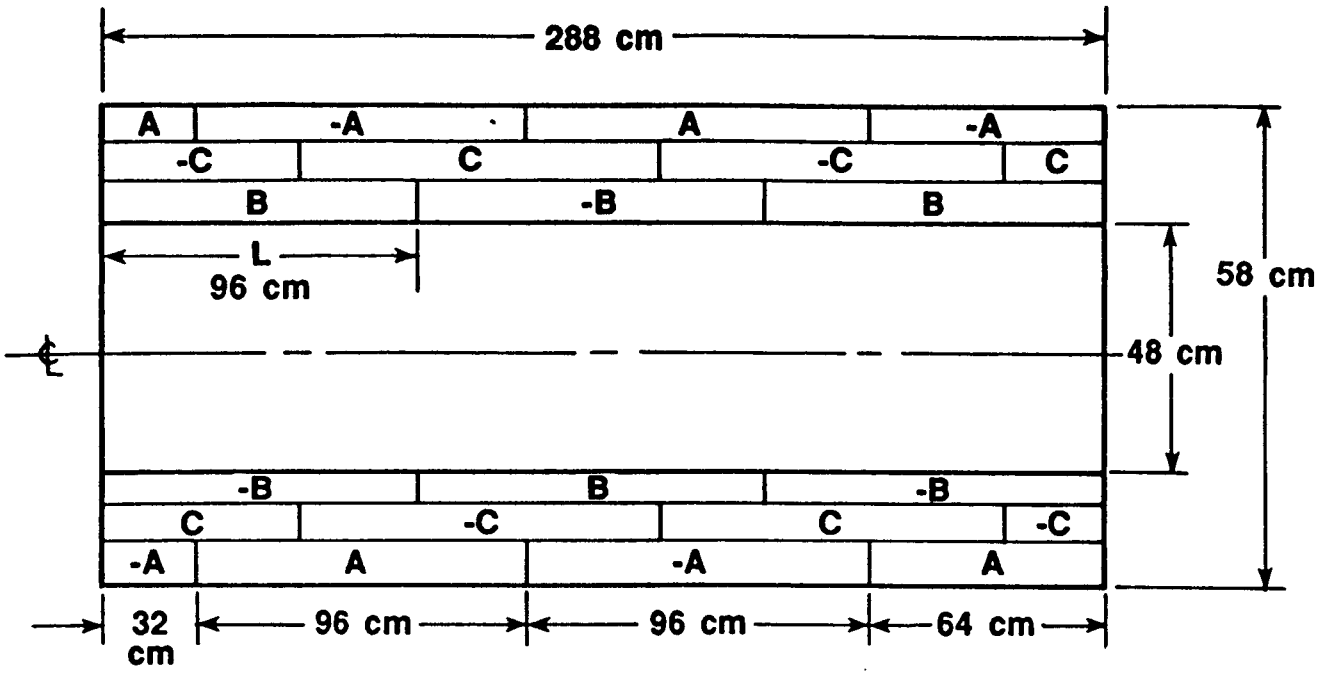

Figure 16. Segment of layered distributed stator winding for the coaxial launcher

Comparing figures 7a and 7b, it can be seen that the distance over which phase B is spread is twice as much in the distributed winding. Then for equal conditions the resulting mmf of the traveling wave is only 4/3 x 1/2 = 2/3 or 66% of the original concentrated winding.

However, the loss of 1/3 of the mmf represents a favorable trade-off not only for the elimination of complicated phase interconnections, but also for an easy manufacturing process. The windings for a phase run continuously, only the polarity being successively reversed. Insulation between phases is applied uniformly. The projectile traveling down the barrel sees along the stator, a distributed voltage, which for all positions is relatively small, requiring comparatively thin layers of insulation.

The trade-off mentioned above is made more attractive by the increase in packing factor for a thinner folded plate conductor. As will be shown at the end of this report the increase in the elementary conductor length, in a stranded and completely transposed conductor using the folded plate method is:

$$K_{\ell} = \frac{\ell^2 + W^2 + h^2}{\ell}$$

where

ℓ = length
w = width
h = height

The concentrated winding requires 15 layers per conductor, corresponding to:

$$K_{\ell}' = \frac{(0.74)^2 + (15 - 1)^2 x\ (0.04)^2 + (0.055)^2}{0.74}$$

which leads to a dc resistance increase coefficient of:

$$K_R = (K_e')^2 = 1.578$$

where

K_R = coefficient of resistance
K_e = proportionality constant for eddy current loss

A distributed winding, five layers of thin plate per conductor, leads to a reduced dc resistance coefficient of only:

$$K_R^{11} = (K_e^{11})^2 = 1.16$$

which partially off-sets the loss of effective turns.

There is a disadvantage in using the layered, distributed winding, introduced by the difference in the diameter between the outer and inner phase. In the present case, however the relative difference is small (the phase conductor is only 5 mm thick, compared to 467 mm-the ID of the launcher bore). Provisions have been made in the design that the phase layers change places (transpose) 16 times for the 6 km/s launcher which will produce the desired symmetry.

The stator winding has four electrically distinct parts. Each part is 48 m long and is energized from a separate compulsator. While electrically distinct, they are magnetically continuously connected, producing an uninterrupted traveling field wave, such that the secondary (projectile) passes smoothly from one part to another. Each part has a different number of segments, each having a different pole pitch (the segment length is equal to pole pitch length). Table 2 gives synoptic data for the four parts of the launcher winding. Tables 3A, B, C and D give the dimensions of individual segments in different parts of the winding which, when energized with the corresponding frequencies will provide the continuous traveling wave. The winding is manufactured from elementary turns of 15 cm length, carrying a current of 238.5 kA (rms) each or 1.59×10^6 A/m--producing a flux density linking the secondary of 1.95 T (rms) or 2.75 T (maximum)--as a result of a joint action of all three phases. The thickness of a phase conductor is 0.5 mm and a packing factor of 0.5. The heating of the primary winding is 79.6 °C above the ambient temperature, including the effect of the higher harmonics.

The winding requirements described in tables 3A to D do not include two special sections of the launcher. The first is the "starter coil" necessary for inducing the secondary current in the armature, right before launching. As documented, such a starter coil reduces the necessary "slip", eliminating the necessity to produce much stronger fields for initiation of secondary current leading to a more economical stator design and an improvement of overall performance of the en-tire system. The second special section of the launcher is a final section 4.2 m long which has the role of producing a gradual decreasing impulse as the projectile leaves the active part of the barrel. This gradual flux change avoids high transient current bursts and unnecessary projectile beatings. It also prevents high force transients which will negatively effect not only the projectile but also the last section (muzzle) of the barrel.

Starter Coil (Secondary Current Initiation)

An essential difference between the induction accelerator and its steady-state counterparts, (linear or rotating induction motors) is the initial rate of current

Table 2. Stator parameters

Part #	Total # of segments	Frequency range (Hz)	Accelerator segment
I	14	240 to 110	0 to 48 m
II	8	320 to 225	48 to 96 m
III	7	400 to 280	96 to 144 m
IV	7	480 to 340	144 to 196 m

Table 3A. Stator winding (barrel) with variable pole pitch, part I, L = 48 m

Segment number	Length	Total length
1	0.30	0.30
2	0.60	0.90
3	0.90	1.80
4	1.50	3.30
5	1.95	5.25
6	2.40	7.65
7	2.85	10.50
8	3.30	13.80
9	3.90	17.70
10	4.50	22.20
11	5.10	27.30
12	6.00	33.30
13	6.75	40.05
14	7.95	48.00

Table 3B. Stator winding (barrel) with variable pole pitch
L = 48 m, f = 320 to 225 Hz

Segment number	Length	Total length
1	4.95	4.95
2	5.10	10.05
3	5.25	15.30
4	5.40	20.70
5	5.70	26.40
6	6.30	32.70
7	7.05	39.75
8	8.25	48.00

Table 3C. Stator winding (barrel) with variable pole pitch
L = 48 m, f = 400 to 280 Hz

Segment number	Length	Total length
1	5.85	5.85
2	6.00	11.85
3	6.30	18.15
4	6.60	24.75
5	6.90	31.65
6	7.65	39.30
7	8.70	48.00

Table 3D. Stator winding (barrel) with variable pole pitch
L = 48 m, f = 480 to 340 Hz

Segment number	Length	Total length
1	6.00	6.00
2	6.15	12.15
3	6.45	18.60
4	6.75	25.35
5	6.90	32.25
6	7.35	39.60
7	8.40	48.00

build-up in the secondary. The acceptable rates for the steady-state induction machines is between four and seven cycles of the power supply voltage (0.066 to 0.12 s) for a 60-Hz frequency--an acceptable delay when compared with the 1 to 3 s, electromechanical starting time. For the proposed induction launcher the total launch time is 0.061 s, which requires special means to reduce the current build-up time in the projectile.

Such considerations have led to "starter coil" as a preliminary stage of the accelerator. It represents the integration of a pulsed transformer with the low speed of a linear motor, inducing the necessary secondary current from the beginning of the cycle, and injecting the projectile. The starter coil is a 0.9 m long coil with an ID of 0.467 m and an OD of 0.74 m. It has a velocity of 10 m/s for the traveling field.

The starter coil power supply is a separate 25 kVA, 3,000 V, synchronous machine modified to operate in pulsed mode. The changes consist in rewinding the armature in order to fit the parameters of the starter coils and to passively compensate it by using a copper squirrel cage on the field part and lateral copper rings, to shield the endturns. Figures 17a and b show the super-position of the magnetic field in the starter coil and the magnetic field created by the induced current in the projectile. Figure 18 shows a variation in time of the current in the secondary of two different types of projectiles considered.

Power Supply Characteristics

The power supplies are electrical machines, low impedence compensated alternators. They discharge, transforming the kinetic energy stored in the rotor into a train of sinusoidal pulses of high voltage, high current of appropriate frequency in order to produce the accelerated traveling field wave.

The compulsator was invented at CEM-UT in 1978. CEM-UT is under contract (number DAAA-21-86-C-0281) to build a self-excited compulsator. Such a machine has a voltage of 8,500 V and a current equal to 5×10^6 A, storing 236 MJ of kinetic energy. The apparent power of the machine is:

$$S = 8.5 \times 10^3 \times 5 \times 10^6 = 42.5 \times 10^9 \text{VA} = 45.5 \text{ GVA}$$

Table 4 shows the characteristics for the four compulsators proposed to drive the four parts of the coaxial accelerators, 6 km/s variant. They are connected for a constant current of 0.477 MA, corresponding to 0.3 m of barrel length. Since the stator of the launcher is modular, connecting elementary coils in series and parallel, the necessary voltage and current can be changed, the apparent power (GVA) remaining the same, and serving as a basis for comparison.

From the comparison, the conclusion can be reached that the compulsator being built at CEM-UT has parameters which are of the same order of magnitude as those for generators I to IV required to energize the coaxial launcher.

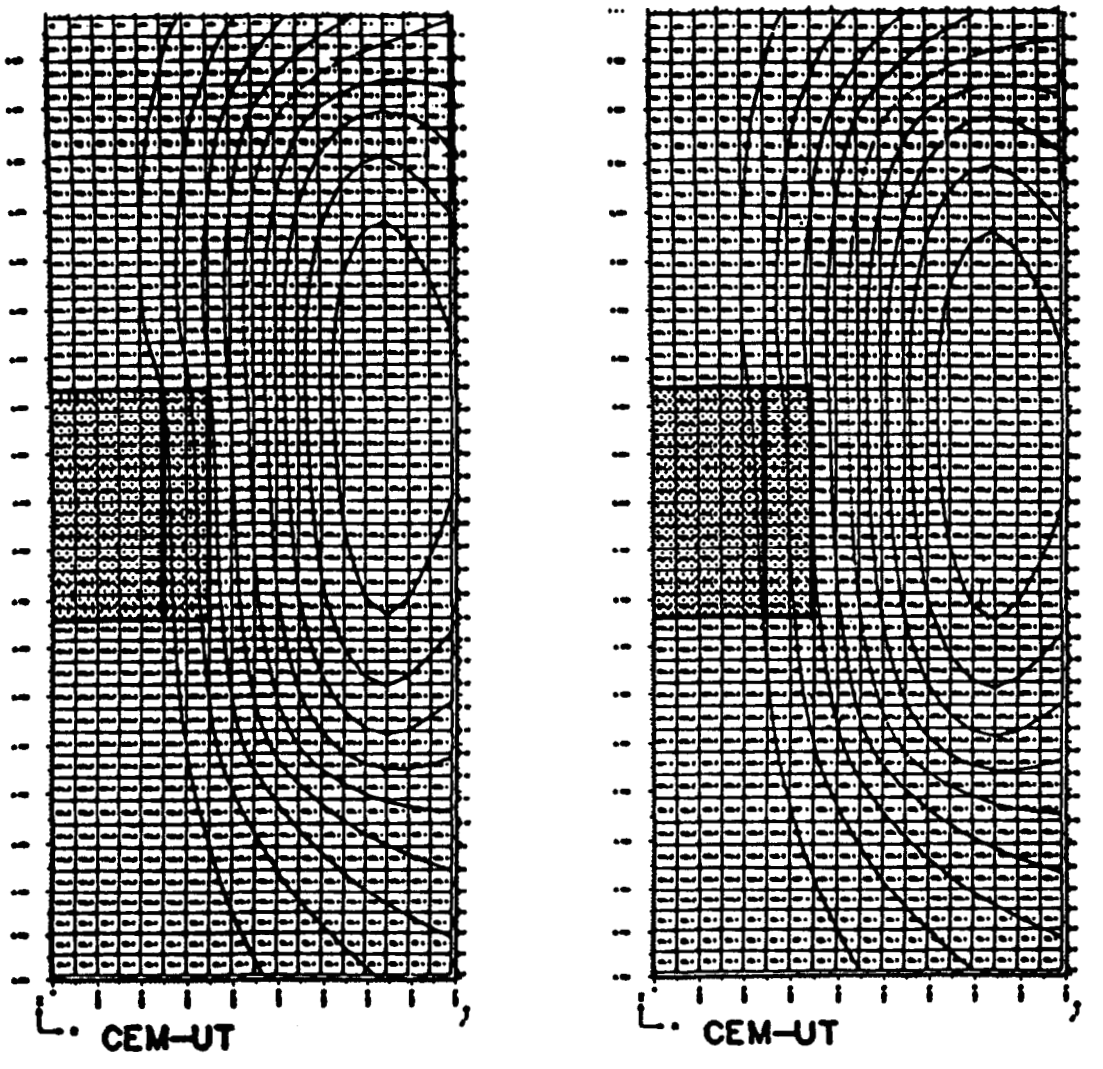

Figure 17. Transient magnetic field projectile in stator coil

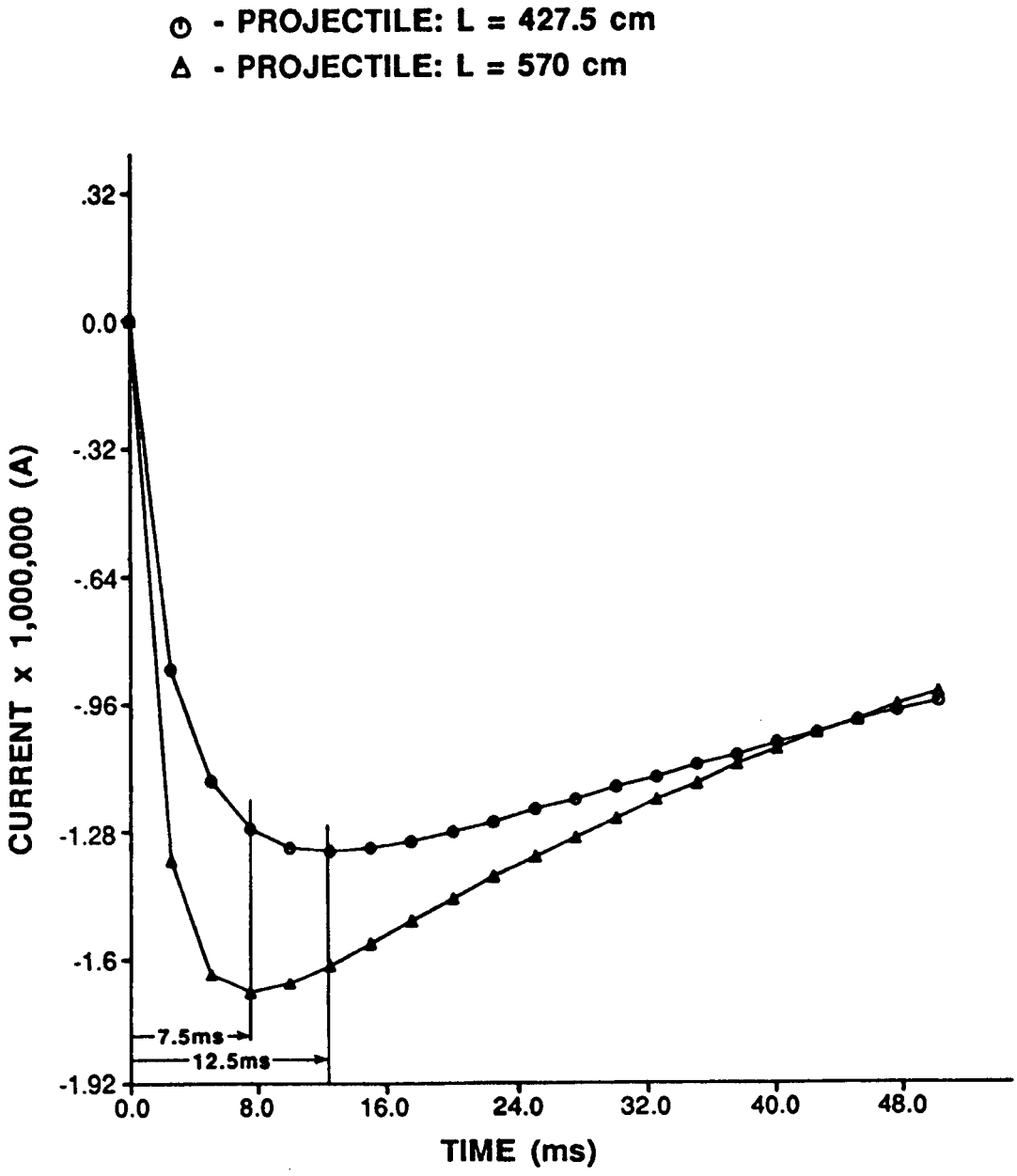

Figure 18. Variation in time of the current induced in the projectiles

Table 4. Generators: voltages, currents, and instantaneous power

Generator	Voltage range (kV)	Current (MA)	Maximum apparent power (GVA)
I	14.95 to 10.50	0.477	21.10
II	14.95 to 14.00	0.477	28.16
III	24.90 to 17.45	0.477	35.14
IV	29.92 to 21.20	0.477	42.82
UT-CEM Compulsator	8.500	5.000	42.50

The compulsator uses inertial energy storage and can produce a burst of pulse or even a continuous chain of pulses. Since its invention in 1978, CEM-UT has built and tested three compulsator variants. The machine listed at the end of table 4 is the fourth generation, and is being designed, built and tested under U.S. Army contract to demonstrate a field portable "rapid fire electromagnetic gun system". Due to the field portable condition, this iron-less compulsater has to satisfy very stringent weight and compactness requirements which greatly affects its design. For the NASA launcher project which is a stationary power supply, with relaxed weight and compactness requirements, a less expensive electrical machine will be built. Such a machine might have an iron core.

Another possibility considered in this project was to compensate and mechanically and electrically upgrade, for pulsed operation, large synchronous machines manufactured by one of several established companies in the U.S. or Europe. Suitable designs are manufactured by General Electric, Allis Chalmers, Westinghouse in the U.S., ASEA in Sweden, Siemens in West Germany and Brown-Boveri in Switzerland. An example in this direction is the upgrade of a water-wheel alternator as the pulsed-power supply--the Texas Experimental Tokamak, for which a detailed design was performed [6]. Table 5 shows the energy stored and the frequency range for the four generators used in this project.

For the 11 km/s variant, the coaxial launcher remains the same. It will be, however split in 8 parts of 24 m each and several connections will be modified. A separate electrical machine, using identical storage will pulse each of the eight parts. The current through the elementary coil 0.15 m wide is 432 or 864 kA through a 0.3 m wide coil. Table 6 gives voltage ranges and the maximum instantaneous power for the four pulsed, compensated generators.

The current has considerably increased from the 6 km/s variant. Also, to keep the phase voltage within reasonable bounds several paths in parallel have been introduced--leading to some parallel connections between the elementary coils. In spite of doubling the number of machines, due to the increasing frequency, and the increase in the velocity--the apparent power has very large values. Table 7 gives the values of kinetic energy stored by each machine and the corresponding frequency range (initial and final).

Projectile

The secondary of the coaxial launcher is a shell of aluminum 0.457 m in diameter, 0.30 m long and 0.004 m thick. Aluminum was chosen after a study to find the material which has the optimum balance of the density, strength, electrical conductivity, and specific heat.

Initially, using the starter coil a current of 1.49×10^6 A will be induced in the armature, corresponding to a current density of 1.24×10^9 A/m^2 in the conductor volume of 1.723×10^{-3} m^3.

The total heating of the secondary during the launching is $t = 246°C$ above the ambient temperature due to the slip, joule losses in the armature and eddy currents

Table 5. Generators: frequency range and energy stored

Generator	Frequency Range (Hz)	Energy Stored (MJ)
I	240 to 170	179
II	320 to 225	211
III	400 to 280	242
IV	480 to 340	274

Table 6. Generators: voltages, currents, and instantaneous power

Generator	Voltage range (kV)	Current (MA)	Maximum apparent power (GVA)
I	1.72 to 1.2	1.72	2.96
II	3.43 to 2.4	1.72	5.92
III	5.2 to 3.6	1.72	8.87
IV	6.9 to 4.8	1.72	11.83
V	8.6 to 6	1.72	14.79
VI	10.3 to 7.2	1.72	17.75
VII	12 to 8.4	1.72	20.7
VIII	13.7 to 9.6	1.72	23.7

Table 7. Generators: frequency range and energy stored

Generators	Frequency range (Hz)	Energy stored (MJ)
I	110 to 77	274
II	220 to 154	286
III	330 to 231	303
IV	440 to 308	338
V	550 to 385	375
VI	660 to 462	424
VII	770 to 539	477
VIII	880 to 616	542

due to the magnetic ripple. If the influence of the higher field harmonics is added, the total heating above the ambient temperature reaches (Δt) total = 268°C. The secondary will be initially cooled at liquid nitrogen temperature in order to increase its time constant.

RAILGUN ACCELERATOR

Introduction

Another candidate technology for the EML is the railgun. The railgun armature is driven by a body force resulting from the interaction of a self excited magnetic field and the current in the armature (fig. 19). Unlike conventional guns, which are limited by the expansion rate of chemical gases, the railgun can achieve much higher velocities. Velocity limits encountered to date are due in part to armature instabilities and current diffusion characteristics. As of 1986, projectiles launched from small railguns have achieved velocities of 10 km/s.

The simplified equation of force in a railgun is:

$$F = 1/2 L' I^2$$

where

F = force on the projectile
L' = inductance per unit length of the railgun
I = current in the armature or projectile.

Railguns accelerate projectiles by passing a high current through an armature positioned between two rails. As the current passes through the armature the interaction of the magnetic field and the current creates a force which accelerates the armature and projectile along the rails. The force is proportional to the square of the current. Using this technique, very high currents create acceleration forces leading to hypervelocities.

Background

The Center for Electromechanics at The University of Texas at Austin is currently launching small projectiles at 6 km/s, and expanding this capability toward the energy levels required by the hypersonic real-gas facility. Power supplies are now available and accelerators are being built to launch 2 kg at 3 km/s. Our ongoing research in high speed solid armatures resulted in concepts for the successful repetitive launch of high mass payloads (10 kg) at hypersonic velocities (6 km/s). Previous and on-going studies performed by CEM-UT are listed in Appendix B.

To perform this type of launch CEM-UT proposes the construction of a multi-rail railgun with plasma gas bearing sabot (launch vehicle), which can be used repeatedly without reworking or replacing accelerator components (fig. 20).

The following is a listing of goals and constraints necessary to launch high-mass vehicles in the hypersonic facility:

Total projected mass: 14 kg

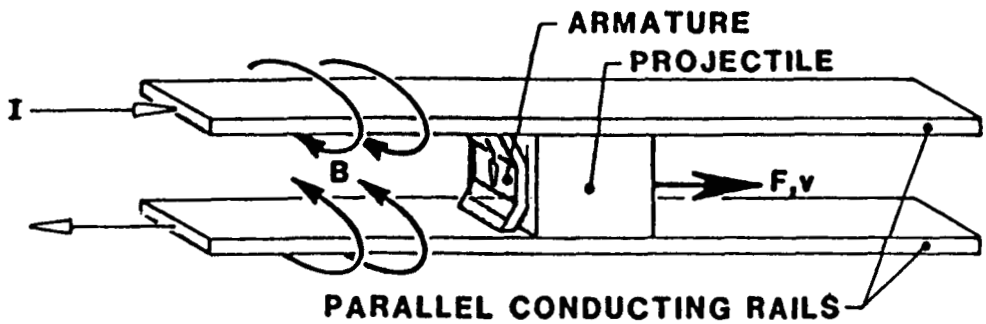

$$F = \frac{L' I^2}{2}$$

Figure 19. Railgun basic concept

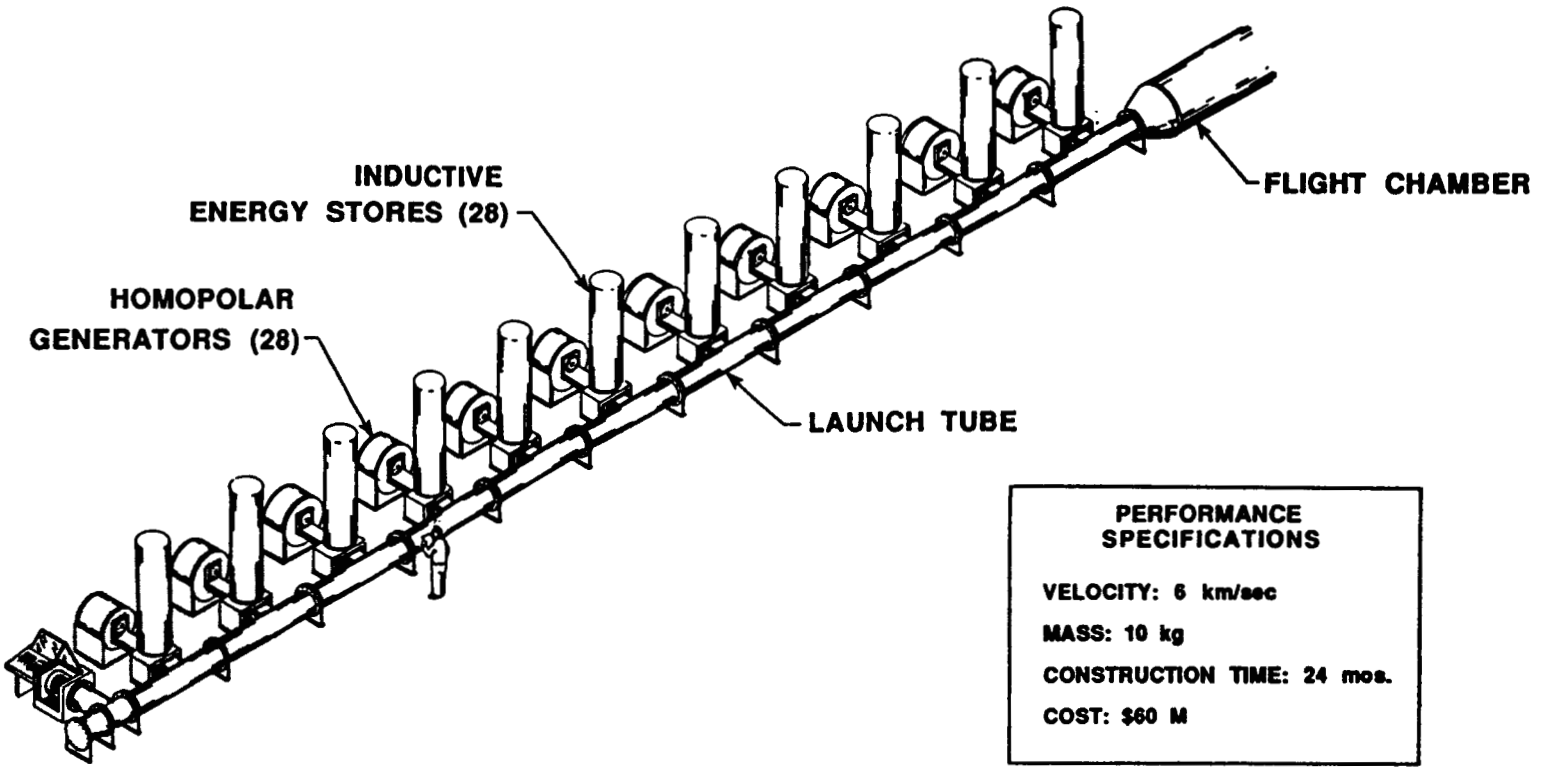

Figure 20. Railgun launcher

Velocity: 6 km/s
Projectile kinetic energy: $E = MV^2/2 = (14)(6{,}000)^2/2 = 225$ MJ
Maximum acceleration: 98,100 m/s^2, 10,000 gees
Minimum launch time: $t = V/A = 6{,}000/98{,}100 = 61$ ms

To launch a total projectile mass of 10 kg in the form of a flight model to the velocity of 6 km/s would require a constant force of 98,100 N.

$$F_{max} = MA_{max}, \text{ where M is mass, A is acceleration}$$

$$f\ F_{max} = 14 \text{ kg} \times 98{,}100 \text{ m/s}^2, \text{ where } \alpha_f = \text{friction factor} = 0.8$$

$$F_{max} = 1.72 \times 10^6 \text{ N}$$

$$0.25\ F_{max} = 0.43 \times 10^6 \text{ N for each of 4 rail pairs}$$

The current necessary to generate this force is, based on the equation:

$$F = L'I^2/2$$

Solving for the value of I, assuming a value of 0.41 μH/m for L', and also assuming uniform current distribution over the cross section of the railgun.

$I = 1.45$ MA for each of the four rails
I_{peak} from the HPG/I = 2.9 MA

This special four rail railgun configuration (fig. 21) has the advantage of lowering the individual rail currents to achieve the initial launch objective, and allows an increase in current as the launch objectives advance, without melting the rails. Opposing rails are wired in series to insure equal currents (and equal forces) along an axis (fig. 22), and serial pairs of rails connected in parallel to a single power source.

The value of L' is dependent on the current penetration in the rails near the projectile. Although the value of L' varies little over a wide range of gun constructions, the value was calculated using finite element methods to determine the gun performance and was found to be 0.41 μH/m for one of the four rail cross sections shown in fig. 23. I (1.09 MA) is the current in each rail with the assumption that the current density is uniform over the cross section.

Railgun Construction

Because of the inherent resistance in a long railgun, and the large current required to propel the projectile, normally, short rail sections are used to reduce the ohmic loss. For this design, however, the individual storage modules are connected to sections of the continuous rails and switched in very close to the armature. This is referred to as distributed energy store (DES) [7] (fig. 24). DES guns have two major advantages where rail length is a factor; first, switching in

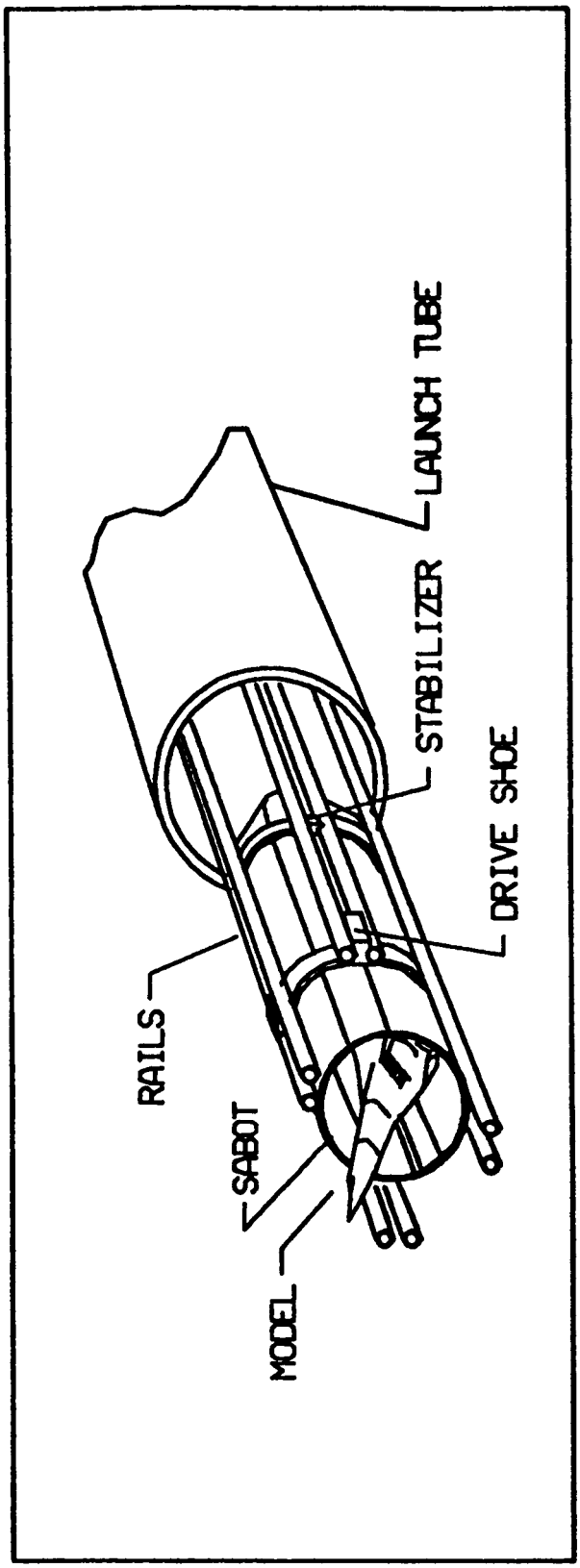

Figure 21. Multi-railgun configuration

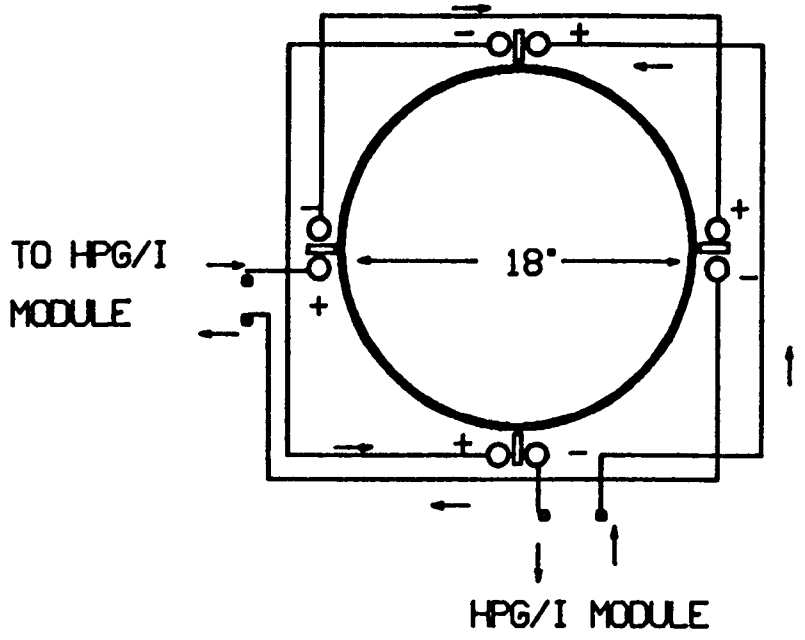

Figure 22. Electrical hook-up for multi-railgun

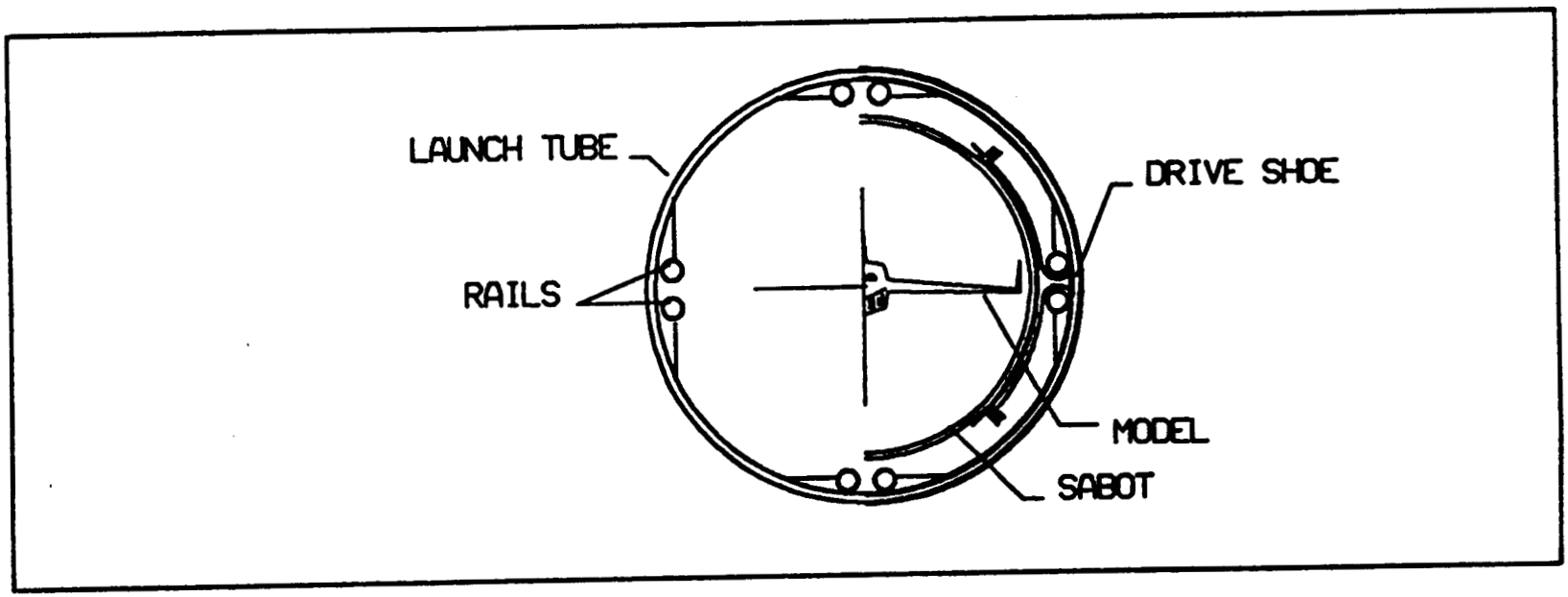

Figure 23. Cross section of multi-railgun

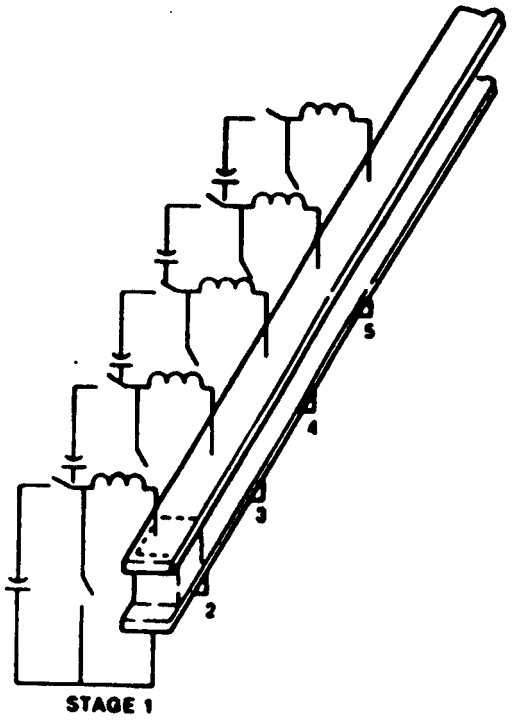

Figure 24. Distributed energy source

stored energy at discrete locations along the rails minimizes the resistive losses that a breech-fed gun would need to overcome. Second, a number of discrete power supply modules can be used to add up to the total amount of energy required for the launch.

Railguns can be repeated subassemblies of energy store, and switching elements, powering the continuous rails of the launcher. This modularity will be an important aspect in achieving the operating performance and for varying the capabilities of the hypersonic facility. The minimum length of the launcher is represented by the equation:

$$V = (2As)^{1/2}$$

where

V = velocity
A = acceleration
s = distance traveled,

s = 180 m

This assumes a constant acceleration on the armature, that would result in a minimum launch length. However, because of the discharge and switching characteristics of the power source (HPG/I), there is a drop in current as each section discharges which necessitates additional gun length for each segment.

Synchronous Switching of Energy Store

In a DES launch system, it is important to time the discrete charging of the rails with the acceleration of the projectile along the rails. An obvious way to time the switching is to detect the arrival of the projectile at different points along the launcher and switch in the next energy store. The projectile essentially rides a magnetic wave which is easily detected as a sharp field reversal and this signal can be detected and used to switch in the next store with an accuracy of 1 μs.

The shape of the magnetic wave which accompanies the armature, being sharp, provides an edge to time a switching sequence connecting the next energy store to the next rail module. The previous store must also be disconnected when discharged to prevent reversal of energy flow.

Initial Acceleration

To reduce the chance of damage at the railgun breech when the projectile is accelerated from rest, the projectile can be prelaunched and moving before the rails are energized. A simple pneumatic cylinder will give the projectile an initial velocity of 20 m/s (fig. 25). Compressed air at a pressure of 1,000 psi can be

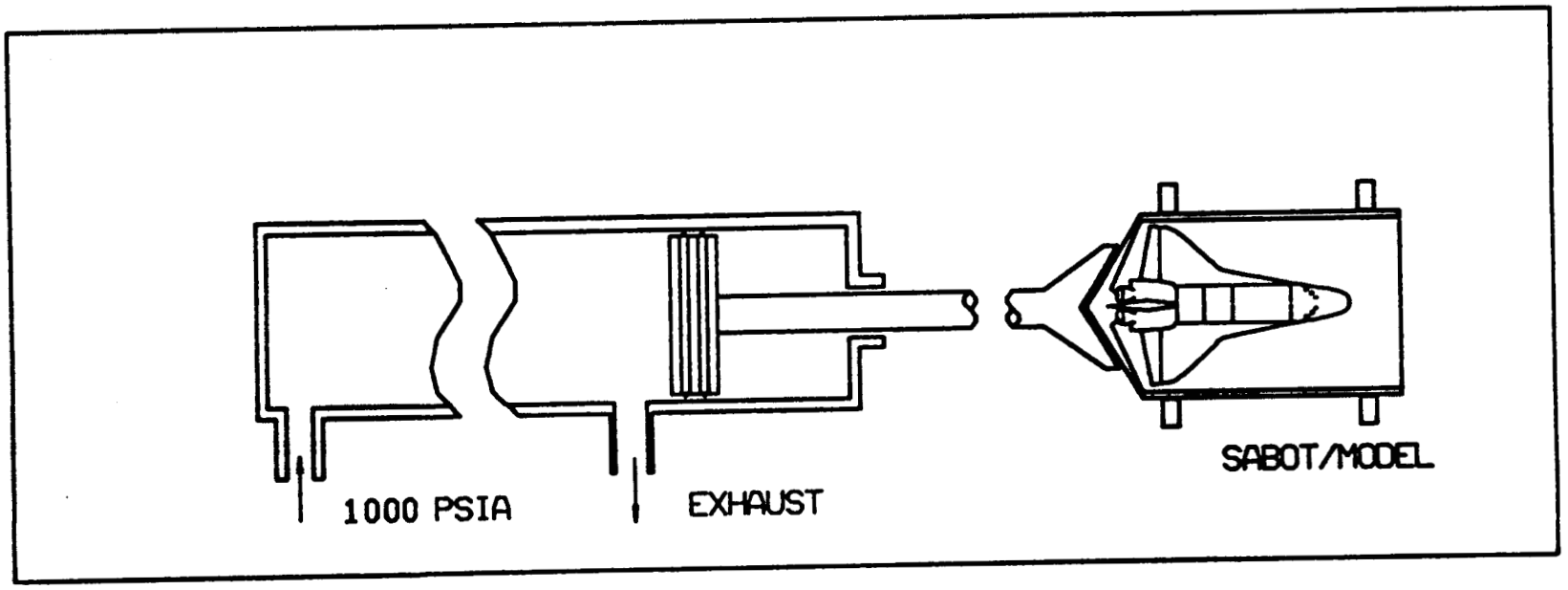

Figure 25. Pre-launch mechanism

switched into the cylinder by a fast acting electric valve. As the piston, which pushes the sabot, reaches the extended position, the EML cycle will begin.

Method for Decelerating Sabot

An important aspect of the launch is the model separation from the sabot. The model must be allowed to fly clear of the sabot without tipping or interfering in any way with the designed launch attitude.

An opportunity exists with the EML to reverse the launch system (fig. 26) to decelerate the sabot alone. This sudden deceleration of the sabot will allow the model to launch at the desired velocity of 6 km/s. To perform the deceleration, a final railgun module is engaged.

This final module would be pre-energized with two capacitor banks to establish a reverse field between the rails. In this arrangement, the sabot is acted on by a high force in the reverse direction from that of the launch. The power generated could be wasted by heating a water vat with submerged resistors during this deceleration phase of the launch, (fig. 27).

The load resistors should be adjusted to provide controlled deceleration for the sabot and allow the model to fly clear, sending the model on its way through the flight chamber. After the model clears the sabot, the sabot can be decelerated with much more authority, dumping approximately 80 MJ of kinetic energy into hot water. It requires approximately 1 MJ to boil a pound of water, so 15 gal would need to be added to the tank before each launch. This may be an important feature of a quick turnaround cycle for the hypersonic laboratory. It is ironic that the power capacity from across two states cannot deliver the power for a launch yet the energy to boil 3 buckets of water will quench it.

Power Source

A 14 kg mass stores 252 MJ of kinetic energy at 6 km/s. The railgun must impart this same amount of energy into the model during the launch in order to successfully achieve the launch objective. To achieve a controlled surge of current of this order of magnitude, railguns are powered by homopolar generator/inductor (HPG/I) systems, compulsators, or capacitors.

Capacitors are quite often used as a primary energy storage device for small railguns. With the use of a closing switch, this energy can be applied to a launcher by allowing current to flow from a bank of many capacitor stores. Capacitor banks are readily available that can store 60 MJ, but at significant cost. Current gathering from the large bank required for the program is the problem.

Compulsators, are the first fundamentally new rotating electrical generators invented in the twentieth century. A compulsator operates by compressing magnetic flux between two identical sets of wave windings, one moving and the other

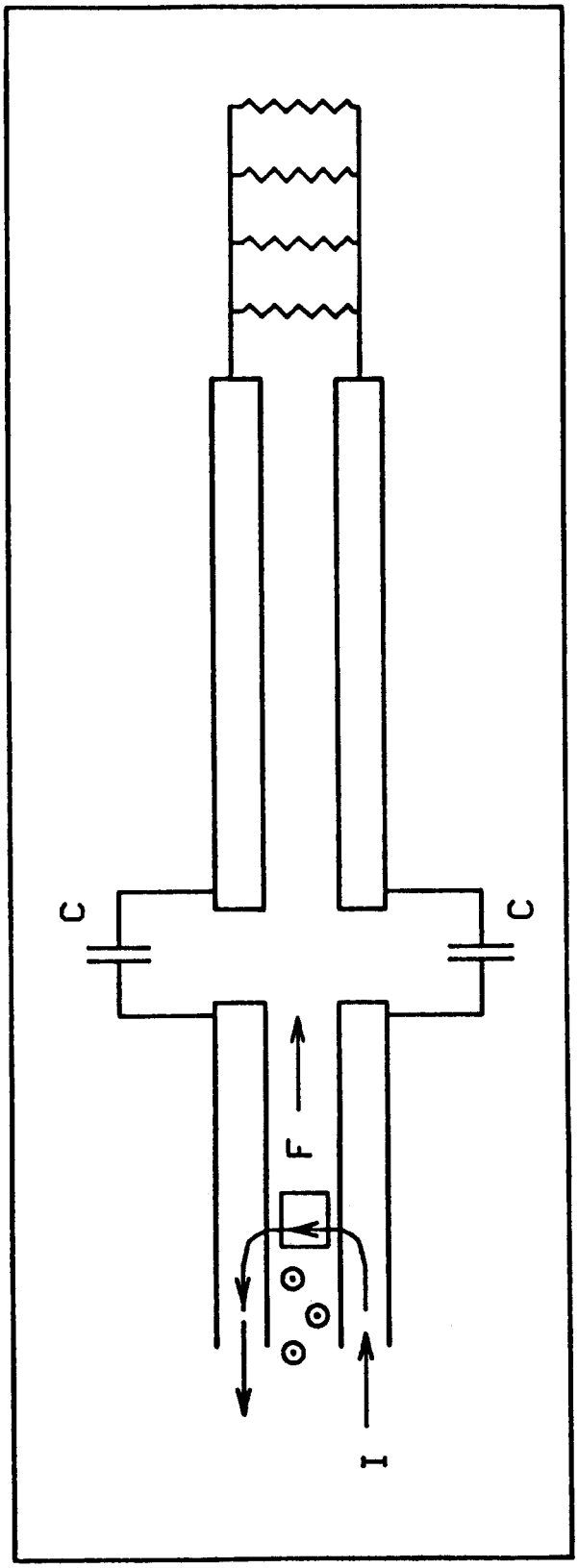

Figure 26. Railgun decelerator at the ready

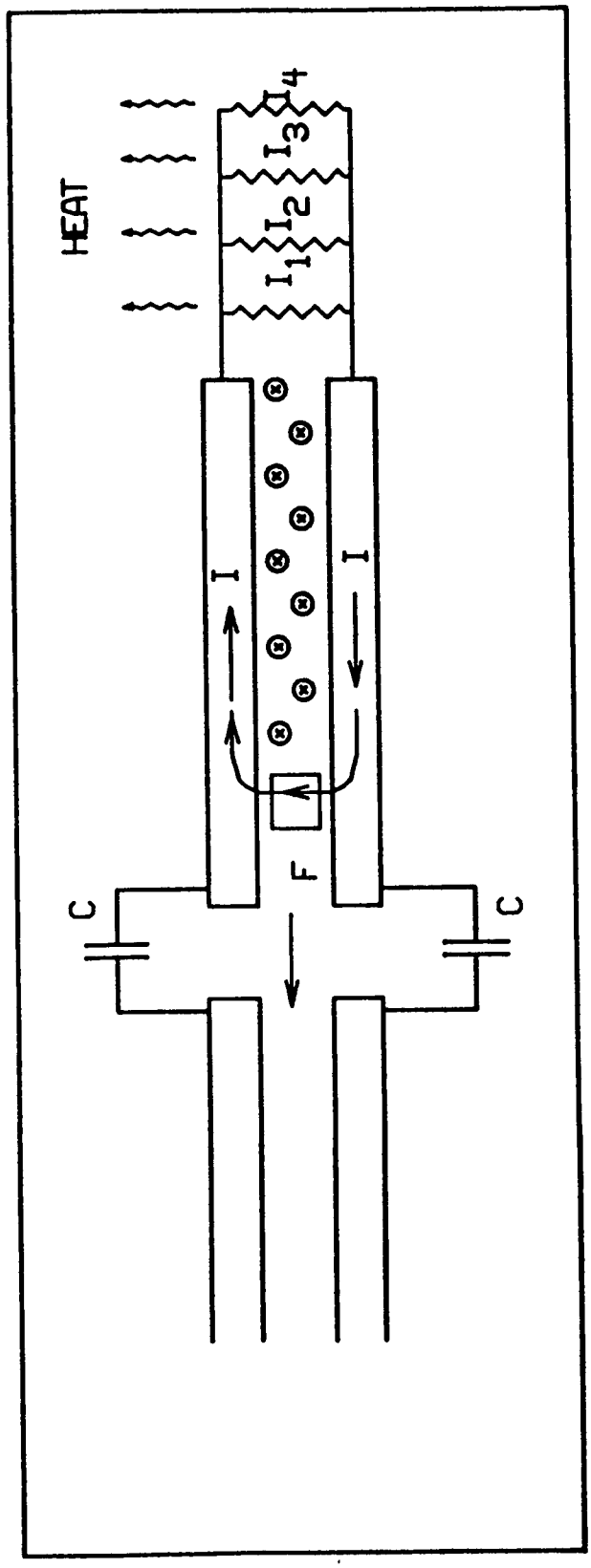

Figure 27. Railgun decelerator converting kinetic energy into heat

stationary. Kilovolt-level pulses of megampere current may be generated; however, the millisecond duration pulses of existing compulsators are too short to make long barrel railgun launches possible. Future machines with long, square pulses shaped specifically for railguns are being developed and could be a viable alternative. The advantage of a compulsator is that it can be tied directly to the railgun without the power conditioning components required by homopolars or capacitors.

The homopolar generator (HPG) (fig. 28), old in principle, was the first pulsed-power supply developed at CEM-UT. Homopolar generators can deliver large pulses of electric power at very high currents (multi-MA), but with comparatively low voltage. In operation, mechanical energy is stored by slowly spinning up the rotor which is situated in a magnetic field. After the rotor is spinning at high speed, the magnetic field is applied. On closing a switch in the output circuit, the stored energy is converted to an electric pulse which peaks into an inductive load in about 0.25 s.

One problem, however, with the HPG is the low voltage which makes energy transfer to the railgun difficult. The voltage requirement at the end of the launch is:

$$V = L'Iv = (0.4 \times 10^{-6})(1.5 \times 10^{6})(6{,}000) = 3{,}690 \text{ V}$$

One means of overcoming this difficulty is to use intermediate inductive storage for power conditioning (fig. 29). The inductor, which is switched into the railgun with a high current opening switch at peak current, will develop voltage as required to transfer current into the railgun.

CEM-UT is currently using, in research, a 60 MJ modular system of six, 10 MJ drum type (iron-core) homopolar generators (fig. 30). These generators are now commercially available. However, CEM-UT has designed a single HPG capable of 60 MJ storage, which is proposed for use at the hypersonic real-gas facility. Two hundred eighty MJ modules have also been designed and could be used. The 60 MJ modules, because there are more of them, would minimize jerk on the projectile.

A preliminary design for a single rotor 60 MJ HPG calls for a drum type, iron-core generator with an average magnetic flux density of approximately 1.6 T, and a maximum tip speed of 180 m/s. The design specifications for this new HPG have been defined as follows, (see fig. 31).

$$\text{Mass of rotor} = m = r^2 \ell_r \rho$$

where

r = radius of rotor
ℓ_r = length of rotor
ρ = mass density of iron = 7,860 kg/m^3

Polar moment of inertia of the rotor is

$$J = \tfrac{1}{2} m r$$

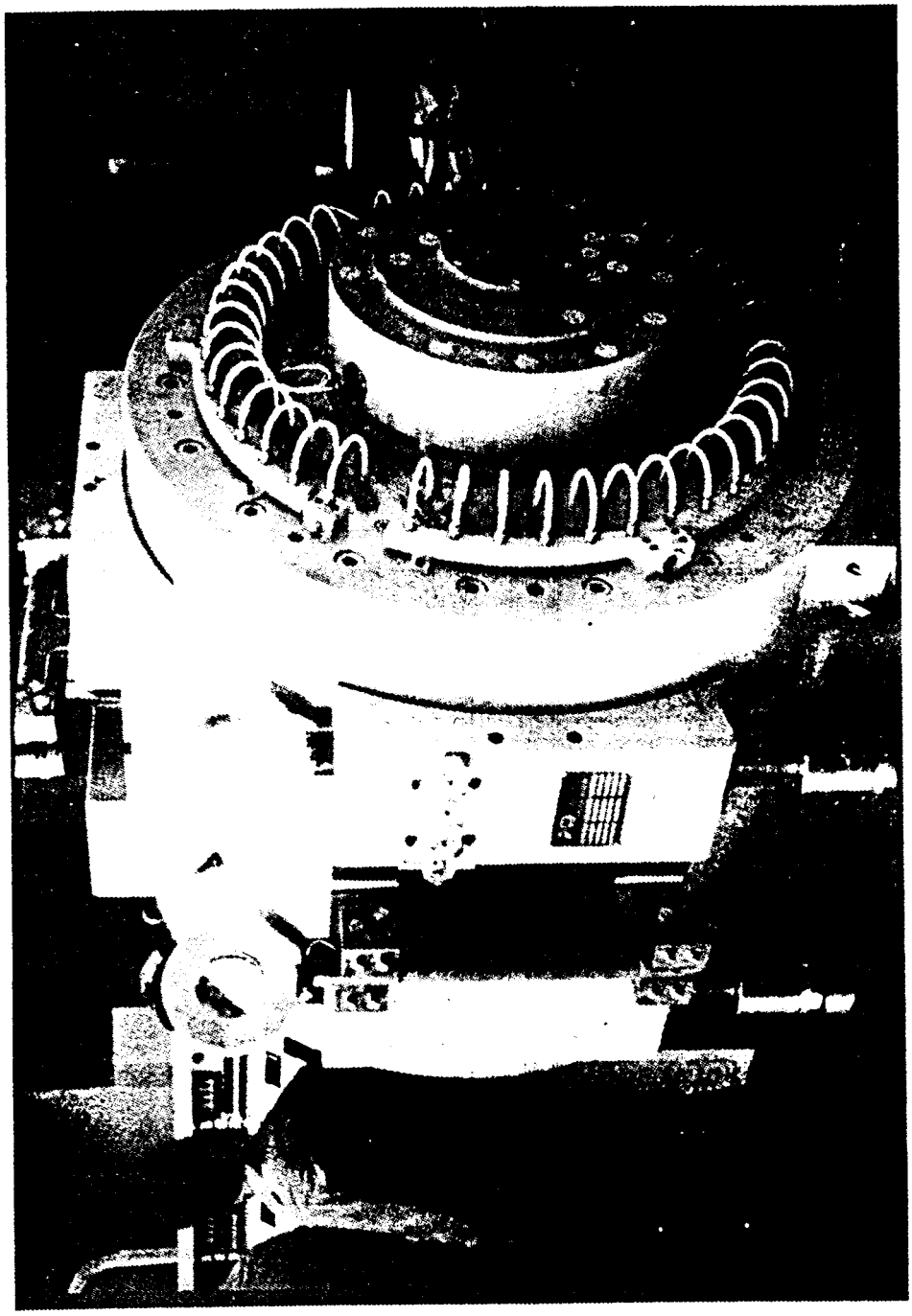

Figure 28. Balcones homopolar generator

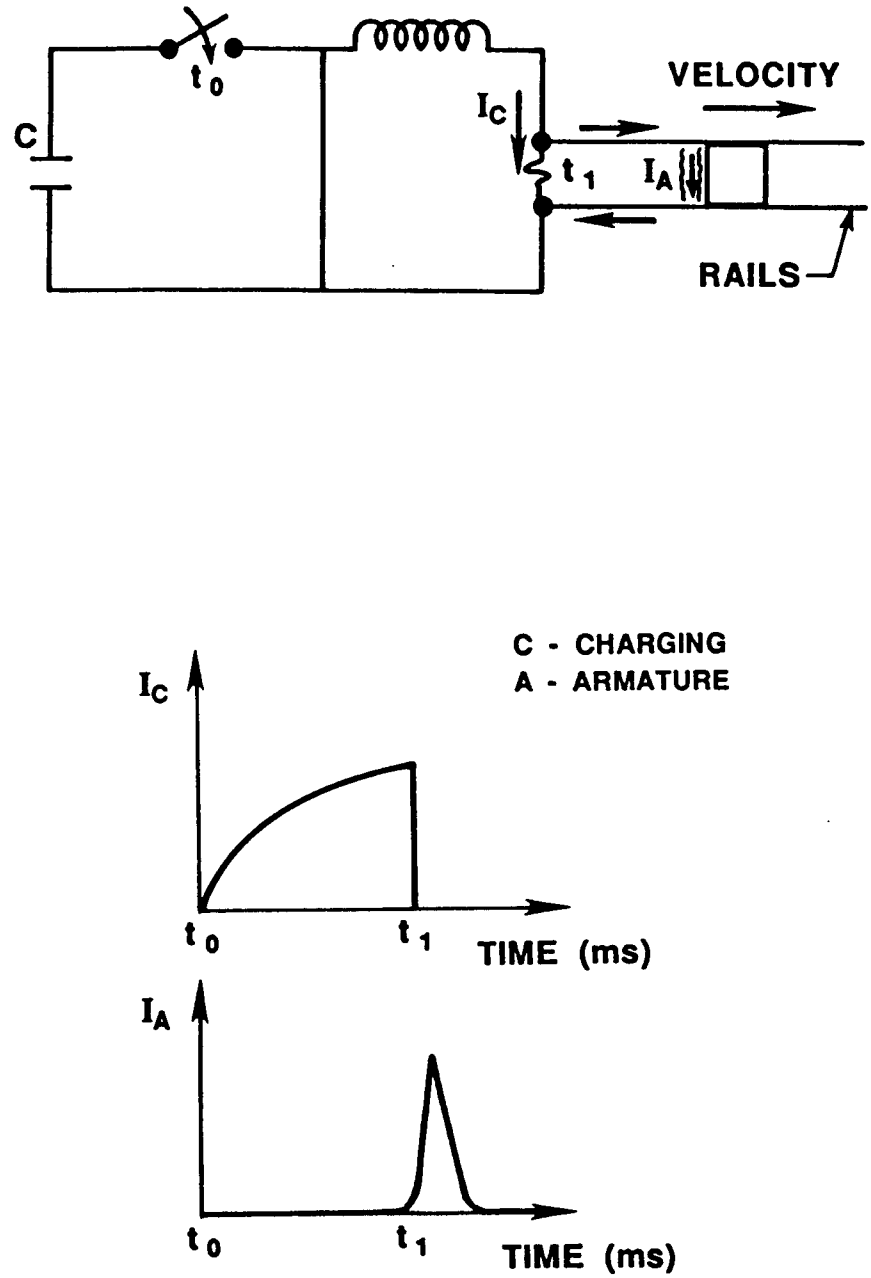

Figure 29. HPG/I circuit

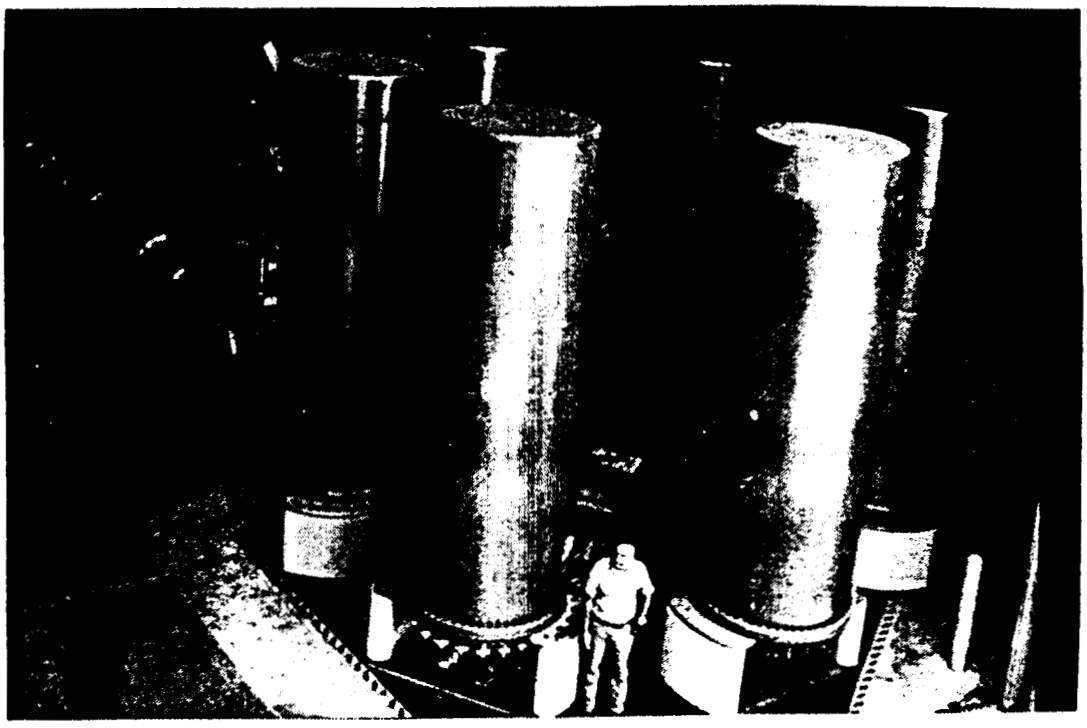

Figure 30. 60 MJ homopolar/inductor power supply at CEM-UT

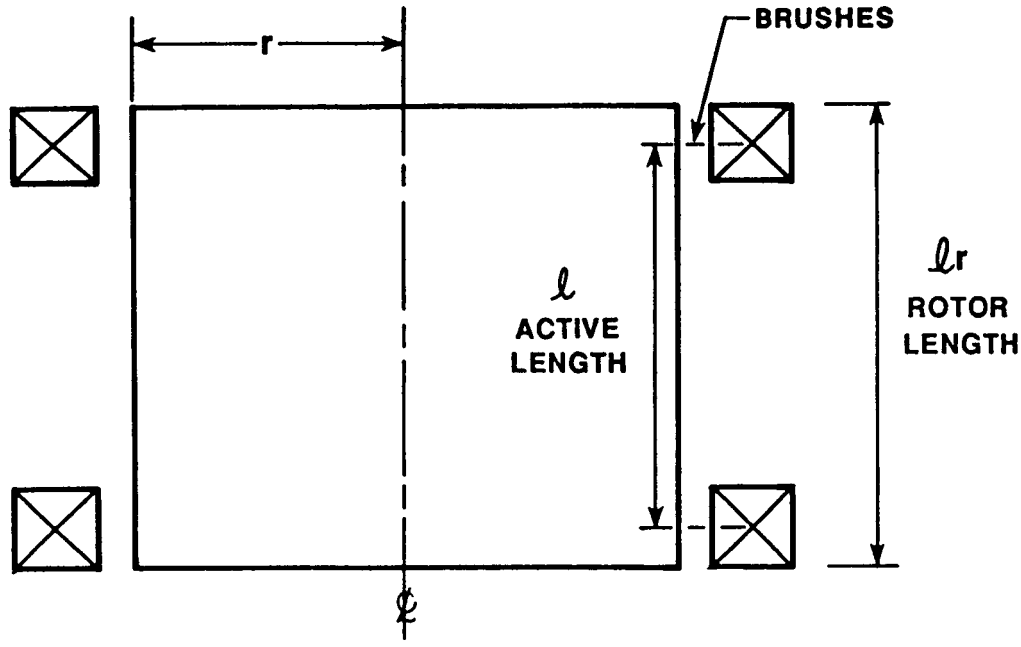

Figure 31. Preliminary design layout (HPG)

$$= 1/2(\pi r^2 \ell_r \rho) r^2$$

$$= \frac{\pi}{2} \ell_r \rho r^4$$

Then, when the angular velocity of the rotor is ω, the kinetic energy stored in the HPG is

$$KE = 1/2 J\omega^2$$

Applying the equation

$$J = \frac{\pi}{2} \ell_r \rho r^4$$

and $\omega r = 180$, which is the limiting slip speed,

$$KE = \frac{1}{2}\left(\frac{\pi}{2} \ell_r \rho r^4\right)\left(\frac{180}{r}\right)^2 = 8{,}100\ \pi \ell_r \rho r^2$$

where all dimensioned parameters are in SI units.

Since we required

$$KE = 60\ MJ = 60 \times 10^6\ J,$$

equating $8{,}100\ \pi \ell_r \rho r^2$ to 60×10^6, we have

$$\ell_r \rho r^2 = \frac{60 \times 10^6}{8{,}100\ \pi} = 2{,}358.$$

The mean distance between the brushes at the two ends of the rotor is defined as the active length = ℓ and let $\ell = 0.8\ \ell_r$.

For iron-core HPGs, most of the magnetic flux lines stay within the iron rotor, as opposed to spreading everywhere in the case of air-core machines. The flux that goes through the side and into the rotor drum must be equal to the flux that comes out from the ends of the rotor. In the case of an iron-core machine, the excitation field should be at magnetic saturation. Therefore, the sum of the rotor surface areas at the rotor ends should be equal to the area enclosed by the locus of the brushes on the rotor surface. Algebraically,

$$2(\pi r^2) = 2\pi p \ell$$

$$\rightarrow r = \ell = 0.8\ \ell_r.$$

Substituting $r = 0.8\ \ell_r$ into $\ell_r \rho r^2 = 2{,}358$, we have

$$\ell_r \rho\ (0.8\ \ell_r)^2 = 2{,}358 \rightarrow \ell_r = 0.78\ m$$
$$\ell = 0.8\ \ell_r = 0.62\ m$$
$$r = \ell = 0.62\ m$$

$$\omega_r = 180 \rightarrow \omega = \frac{180}{0.62} = 290 \text{ rad/s}$$

$$\phi = (1.6)(2\pi r \ell)\text{Wb} = 3.86 \text{ Wb}$$

$$V_o = \frac{\omega\phi}{2\pi} = \frac{290\ (3.86)}{2\pi} V = 178 \text{ V}$$

$$m = \pi r^2 \ell_r \rho = \pi\ (0.62)^2 (0.78)(7{,}860)\text{kg}$$

$$= 7{,}404 \text{ kg}$$

$$\text{Machine equivalent capacitance} = C = \frac{2W}{V^2} = \frac{2(60 \times 10^6)}{(178)^2} F = 3{,}787 \text{ F}$$

$$J = \frac{1}{2} mr^2 = \frac{1}{2} (7{,}404)(0.62)^2 \text{ kg} \cdot \text{m}^2 = 1{,}423 \text{ kg} \cdot \text{m}$$

Inductor Design

The purpose of the energy conditioning inductor is to store the electric energy supplied by the HPG, which is a relatively low voltage device, and discharge to the railgun, which requires a high voltage supply such as an inductor. The inductor should be designed to maximize the energy transfer from the HPG to the inductor, and the ohmic resistance of the inductor should be minimized to keep ohmic loss low.

Given an inductor charging circuit in which the circuit parameters for the buswork and the HPG are known, and the only unknowns are R_L and L_L, the resistance and inductance of the inductor. R_L and L_L, can be defined as the desired peak current and energy transfer efficiency. Once the current and efficiency requirements are determined, R_L and L_L can be obtained mathematically. However, R_L and L_L cannot be obtained directly from current and efficiency for the following reasons:

1. Generally, for an RLC circit as shown in figure 32A, R and L cannot explicitly be expressed (mathematically speaking) as functions if I_p, the peak current, and η, the energy transfer efficiency.

2. Even if a unique pair of R_L and L_L are found for a given i_p, η pair, a better perspective can be obtained of how I_p and η change with a change in the computed R_L and L_L. One reason to look at the effects of R_L and L_L is that the R_L and L_L computed directly from I_p and η may be a realistic solution. For example, to specify a very high η and a rather high I_p, the R_L and L_L computed from I_p and η will place the L/R ratio unrealistically high.

The methodology of inductor design is 1) investigate the parameters of space, R_L and L_L, 2) compute the I_p and η for a range of R_L and L_L, and create either contour plots or charts shown I_p and η as function of R_L and L_L for a range of R_L and L_L. CEM-UT's inductor designs efficiently locate a subspace of R_L and L_L to obtain the energy storage effectively, and with economy.

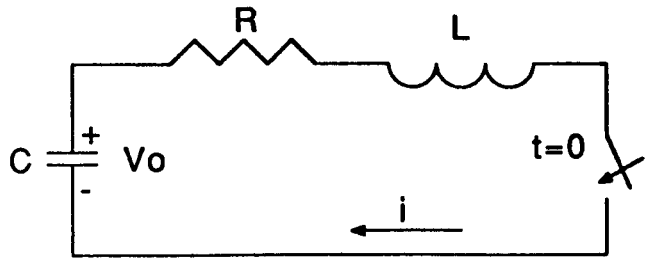

Figure 32A. RLC serial circuit

A charged HPG can be treated as a capacitor with a certain V_o, initial voltage, neglecting friction loss due to windage and bearings. Typically, HPG friction losses are very small and can be neglected for the preliminary design. By treating the HPG design mentioned earlier as a capacitor, the HPG/I charging circuit can be modeled as shown in figure 32B, where time zero is the time when the brushes are dropped and current begins flowing into the inductor.

In figure 32B, the following applies:

V_p = HPG open circuit voltage when the brushes are dropped = 178 V
C = HPG equivalent capacitance = 3,787 F
R_{HPG} = HPG internal and output bus resistance ≈ 3 μH
L_{HPG} = HPG internal and output bus resistance ≈ 200 nH
R_{brush} = HPG brush resistance ≈ 2 μH
R_{bus} = bus resistance ≈ 5 μH
L_{bus} = bus inductance ≈ 200 nH
R_{sw} = opening switch resistance ≈ 2 μH
R_{sw} = opening switch inductance ≈ 50 nH

For the RLC circuit in figure 32A, the current as a function of time can be expressed as

$$i(t) = \frac{V_o}{L\,(S_1 - S_2)} \left[e^{S_1 t} - e^{S_2 t} \right]$$

where

$$S_{1,2} = \frac{-R \pm \sqrt{R^2 - \frac{4L}{C}}}{2L},$$

Generally, this is a complex conjugate pair.

The time of current peak, t_p, can be expressed as

$$t_p = \frac{1}{S_2 - S_1} \, LN \left(\frac{S_1}{S_2} \right)$$

the current, I_p, is

$$I_p = \frac{V_o}{L(S_1 - S_2)} \left[e^{s_1 t_p} - e^{S_2 t_p} \right]$$

the transfer efficiency, η, is

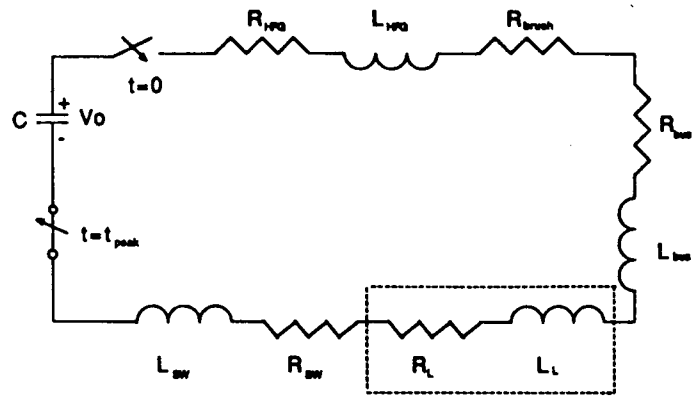

Figure 32B. HPG/I charging circuit

$$\eta = \frac{L_L I_p^2}{C V_o^2}$$

The above equations apply to underdamp, overdamp, and critically damped cases.

The equivalent RLC circuit for figure 32B has the values

$$C = 3{,}787 \text{ F},$$

$$R = 12 \ \mu\Omega + R_L,$$

$$L = 450 \text{ nH, and}$$

$$V_o = 178 \text{ V}.$$

Using a computer code, the parameter space of R_L ranging from 2 to 100 $\mu\Omega$, and L_L ranging from 0 to 100 μH was investigated. Contour plots showing the current peak time, peak current, and energy transfer efficiency as functions of R_L and L_L were obtained. For any combination of peak current and energy transfer efficiency, the values of R_L and L_L can be obtained from the plots.

As mentioned earlier, due to the imposed acceleration limit of 10,000 g, the current in each rail pair is connected in in series, and the two serial pairs are connected in parallel, and the HPG/I module has to supply twice the peak current in each rail pair, so, the HPG/I has to supply 2.9 MA after switching loss. Based on CEM-UT's experience with opening switches, the estimated switching efficiency (in terms of energy) would be 80%. This implies inductor current will drop by 10% since energy in the inductor is proportional to the square of the current. Therefore, each HPG/I module is designed to be charged to 2.9/0.9 = 3.2 MA. The equivalent HPG/I circuit is shown in figure 32C.

From the contour plots, a combination of R_L and L_L was chosen to produce the required current. The parameters are

$$R_L = 20 \ \mu\text{H},$$

$$L_L = 30 \ \mu\text{H},$$

$$\text{peak current} = 1.54 \text{ MA},$$

$$\text{peak time} = 480 \text{ ms, and}$$

$$\text{transfer efficiency} = 60\%$$

A computer was then used to generate feasible inductor designs to match the R_L and L_L. The detailed printout of the design is attached in Appendix B. The inductor is a 4-turn aluminum coaxial inductor with a length of 16 ft (4.88 m), and an outer diameter of 11 ft (3.35 m). The R_L and L_L of the design are 31.2 and 19.6 μH respectively.

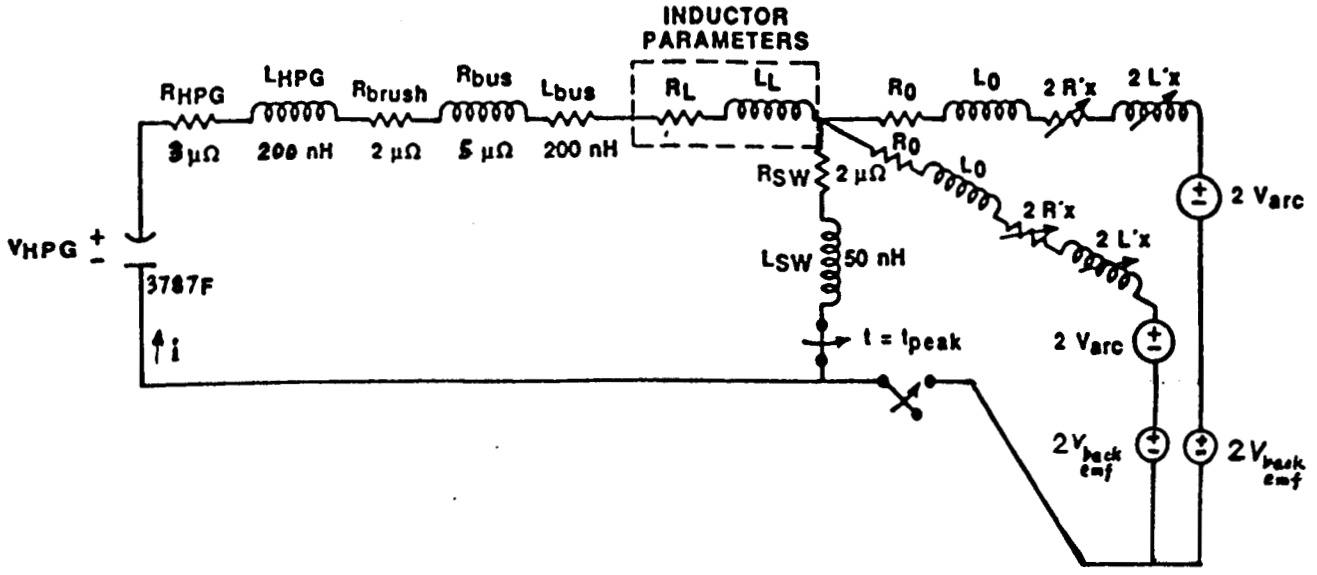

Figure 32C. Equivalent circuit of HPG/I railgun

Railgun Performance

A computer code was developed to analyze the multi-HPG/I powered multiple railgun system. The code numerically solves 30 nonlinear differential equations simultaneously. A sophisticated integrator which solves both stiff and nonstiff differential equations was used. The results from the code are listed in table 8 and plots are attached to Appendix B following the inductor design. To launch a 14 kg total mass to a velocity of 6 km/s, the gun length must be 340 m (1,115 ft). Twenty-one HPG/I modules are used, adjacent HPG/I being placed about 11 to 16 m apart along the railgun. The overall gun efficiency is 20%, which represents the kinetic energy in the projectile divided by the initial kinetic energy in the HPG. The launch time is 107 ms.

Sabot Design

The sabot is the launch vehicle which will carry the model during acceleration, and from which the model will begin its flight upon deceleration. This launch vehicle will experience high forces (981,000 N), and high currents (1.09 MA) during acceleration. In the sabot designed for the special multi-railgun proposed, the armature, is actually part of the sabot.

The suggested design of the sabot (fig. 33) is a cylindrical "can" with an interior diameter of 18 in., with four armature shoes and four trailing shoes for support. As stated earlier the sabot is the supporting structure which is used to carry the model during launch. The sabot aligns the model in the gun, prevents model contact with the rails, and possibly insulates the model from the driving forces. It is frequently necessary to use models which are structurally weak relative to the predicted launch loads. In such cases, the sabot may completely enclose the model allowing greater launch forces while compromising the release process.

The sabot design utilized here is an open support system, which maintains the launch attitude of the model while allowing an undisturbed release upon deceleration. This open support system includes the use of pins upon which the model will sit, utilizing the forces of acceleration to pin the model to the rear wall of the sabot. The length of the sabot may range from 0.6 to 1.0 m.

A long cylindrical projectile (sabot) will be greatly stressed during high acceleration. The forces will be more easily managed by using a pull method of acceleration, therefore, it is proposed that the front shoes of the sabot, riding on the set of four rails, will be the plasma armature shoes providing the Lorentz forces for acceleration at the front of the sabot. This method of "tractor pulling" will place the sabot in tension during launch which is easier to manage than compression loading. However, during deceleration, compression stress will occur which the sabot design must accommodate, or the resulting collapse could endanger the railgun, and launch.

Table 8: Computed Railgun Performance

HPG/I rise time = 480 ms
HPG/I #1 and #2 discharged simultaneously at time zero

	Time since 1st HPG/I discharged [ms]	Armature Displacement [meter]	Armature Velocity [km/s]
HPG/I #3 discharged	20.8	16.2	1.33
HPG/I #4 discharged	30.3	32.1	1.90
HPG/I #5 discharged	38.4	49.0	2.31
HPG/I #6 discharged	44.5	64.7	2.65
HPG/I #7 discharged	50.0	80.3	2.97
HPG/I #8 discharged	55.3	96.7	3.25
HPG/I #9 discharged	60.0	112.8	3.52
HPG/I #10 discharged	65.0	131.1	3.77
HPG/I #11 discharged	69.5	148.7	4.01
HPG/I #12 discharged	73.8	166.3	4.24
HPG/I #13 discharged	78.0	184.9	4.46
HPG/I #14 discharged	82.0	203.2	4.68
HPG/I #15 discharged	85.8	221.2	4.89
HPG/I #16 discharged	89.3	238.7	5.08
HPG/I #17 discharged	92.8	256.9	5.27
HPG/I #18 discharged	96.0	274.4	5.46
HPG/I #19 discharged	99.8	295.2	5.64
HPG/I #20 discharged	103.0	313.9	5.82
HPG/I #21 discharged	106.5	334.6	5.99
	107.0	337.6	6.01

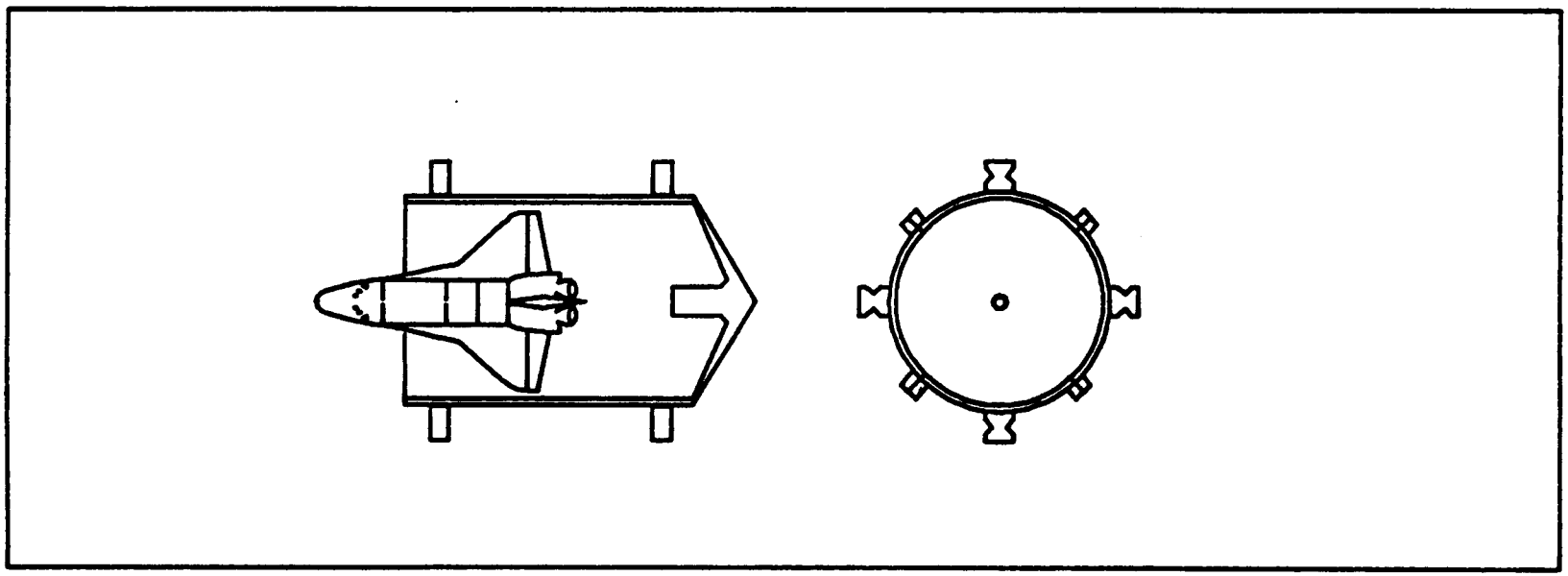

Figure 33. Proposed sabot configuration

One of the major problems in designing the sabot, and the model, is providing the strength necessary to withstand the launch loads. The customary procedure is to first calculate the constant acceleration factor in the gun (ideal operation) which would give the desired velocity, given the length of the launch tube. The appropriate equation is:

$$A = \frac{V^2}{2L}$$

where

A = acceleration constant
V = desired velocity
L = length of the launch tube (railgun)

A factor which represents the ratio of peak acceleration to this constant acceleration is then applied to estimate the maximum acceleration. Thus knowing the peak acceleration, a stress analysis is applied to critical sections of the sabot. It is assumed that the load across any section is that required to accelerate all the mass ahead of that section. Therefore, the stress analysis is fundamentally treated as a static loading. Dynamic effects are very difficult to estimate and so are not usually considered in the initial design.

Plasma Bearings

There are significant problems in maintaining the electrical contact between the armature and the rails at 6 km/s. Brushes vaporize as the current passes through the armature; the current is then carried by a plasma. The rails and insulating walls of the gun immediately behind the sabot must confine the high pressure plasma as it accelerates forward due to the Lorentz forces applied through the armature and plasma.

The accelerating plasma-armature occupies a volume in the immediate region between the rails and requires plasma confining walls if the projectile is to be accelerated. Continuous walls for each of the rails can be formed by the shoe to contain the transverse forces of a high pressure plasma armature. A moving cavity is formed in the shoes of the sabot. This cavity then contains the plasma as illustrated (fig. 34). If deliberate, controlled leak is allowed through a labyrinth seal, a plasma bearing can be formed to reduce the shoe and rail wear. This is an effective way to control the plasma leaking around to the front of the projectile, retarding the acceleration.

The hot gases vented behind the sabot, through grooves in the shoes, also provide a potential path for a shorting arc between the rails. The size of the rear grooves can be enlarged to increase the venting of electrically neutral gases and any ionized particles whose kinetic energy is high enough to escape from the magnetic confinement within the cavity. This enlargement enables any vented gas to expand behind the sabot. This expansion and the associated cooling of the exhaust gases will reduce the ionization and lower the conductivity of the gases. The reduction in conductivity will decrease the probability of an arc across the rail gap.

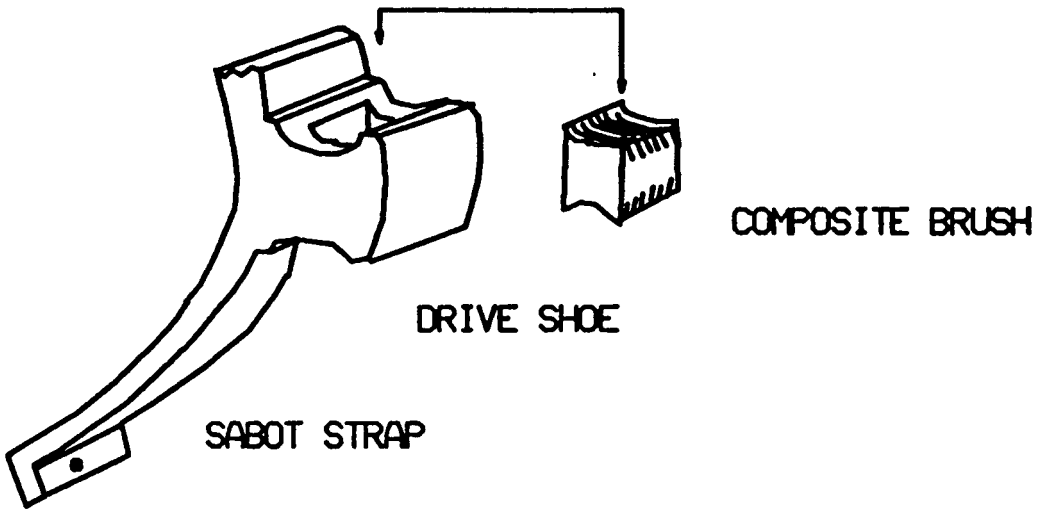

Figure 34. Drive armature

To prevent pressure against the top and bottom faces of the armature shoes from splitting or flexing during the launch, 2 mm thick Kevlar®, 49 winding, 13 mm wide, can be machine wound around the segments of the armature (fig. 35), using araldite epoxy as the adhesive. This Kevlar® winding is considered in the design of the shoes, and therefore does not detract from the performance of the sabot.

Armature Consideration

For plasma generation on the armature, a special sintered matrix brush construction is proposed to initiate and maintain the armature current throughout the launch. The requirements for high speed brush operation followed by plasma conduction are as follows:

1) Sufficient contact should be made between rail and armature to conduct the current necessary to produce the driving force.

2) The arrangement should have many good contacts, wiping between rails throughout the launch.

3) The contacts should do a minimum amount of damage to the rails while conducting current.

4) The brush configuration should be configured to support plasma and not affected by the 14,000 psi plasma pressure or the pressure of the electric field, while offering the least amount of resistance to the current flow which would result in heating.

5) The melting point of the brush material should be high so as not to boil away and short the rails during the next launch.

Although these are formidable requirements, one engineering solution would use a sintered metal, composite brush construction. The armature will have compliant members and the magnetic pressure will help feed new contacts toward the rail. The tungsten wires are short nubs sticking from the sintered aluminum contact. The tungsten is heated to boil the aluminum between the fibers to dissipate large amounts of energy.

Finally the unsupported tungsten wires and new fibers are fed into the contact surface by the compliance of the contact finger. Once all the stroke of the compliant members is used, aluminum vapor provides the conducting path.

New armatures would be installed and aligned to the sabot prior to launch. The brushes, conductors, and alignment shims would be discarded as expendable items after deceleration of the sabot. Another portion of the projectile that will wear and need to be replaced are the shoes that guide the sabot along the rails.

A similar support system as the main armature drive of the sabot is used to launch stabilize the back of the sabot. This can be accomplished by using electrically isolated guides in place of the brushes. Because current sharing can

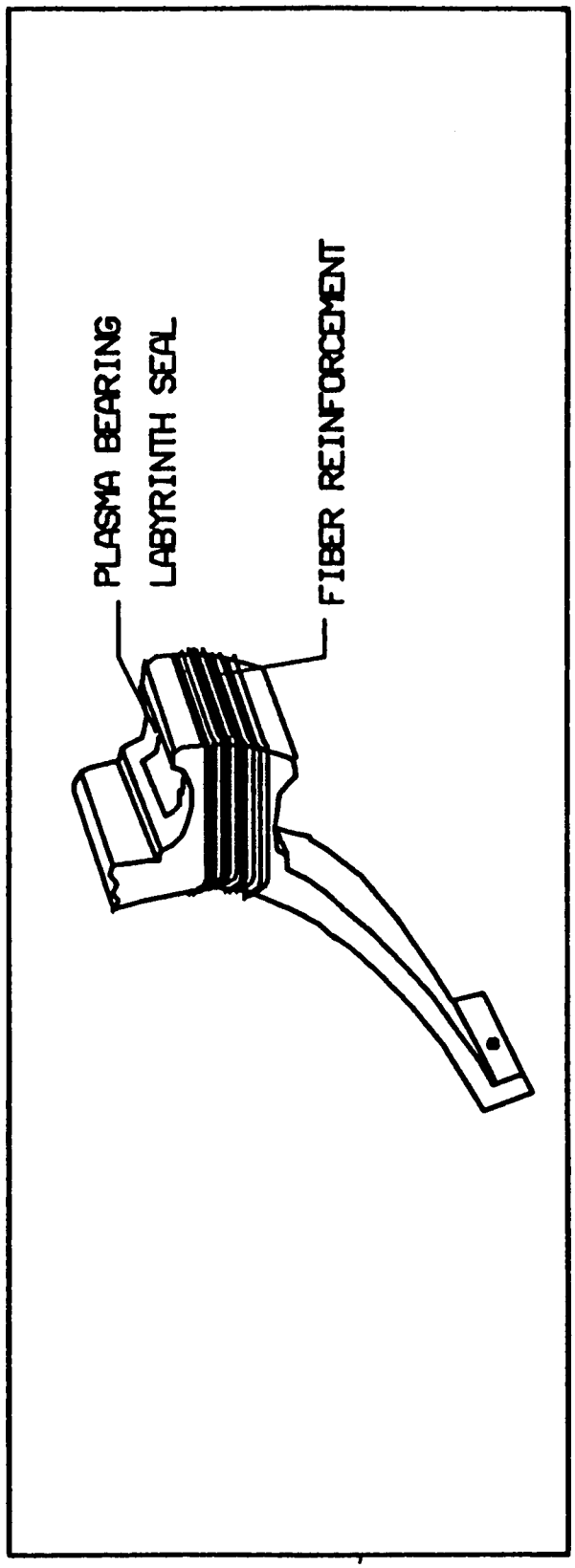

Figure 35. Armature re-enforcement

be a problem for multiple brush rail systems (fig. 36), the back graphite shoes will serve only to stabilize the sabot. These parts would also be removed from the sabot and replaced for the next launch. All of these mechanisms can be tested at CEM-UT prior to commitment.

Maintenance

One disadvantage of the conventional railgun concept is the arc damage caused to the rails during firing. This effect is characterized by high metal spots and pitting on the rails which causes interference for the sabot during the next launch. The rail sets can be processed by a honing fixture to clean away and remove all high spots so the next projectile can slide easily during firing. This process can take place between each launch. Instrumentation on-board the self propelled hone will provide a quality audit of the launch system.

Model Design

In a railgun, current flows through a discrete armature, resulting in no ohmic heating of the model. However, the sabot transmits the accelerating forces to the model, resulting in high compressive and/or shear stresses on the model.

Design considerations of the model, and instrumentation are discussed in the section entitled "Instrumentation" described later in this study.

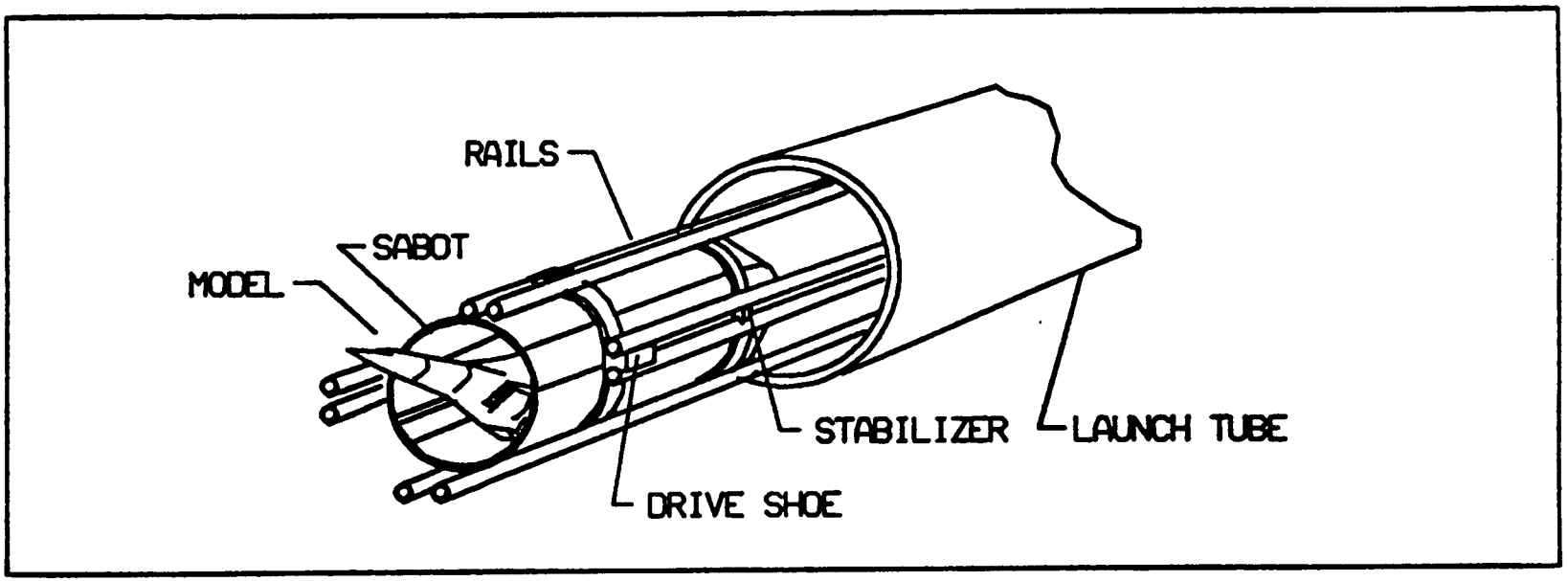

Figure 36. Multi-railgun configuration

Electromagnetic Launch Model Electronics

During the conversion of electrical energy in the launch tube to kinetic energy in the flying model, electromagnetic waves are produced which will significantly affect the on-board electronics of the model. In a railgun the plasma arc can be detrimental to electronics; and in the coil gun, the changing magnetic field (B-dot) sweeping through the electronics acts as a random voltage source.

Digital electronics makes use of a bus structure for the transmission of data to addressed locations in memory, to receive instructions or store information. The bus may contain 16 to 72 parallel conductors, traveling the entire electronic system. Bus structured sensors can reside on a bus for fast access and storage of data. Depending on the layout and complexity of the electronics used in the flight instruments, a bus can be 20 m long or more. This long bus, even though it may be folded, and many of the lines arranged in a parallel fashion, will act as an antenna, or search coil, in an EML field.

The rising and falling electric fields in the EML are necessarily large. Because of this, another element which is sensitive to the EML field is the antenna required to transmit data from the discrete model during flight (which is a good argument for infrared data transmission). The effect of this field on the model electronics is a major concern for a successful launch.

To provide hardened electronics for models in the EML environment, consider the following critical cases:

- the model is being accelerated, yet slipping backward slightly through an accelerating magnetic wave
- the model is separating from the sabot in a decelerating magnetic wave
- arcing contacts in armatures & switches
- self excited fields associated with megamp currents

In the first case, the electric field of a coaxial accelerator is produced by currents in each two adjacent coils, which carry voltages of the same frequencies but with a phase lead of 60°. The antenna is oriented in the same axis as the launch progresses backward in the field from wave to wave. The antenna (and bus structure) is subjected to a maximum, minimum, and reverse maximum flux field as it slips in the rapidly increasing frequency wave. As the model and sabot slip in the field, the direction of this field changes 180°. During a launch of 61 ms with 740 waves and a 2% slip, the electronic package will encounter 15 reversals of the wave that has a frequency range from 25 to 2,000 Hz. The actual frequency the model sees, because it is traveling with the wave, is only 0.5 to 40 Hz. It is the magnitude of the field, how the antenna length fits within the field, and the sweep, that is significant. The $d\Phi/dt$ is on the order of $2T/2 \times 10^{-6}$s or 1×10^{6} T/s.

The above example assumes a frequency of 2,000 Hz as a worse case. The proposed coaxial launcher requires a frequency of less than 500 Hz. In the second case the model is flying through a magnetic field that must terminate abruptly at the end of the deceleration region. However, in the earlier stages of separation, the model is traveling very close to the velocity of the decelerating sabot, so the $d\Phi/dt$ will be less than the slip through the highest launch frequency. This means less than 100 V could be expected.

For a model exiting a railgun muzzle, the case is almost the same with the plasma velocity very close to the velocity of the model. Therefore, $d\Phi/dt$ would produce an induced voltage in the 100 V range.

Only the first two cases produce significant voltages that are beyond the working voltage of the logic device technology. We would like to use complimentary metal, oxide, silicon (CMOS), but can be easily managed with bipolar devices. Although some protection will be offered by the sabot, instrument package, and the filler material of the model, these types of shielding will dissipate the magnetic energy as heat. Alternate methods should be considered that will build protection into the circuits with both shielding, and short circuit methods (while in the launch phase) to shunt the rising and falling voltage on the bus structure and antenna.

Assuming that functional on-board electronics would make an important contribution by collecting parametric data in the free-flying model, there are important design considerations. Multiple shielding of the sabot using laminated dissimilar metals would produce eddy currents which would diminish the magnetic field, but at the cost of dead launch weight. Similar shielding of the electronics directly inside the model would have the same effect; however, this shielding would produce heat, affecting the electronic systems, as well as affecting other parameters of the model such as skin temperature and strength of the air frame.

Another important factor in providing protection for electronic signals is in the basic architecture or building method of the circuit. Because of ongoing development in electronic packaging, methods of manufacture are now available which provide a high degree of shielding from these types of fields. It is interesting to note that the design rules for protecting the bus structures, and devices from electromagnetic interference (EMI) and electromagnetic pulse radiation (EMR) are the same as encountered during EML. Even though the launch fields are orders of magnitude greater in intensity than are experienced in GHz circuitry, the frequency is three orders of magnitude lower, so, the same solutions become relevant.

Data Acquisition

To illustrate a solution for an instrument package on-board scale models in the EML environment, techniques useful for high performance weapons can be reconfigured to tolerate the electromagnetic fields of the launcher. Consider the requirements for a hypersonic model weighing 10 kg to be accelerated at a constant acceleration, 10,000 gees, to a velocity of 6 km/s. After launch, this model will fly along in a 1,000 ft flight chamber which is conditioned to emulate the environment of the upper atmospheric climb, high altitude engine flow and burn, and reentry conditions.

The flight time will be on the order of 100 ms. Instrumentation is needed during this flight for the following parameters: gravity (6 axes), pressure (6 points), temperature (6 points), attitude (3 axes), radiation (4 points), and frame flexure (2 points). To accomplish this task with conventional analog multiplexing, A/D, S/H, with memory storage, this would require approximately 15 ms/data word or 6 words of data could be collected during the flight. This would not represent a viable method of data acquisition for such a time intensive event.

It is common knowledge that hypersonic models sometimes experience from 4 to 40 oscillations during a single flight, experience various pressures on flight surfaces, and undergo temperature changes. Six data words will not be adequate to properly define the parametric growth. A new method of data acquisition must be devised to take full advantage of the hypersonic facility. This method should provide the data in digital form, bus compatible so that the data can be written directly to the on-board memory during an address and write cycle with a single enable of a sensor. This information must also be simultaneously transmitted for data retrieval, in case of destruction of the model during flight (when the soft catch fails). Parallel processors and 3-dimensional computers with improved speed can be used for data acquisition requirements. The more data acquired from a flight, the more effective the development work of the hypersonic real-gas facility.

The process for developing bus configured sensors is as follows:

1. Select operating limits and bracket the range of interest for each of the parameters.

2. Establish mathematical models for each device.

3. Layout the physical devices based on researched performance of available materials.

4. Manufacture, utilizing quick turn CAM system.

5. Provide EMI, EMR shielding as an integral part of the circuit construction.

6. Test sensors for performance (bench test).

It should be noted that once the sensors have been developed, manufactured, and calibrated, each device can be used repeatedly for new instrument packages. Table 9 gives a listing of parameters which could require observation during the model launch and flight, as well as a discussion of the types of sensors and how they could be used in the research facility.

As an example of a device to measure acceleration, consider a physical design where a series of small cantilever beams are arranged to form switches. Each switch can be designed (fig. 37) to close under a different G-load in one axis. These devices, developed by computer aided design (CAD), may be arranged as a cluster of switches (figure 38) each sensitive to a different gravity. Fabrication is by simply dispensing materials (polymer) with an X-Y plotter in the same operation as the printed circuit board (PCB) is constructed.

Table 9. Instrumentation requirements

Parameter	Condition	Range
Acceleration	Launch Free-flight	10 to 30 k gees -300 to -.01
Pressure	Ambient Dynamic	Vacuum to 2 lb/ft^2 0.5 to 1,200 lb/ft^2
Heating range	Maximum Minimum	1, 2, 3, 4 W/cm^2 24 W/cm^2
Radiation Heating		8 to 78 W/cm^2
Spectral Range		0.18 to 0.5 m
Integrated Heat	Maximum	2,196 J
Magnetic Flux	Launch	1.0 T
Gyro (3 axes)		± 4°
Flexure		± 4°

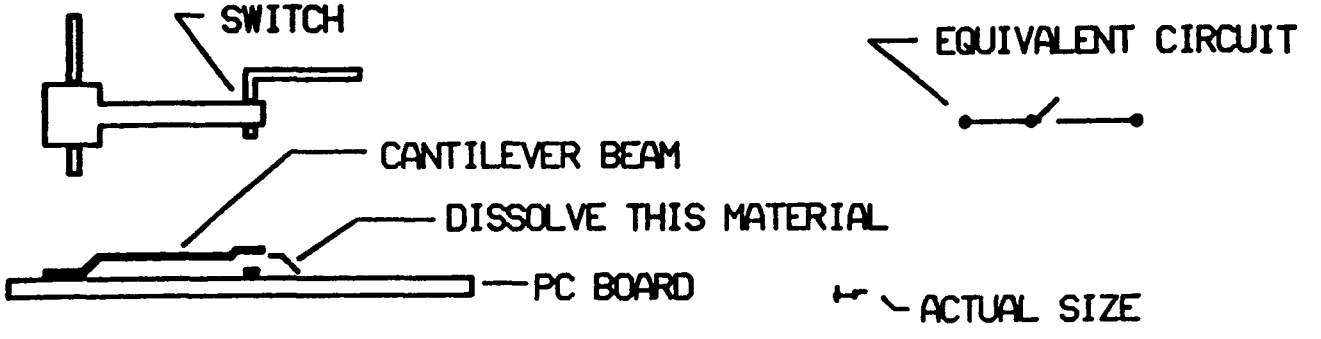

Figure 37. PC board level gravity switch

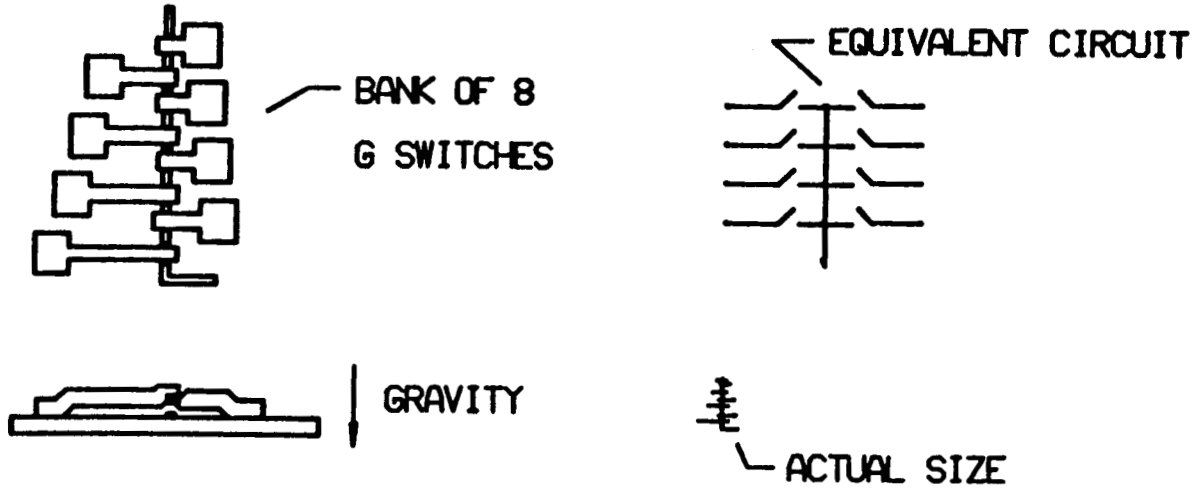

Figure 38. PC board cluster of gravity switches

A mathematical model of such a device can be expressed by the formula for a cantilever beam as follows:

$$R_2 = w$$

$$M_x = -W_x$$

$$M_{max} = -W\ell(x = 1)$$

$$Q_x = -w$$

$$f = \frac{W\ell^3(MAX)}{3EI}$$

where

ℓ = distance between supports
R = reaction
M = bending moment
W = Total distributed load

Then the force on the beam acting through the center of mass:

$$F = MA$$

Using the original criterion, the beam dimensions become as follows for the various G-loads:

By using the (typical) physical layout of table 9, the CAD database of the PC Board can be modified to allow the sensors to be fabricated at the same time the PC Board is formed. The result is an electronic package with integrated electromechanical sensors that began as a requirement, was developed as a computer design and simulation of a circuit and physical sensor, and ended as a computer formed (constructed) electronic package, complete with sensors. After the chips (semi-conductor microcircuits) are placed, the circuit with sensors can be tested. For instance, all the gravity switches of an instrument package can be pre-flight tested and data-logged while being spun in a centrifuge. This data as well as pressure pot and temperature cycle, is recorded through the radio frequency link (RF) and depos-ited as a file in a personal computer. In this way, the data obtained from sensor read-out during a flight can be interpolated using pre-flight and post-flight sensor evaluation. An illustration of a circuit containing both multiplex circuit and sen-sors on the PC Board is in figure 39.

The procedure for building devices of this type is to place a board on an X-Y plotter, plot the first layer with conductive material, bake for 5 min, plot spacers, bake, plot second layer conductor, which includes the cantilever beams, and bake. After bake (cure), the spacer material is dissolved away, leaving the micro-scale beams extended above the lower contact. The physical dimensions of the sensor elements are formed under computer control and therefore, the characteristics are

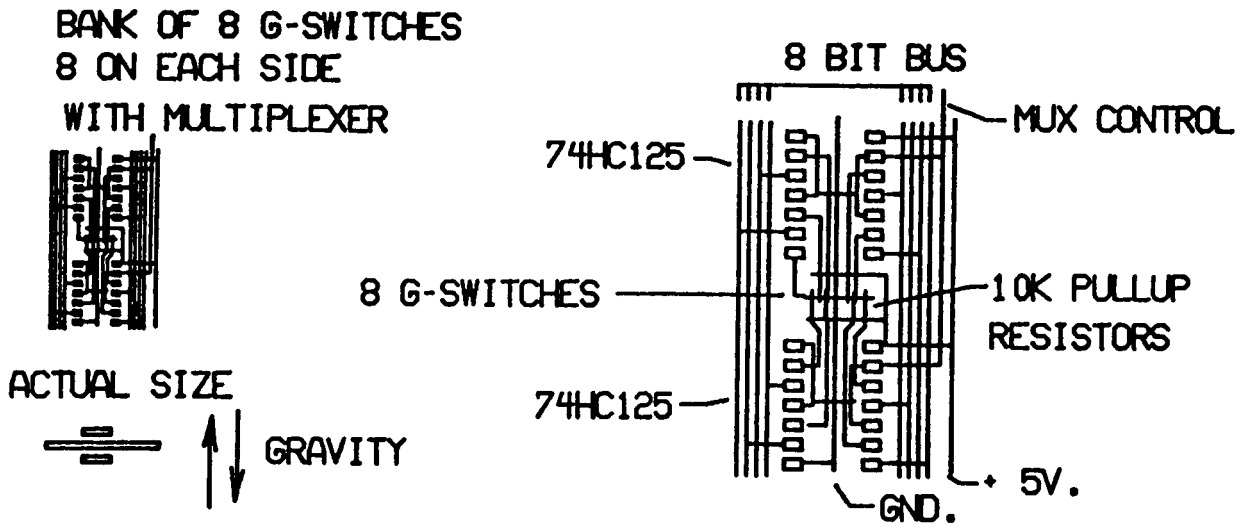

Figure 39. PC Board gravity switch

C-2

reproducable. It should be noted that the sensor fabrication takes place as a part of the complete board fabrication which is together completed in less than 1 hr. This reduces the cost of model instrumentation to a range of $300 to $3,000.

The database describing this sensor can be used with other sensing elements in combination with an on-board computer. In circuit simulation form, adjustments can be made and the results used to modify the design and the end product (data acquisition package). The fine structure of the G-switches requires little real estate compared to the size of the bus structure and gate. The status of any G-switches bank can be written directly to the memory through the bus by simply enabling the tri-state gates. This can be accomplished in 12 ns with HCMOS. A conservative, 15 ns window (clock rate) should be used.

This switch is designed to measure forces in a specified range. Other ranges of interest (finer or wider) could be bracketed by another group of redesigned switches to cover different ranges. A combination of wide and narrow range switches would produce resolution within the range of interest. This can be done by modifying the data base of figure 39. Figure 40 describes a method of folding the board to measure gravity in all six axes of interest.

Should positive and negative gravity measurements be of interest, the gravity sensors must be read out in each axis. This can be accomplished by reorientating the package so the centrifuge applies gravity in all axes of interest during calibration. This type sensor is little affected by forces that are applied normal to the designed direction. They can, however, be damaged by excessive loads applied 180° to the direction of design, resulting in permanently bent beams, away from the switch direction. Additional sensors were developed and can be found in Appendix C.

Circuit Noise Immunity

One of the primary reasons for using conductive polymer, other than ruggedness and the ability to form these circuits easily from the same CAD, is the noise immunity resulting from a shielded communication. The proposed architecture allows the ground shield for each individual line to totally surround the line for the length of the run (fig. 41). This feature will provide noise immunity for the circuit during the electromagnetic launch and also prevent noise injection by adjacent lines in the acquisition system. It should also be noted that these circuit structures are resilient and therefore can tolerate the high decelerations anticipated after flight. The conductive material will be eventually formulated to emulate the high temperature superconducting materials currently under development and this will result in higher speed data acquisition, which will virtually extend the length of the flight chamber by producing more data/meter of flight.

A number of instrumentation packages could be tailored to fit general or specific missions. These packages could be stock piled, awaiting a final model design. A practical memory size would be 64,000 words, however this could easily be pushed up to 256,000. Two Ni-Cad batteries could be charged prior to calibration or flight and used as a regulated primary power source.

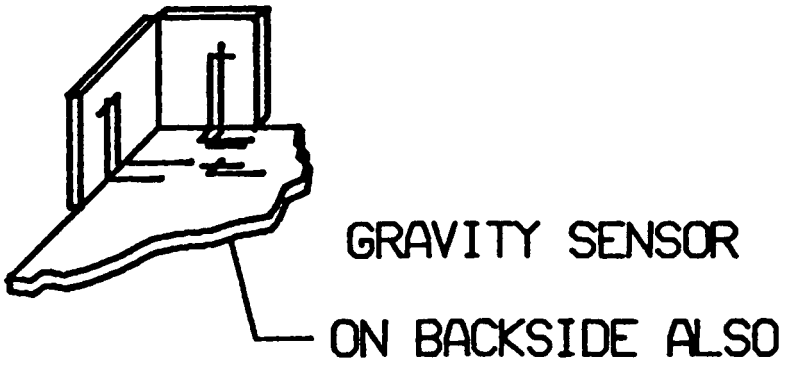

Figure 40. Folded PC board provides six axis gravity instrument

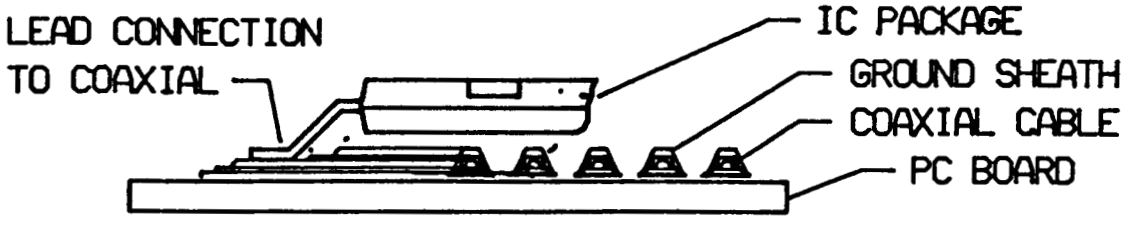

Figure 41. Coaxial shielding bus and PC board interconnection system

A personal computer can be used to perform the sensor set-up, calibration and retrieval. This system was actually configured and tested to prove the data acquisition concept (figs. 42 to 45). Data was loaded in the memory device at a clock rate of 400 MHz, stored overnight, and downloaded to the IBM-PC at 1200 baud.

Soft Model Catches

Of importance, is the recovery of the hypersonic models, intact and undamaged after flight. Projectiles of this mass and possessing this kinetic energy will readily serve as a lethal weapon, capable of piercing the armor of a tank. A soft catch is desirable to provide information on surface damage and for flight recorder readout by cable to the computer. While data can be unloaded during the flight by infrared transmission as well as radio frequency (RF), significantly more data can be obtained if the models could be caught softly. For instance, surface ablation, engine orifice erosion, and even the fuel consumption (for powered flight) and weight loss could be determined and compared with the flight effects and conditions of other models. The onboard sensors could be read out in a retest for postflight calibration. This would be a check of the inflight data. Minor changes could be made to the airframe and the model could be reflown to obtain exact flight data.

A possible method of soft catch would be to impact after the flight, into several large, thin, plastic diaphragms (polyethylene) and then into a bed of very low density expanded polystyrene beads (coffee cup starting material). The plastic diaphragms would tend to contain the beads in the catch zone and reduce the outgasing into the flight chamber.

From impact theory of hypervelocity projectiles, it can be shown that upon impact, the material being impacted, liquifies due to energy transfer. The most convenient material to liquify and become a part of the model, would also be something that would adhere to the model. This would quench the kinetic energy while becoming an attachment to the model. The reason that styrofoam, or melted styrofoam is suggested, is because a simple series of dips in trichlorethlyene (TCE) or methylethylketone (MEK) would dissolve away the styrene and render the model clean and ready quickly for data download, recalibration, and eventually a reflight.

There will be a race after a flight, to unload the data because battery life for the onboard computer system is limited. This is one suggestion, a different density foam system [9] has also been used although this material will require more maintenance and would not be manageable for a fast turn launch and catch system. The beads could be vacuumed from the catch chamber between flights, the model located (there's a radio signal) and then TCE dipped. After the plastic diaphragms are replaced or repaired, the beads could be filtered and reinstalled in the chamber. Additional beads could be added topping off and replacing the beads that were melted by the model. It is estimated that a travel through 20 m (50 ft) of beads would be more than adequate to soft catch even the most energetic models.

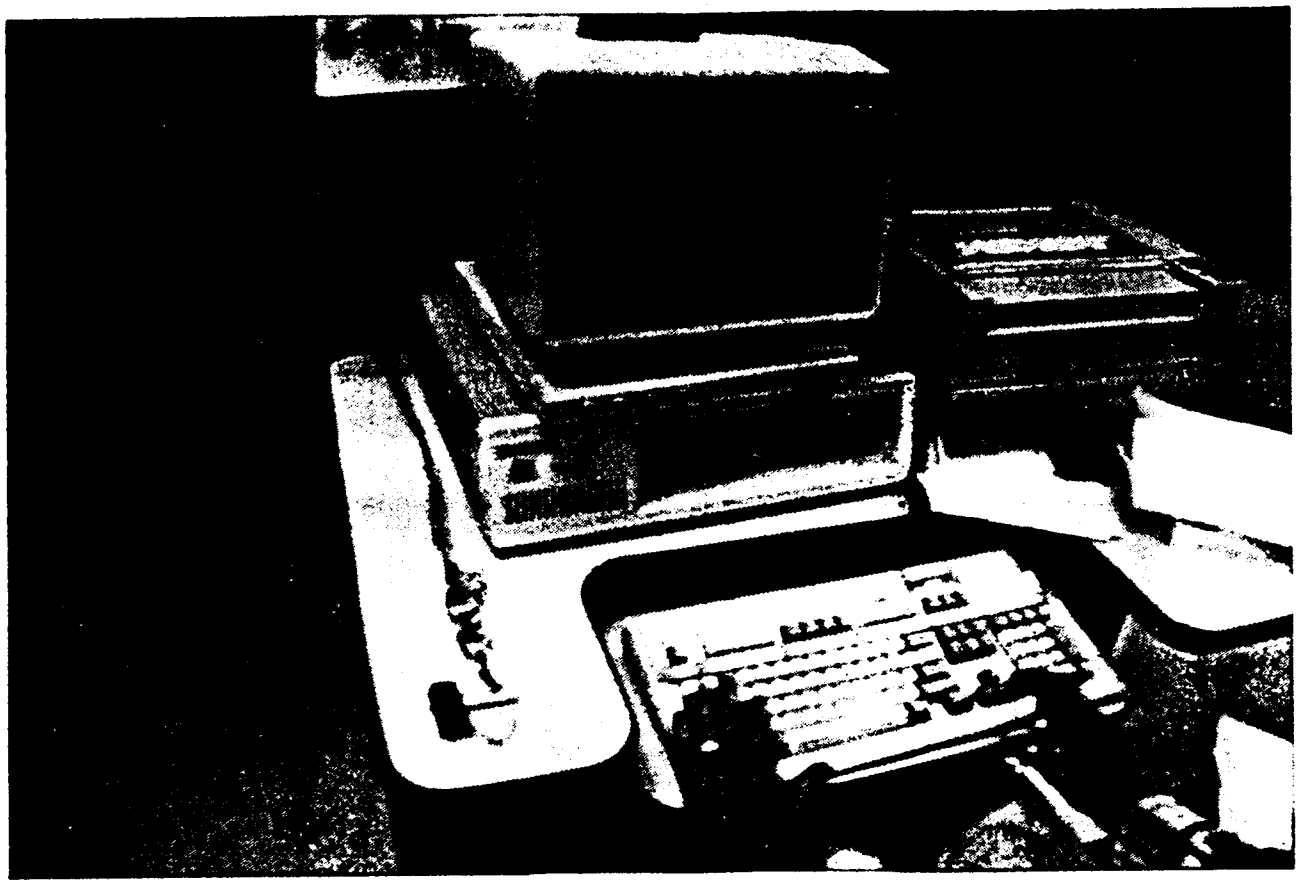

Figure 42. Data acquisition system

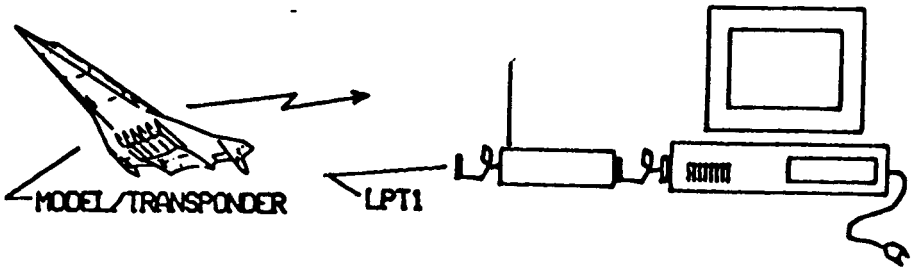

Figure 43. Up/down loading

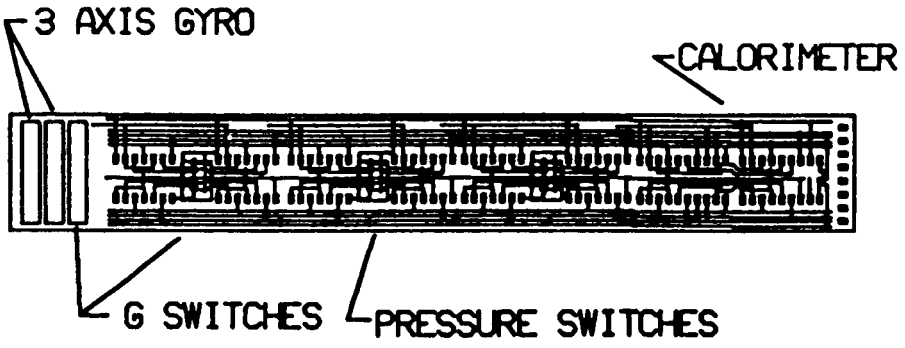

Figure 44. Sensor stick

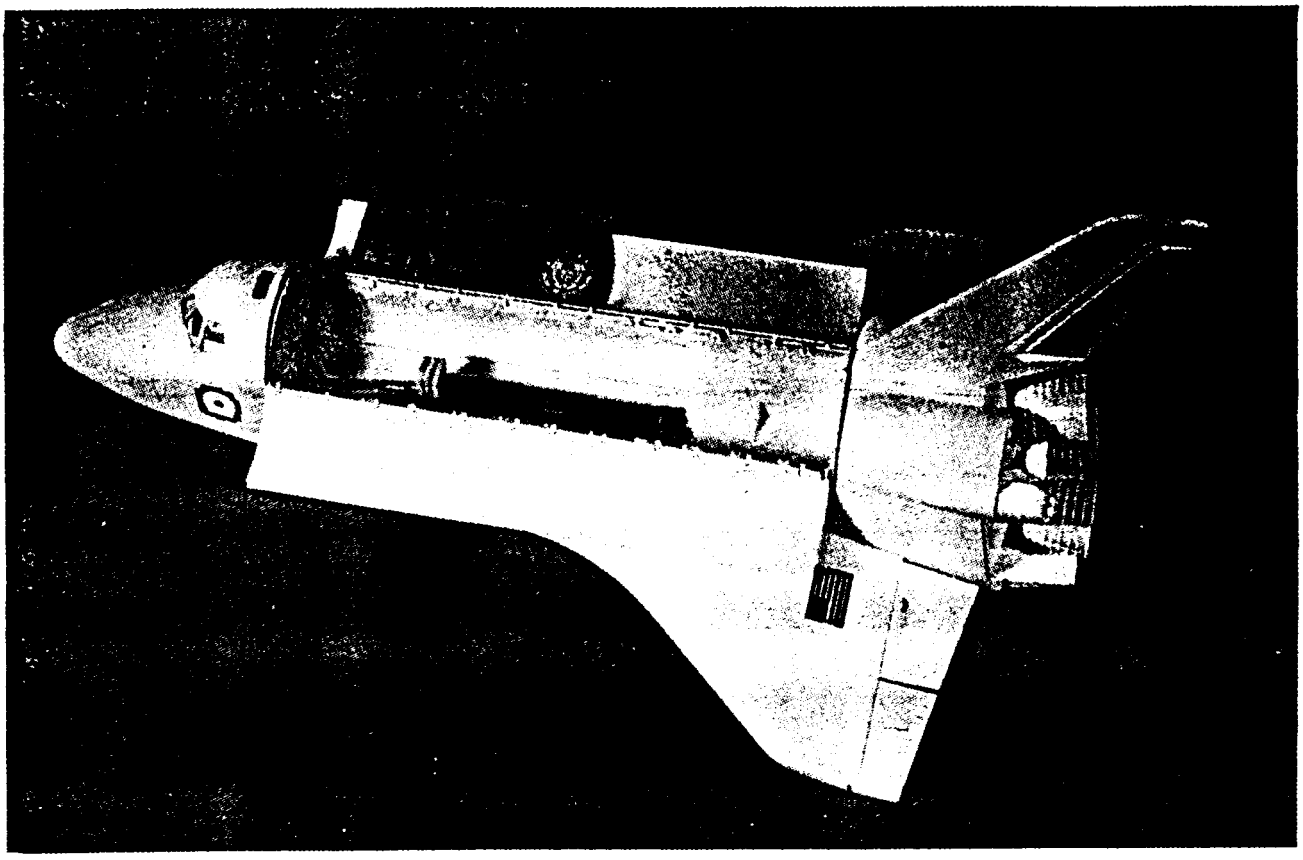

Figure 45. Sensor stick in 17 in. shuttle model

COMPARISON

Both the railgun and the induction accelerator will perform well as the launch system for a hypersonic real-gas ballistic flight facility. It is the understanding at CEM-UT, that the launch system would be useful for aerospace plane transition studies with large scale flying models for computer model validation. If this system could be placed on stream in the near term, the launch and flight facility might hasten the development of next generation flight vehicles. Additionally, it might reduce the overall development costs for such a project. It is with these goals in mind that the selection of a launch system might be made by NASA.

Railgun

For instance, with a railgun system, the homopolar generators (power supplies) are basically off-the-shelf with an 18 to 20 month delivery. Each component of the HPG/I is fully tested and is in use on a daily basis at CEM-UT. This system could be pressed into service, ready for commission in approximately 24 months. Although larger payloads than 10 kg could be accommodated, the rail launch system with solid armatures have only been demonstrated in the 2 km/s regime. The hybrid that was addressed earlier in this report could make the 11 km/s goal. This type launcher will also require more maintenance with down time for periodic exchange of rail sections. It is estimated that the beginning rails will require section exchanges for overhaul with each 100 launches. Rail dressing and inspection should be performed between each launch but this process need not extend launch cycle times. These constraints may be acceptable for a launch system that can be quickly composed of off-the-shelf, proven components. Homopolar generators have been in continuous service for over 35 years, seam-welding pipe. The cost of the rail launch system is estimated to be in the $60,000,000 range.

Induction Accelerator

Should NASA's interests and priorities be based on extended performance, in both velocity and payload, the induction accelerator would be the "system of choice" with low maintenance launch capability and could accelerate 3 kg models up to 11 km/s or 10 kg models could be accelerated to 6 km/s. Accelerating 10 kg masses to 11 km/s would be possible with future installation of additional or higher energy power supplies powering the same as-designed launcher. The cost of this launch system is estimated to be in the $47,000,000 range. Because components are not "off-the-shelf", it would require approximately 30 months to implement this system.

Because no sliding transport of current is required in the Induction Launch design, which is not the case with the Railgun, very little wear is anticipated in the launch tube, resulting in long system life. The projectile is levitated and held away from the walls throughout the launch.

The power supply requirement for the induction launcher consists of four compulsators, configured to operate in the surge mode. This machine was invented

and developed by the University of Texas, and can be used for a number of rail and induction launched systems. The proposed induction launcher, as designed, could accommodate additional power units for more robust launches, should they be needed with future research. Commercially available water wheel alternators would be rewound in the compulsator configuration to economically produce these power supplies.

Cost Summary

A summary of cost, performance, and delivery follows:

Launch Type	Cost	Performance	Construction Time
Railgun	$57.0 M	10 kg, 6 km/s	24 months
Induction	$47.5 M	10 kg, 6 km/s, (or 3 km, 11 km/s)	30 months

Instrumentation

An instrument package was designed for this program that makes use of micro-scale sensors and bus structures useful for "smart weapons". Computer aided design and manufacturing, using a personal computer, allow these packages to be quickly modified and custom manufactured for use with flight models to document flight parameters. The unit cost is believed to be between $300 and $3,000, depending on the combination and resolution expected from the instrumentation.

The manufacturing techniques suggested will allow operation of these packages in both electromagnetic environments. With the use of low cost, on-board data acquisition packages, more information can be derived from each flight, making the facility more efficient as a development tool.

Recommendation

The Center for Electromechanics recommends that this design study be followed by a more detailed engineering study of one or both of the launch systems. The result of this detailed study would produce an engineering design that could be used for preparation of a "Request for Quote". Proof of principle experiments would be performed, with at least two segments of each launch system at full scale. The inner-stage hand-off of projectile for the railgun could be demonstrated, as well as a phasing system between induction stages with multiple ac power supplies.

Both concepts require further refinement and engineering evaluation with full sized launch sections. The decoupling of rails for the rail launcher, as well as the phase matching system between induction sections, can be fully tested to the length of the two sections at designed mass. Tests will also be conducted at near terminal velocity with reduced mass. The starter sections of both systems could also be characterized by launching payloads through the first two stages. These tests and refinements of each concept would produce a high level of confidence prior to proceeding with plans for actual launcher construction.

The development of the electromagnetic launcher for use with a hypersonic real-gas facility will result in a World Class Hypersonic Flight Development Center. Economies can be realized by the technique of rapidly evaluating computer developed designs with the use of large, high mass flying scale models, launched into varied flight environments. This will allow low cost exploration of flight parameters, which can now only be analyzed by the use of space shuttle experiments.

It has been noted that, when major scientific tools become available, especially tools that reduce the cost and time for production of engineering data, new windows of opportunity open. Scientific tools, of this type, can reduce the most complex of problems into simple, yet elegant, engineering solutions. Solving hypersonic aerodynamic flight problems such as successful hypersonic laminar flow, will eventually lead to vehicles that will drastically reduce the cost of placing both man and equipment into space. From these developments, other opportunities will evolve, such as efficient intercontinental transportation. This will further enhance our transportation system as a national resource. The same type electromagnetic launch system used to study computer defined aerodynamic shapes, which are necessarily limited to relatively low acceleration, will eventually be pointed skyward for the low cost launching of cargo into low earth orbit. This will allow non-manned payloads into space as frequent as flights from a metropolitan airport. These concepts will be evolutionary, and the elecromagnetic launcher will have an important role. This hypersonic facility will be a first step in the evolution.

The Center for Electromagnetics at The University of Texas at Austin, is pleased to propose a twelve month, detailed engineering design study of one or both of the described launcher systems (railgun or coaxial). Incorporated in the engineering Design would be "proof-of-concept" experiments, which would make use of at least two of the launch segments. This would provide the empirical data necessary to specify the construction of the total system. Both concepts require further engineering study with test to refine operational performance and maintenance. It is with this additional data that a high degree of confidence can be obtained, prior to final plans leading to the construction and commission of an electromagnetic launcher for the hypersonic facility.

Cost Estimate for Launch Systems

Assumptions:

- 5% energy transfer efficiency for railgun (HPG to payload)
- 50% energy transfer efficiency for induction accelerator (compulsator to payload)
- NASA LANGLEY will supply the following:
  - foundation
  - enclosure
  - free-flight range
  - flight data instrumentation (stationary)
  - grid power

Railgun Launch System

Power Supply:

(21) - 60 MJ, HPG's at $0.02/J.....	$ 25.2M

Inductors:

(21) - 30 MJ, at $0.01/J.....	6.3M

Railgun Launcher:
(includes structure and spare parts)

1,115 ft at $10.00/ft.....	11.5M

Accessories:

(vacuum system, valves, controls, switches, and site preparation).....	12.0M
Total.....	$ 55.0M

Induction Accelerator Launch System

Power Supplies:

(4) compulsator power supplies (Task C) at $6.0M/ea.....	24.0M

or, (4) compensated, rewound water wheel alternators stressed for surge operation.....(same as above)

Drives:		
(4) at $0.5M		2.0M
Starter Coil:		
(1)		0.5M
Induction Launch Tube:		
600 ft at $15,000/ft		9.0M
Accessories:		
(vacuum systems, valves, controls, switching, site preparation)		12.0M
Total	$	47.5M

REFERENCES

[1] I. Boldea and S. A. Nasar, "Linear Motion Electromagnetic Systems", John Wiley and Sons, New York, USA, 1985.

[2] E. R. Laithwaite, "Induction Machines for Special Applications", Chemical Publishing Co. Inc., New York, 1966.

[3] T. Onuki and E. R. Laithwaite, "Optimized Design of Linear-Inductor-Motor Accelerators", Proceedings of IEEE, Volume 118, February 1971, (pp. 49-355).

[4] A. E. Fitzgerald, E. Kingsley, Jr., and A. Kusko, "Electric Machinery, the Processes, Devices, and Systems of Electromechanical Energy Conversion", Third Edition, McGraw-Hill Book Company.

[5] D. V. Richardson, "Handbook of Rotating Electric Machinery", Reston Publishing Company, Inc.

[6] P. Wildi, L. C. Elliott, and A. R. Gilmour, "Motor-Generator for the Texas Experimental Tokamak", IEEE 12th Symposium on Nuclear Energy, Austin, TX, 1979, CH 1441-5/79.

[7] R. A. Marshall and W. F. Weldon, "Analysis of Performance of Railgun Accelerators Powered by Distributed Energy Stores", 14th Pulse Power Modulator Symposium, Orlando, FL, June 3-5, 1980.

[8] B. M. Rech and R. C. Zowarka, Jr., "Design and Construction of a Two-Stage Opening Switch", IEEE 3rd Symposium on Electromagnetic Launch Technology, Austin, TX, March 1986.

[9] J. Thoman, "Railgun Materials Survey Summary and Launch Environment Simulator Description", Boeing Co., presented at Electromagnetic Launcher Association second meeting, July 9-10, 1986, General Dynamics Corporation, Pomona, CA

APPENDIX A

RISING FREQUENCY GENERATOR

As another step to improve the integrated power supply and coaxial accelerator system, the synchronous generator with constant frequency previously reported (see September 1986 Monthly Report) has been replaced by a Rising Frequency Generator (RFG). An initial design was performed in order to satisfy the requirements of the system. The resulting RFG will have the characteristics given in table A-1.

The initial frequency applied by the RFG will be 427.5 Hz, and for a drop in the peripheral speed of the inner rotor of 60% (to 40% of the initial rotor speed) the frequency will rise to 2,736 Hz.

At fist sight, the initial frequency seems high, but it is responsible for low efficiency only in the very beginning of the acceleration, which plays an almost negligible role in the overall efficiency. The basic machine frequency is high (4.275 kHz) and requires special consideration of the conductor construction, shielding, etc. The influence on the designs of a large number of poles has been offset by the large diameter and the polar pitch results as $\tau = 9.24$ cm or $2\tau = 18.48$ cm which is manageable. The machine has a "slim" construction - the active length being only 0.36 m for the machine and 0.2 m for the auxiliary alternator (self excited synchronous machine operating in pulsed mode) necessary to provide the excitation for the RFG. The presence of the rotor of the auxiliary alternator on the same shaft as the inner rotor of the RFG is essential in assuring the desired cycle of the operation for the system. The inertia of the rotor of the auxiliary alternator counts in the discharge pulse. The self-excited alternator has both a three-phase and single-phase armature winding, electromagnetically decoupled. A schematic representation of the general circuit is shown in figure A-1. This circuit functions as follows: the power supply on the left-hand side of the circuit provides a pulse of current (approximately 10% of operating current or 1% of excitation energy) to the self-excited alternator excitation (stator) winding. As this initial current produces flux in the alternator air gap, the three-phase alternator rotor winding begins to generate an alternating voltage which is rectified by the stationary self-excitation rectifier and the current I_A is supplied to the alternator stator winding causing the alternator to self-excite (fig. A-2b). As the alternator self-excites, the voltage produced by the single-phase armature winding (V_A) rises as shown in figure A-2a. As V_A reaches a peak value after 220 ms, it is connected to the RFG rotor winding through a making switch producing the current shown in figure A-3a.

After allowing 1 ms for the excitation current in the RFG to rise, the RFG output is switched into the stator of an induction accelerator designed to accelerate a 1-kg projectile to a velocity of 10 km/s in a distance of 18 m. The launch requires 3.6 ms to complete. During this time the RFG output frequency rises from 427.5 to 2,736 Hz and the output voltage rises to accommodate the rising impedance of the load as the driving frequency increases (fig. A-3b). This results in an essentially constant output current value (fig. A-3c). The physical parameters of the combined RFG/excitation alternator are given in figure A-4 and table A-1.

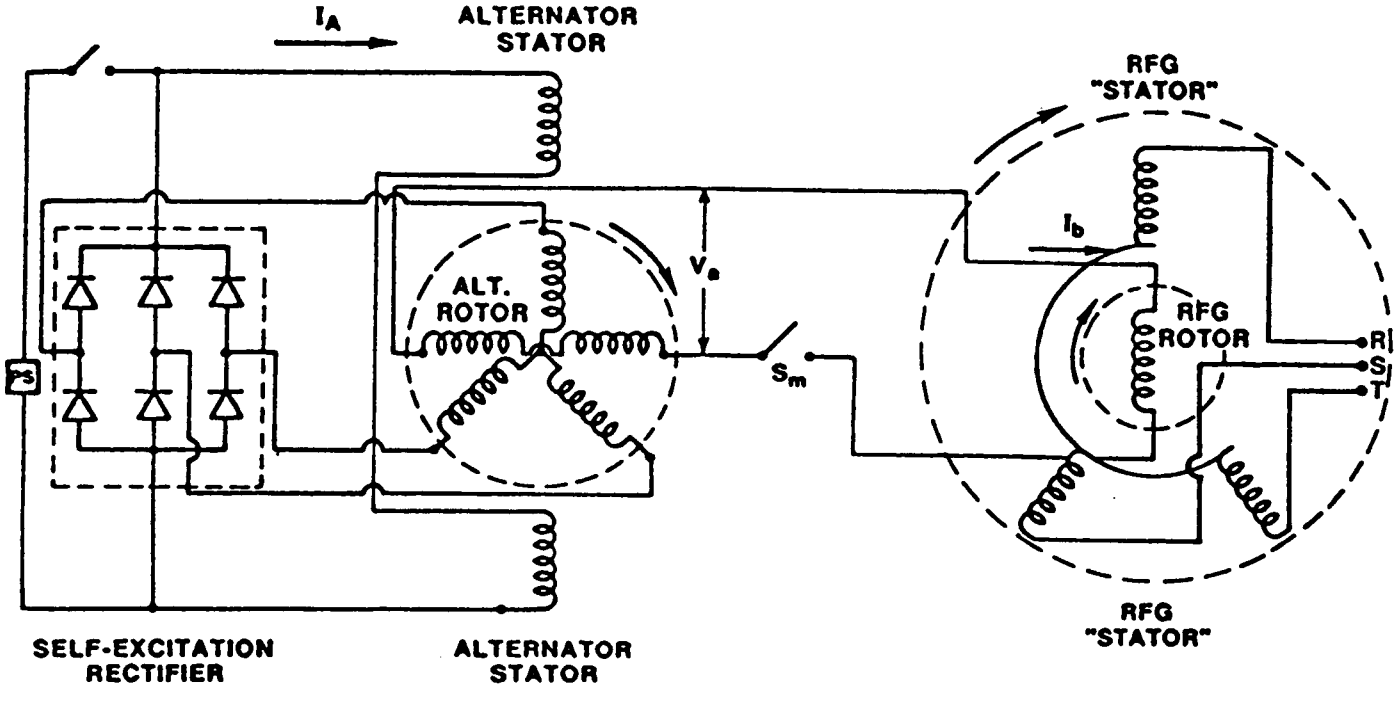

Figure A-1. Schematic of single-phase rising frequency generator (RFG) with self-excited compulsator (CPA) excitation on a common shaft

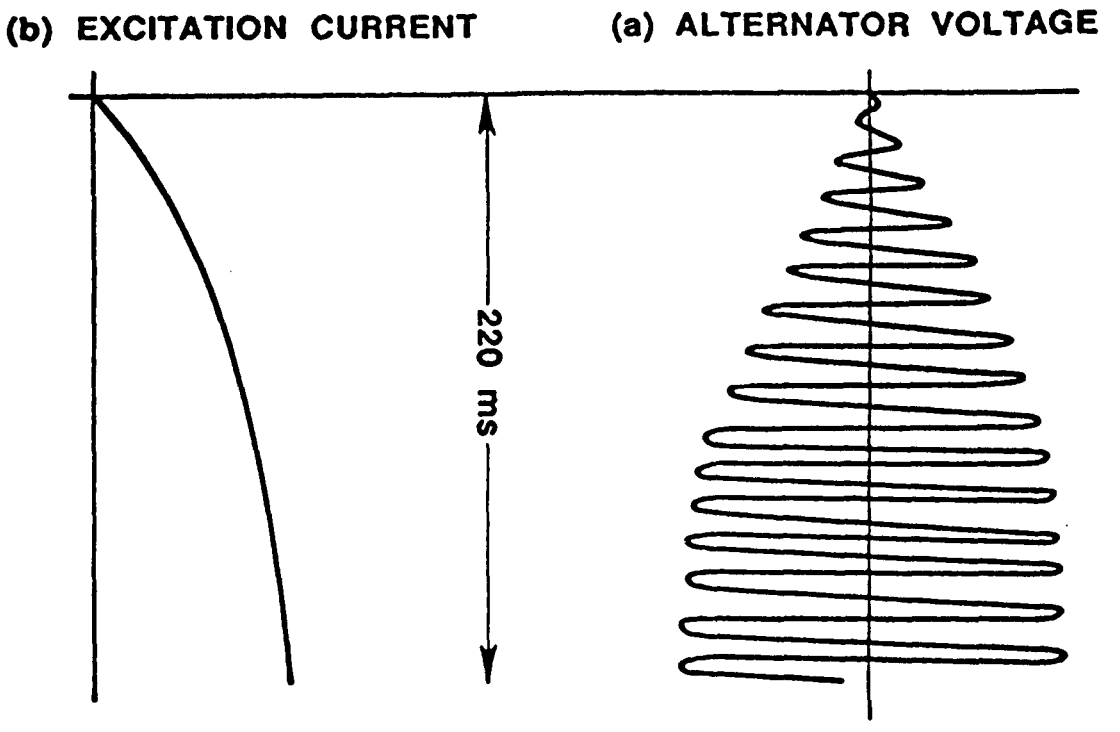

Figure A-2. a) Alternator voltage V_A resulting from
b) excitation current I_A for RFG circuit

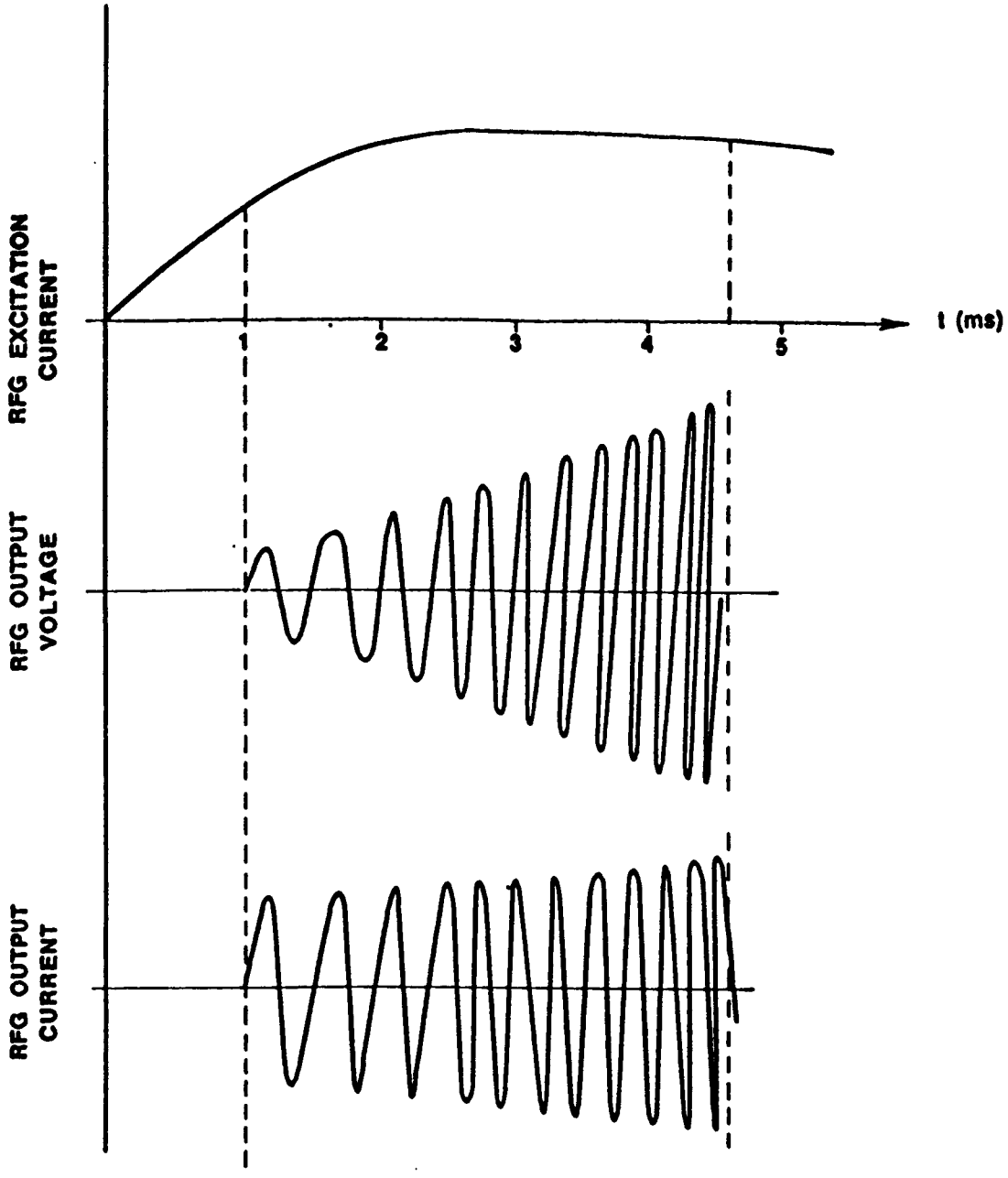

Figure A-3. Rising frequency generator performance in driving a coaxial induction accelerator

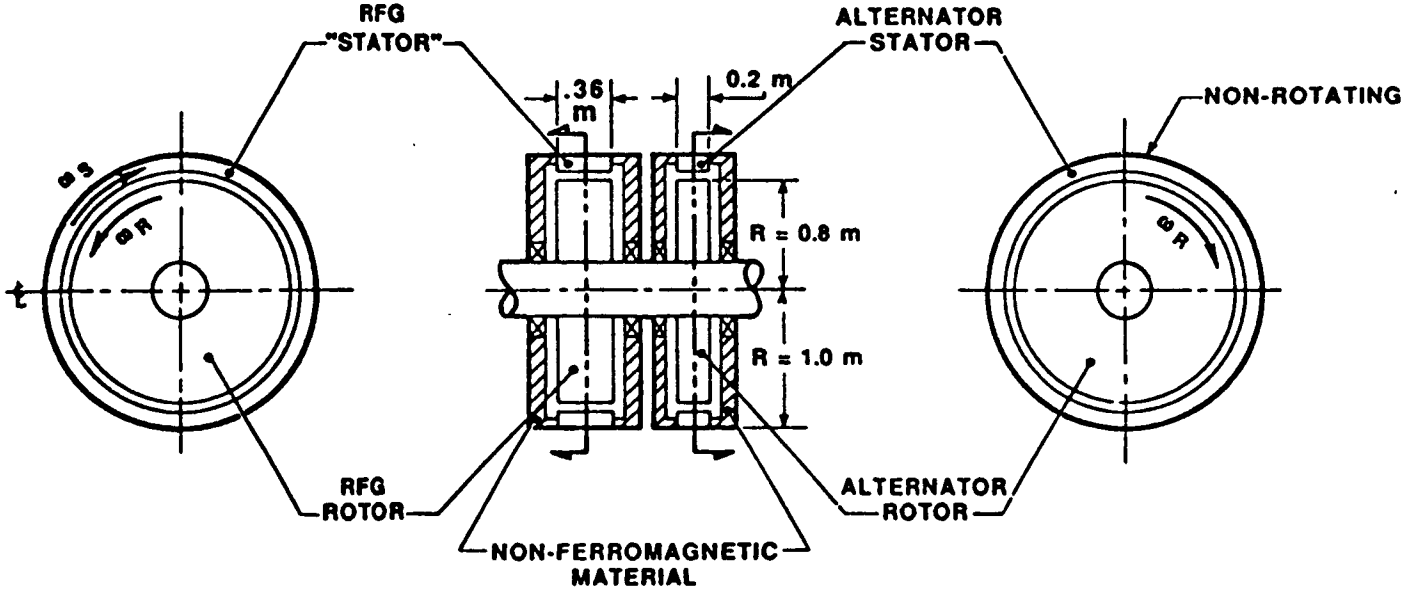

Figure A-4. Combined RFG and self-excited alternator

Table A-1. Rising frequency generator

"Stator" (outer rotor)		
Diameter	2.0	m
Active length	0.36	m
Initial Angular Velocity	790	rad/s
Stored Energy	208	MJ
Inner Rotor		
Diameter	1.6	m
Active Length	0.36	m
Initial Angular Velocity	711	rad/s
Stored Energy	108	MJ
Number of Poles	68	
Output		
Energy	124	MJ
Initial Frequency	427.5	Hz
Final Frequency	2,736	Hz

EDDY CURRENT LOSSES IN THE SUPPORT STRUCTURE

As stated in the September report, the use of conducting materials for stator coil support will result in eddy current losses if placed in the high magnetic field near the coils. Electromagnetic analysis was performed using an EM finite element code to design a support structure. By using ceramic to transfer the force to an outer steel structure, the steel is displaced out of the high magnetic field. For a structure having 5 cm radial thickness of ceramic and 2 cm radial thickness of steel on the radius (fig. A-5), the eddy current losses are 4.8 MJ in 3.6 ms or 1.6% of the total launch energy. However, if high strength, boron-reinforced composite is used, the eddy current losses become negligibly small (64 kJ in 3.6 ms).

System Electrical Configuration

The passive coaxial accelerator will be connected as a delta load to the rising frequency generator. This allows each phase of stator coils to be driven with the same voltage as the phase to phase voltage (fig. A-6) of the generator, also allowing higher harmonics in the system to be damped as circulating currents.

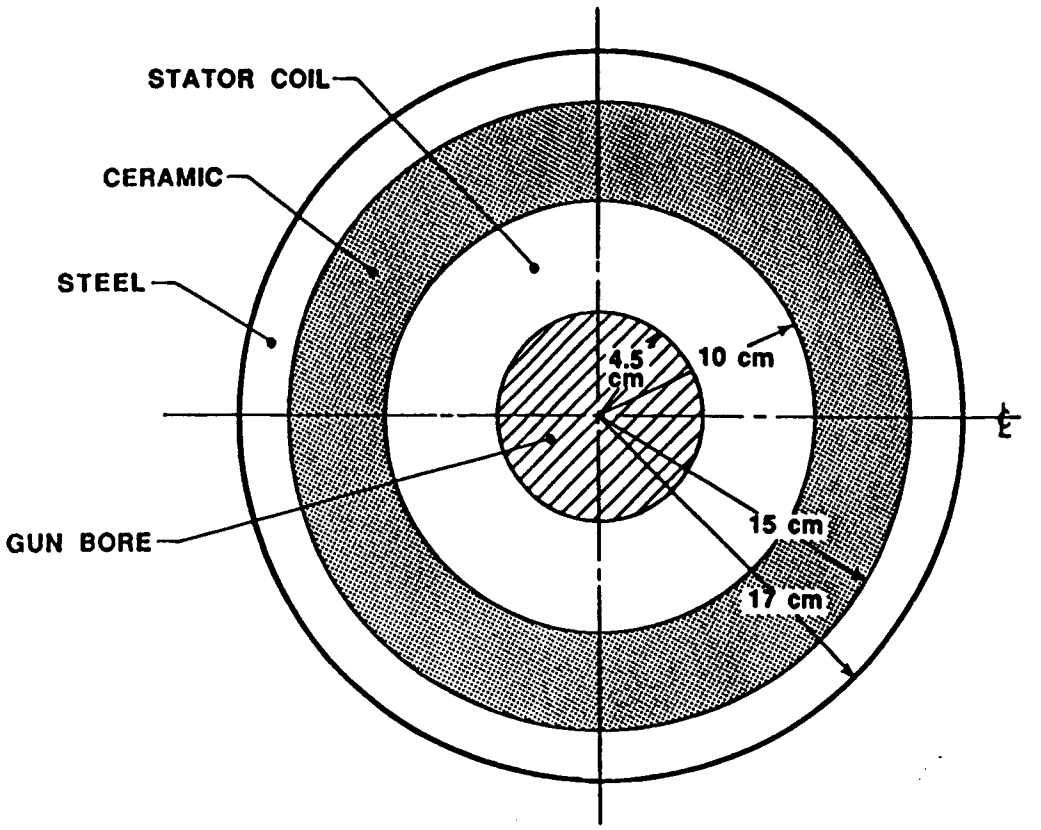

Figure A-5. Support structure

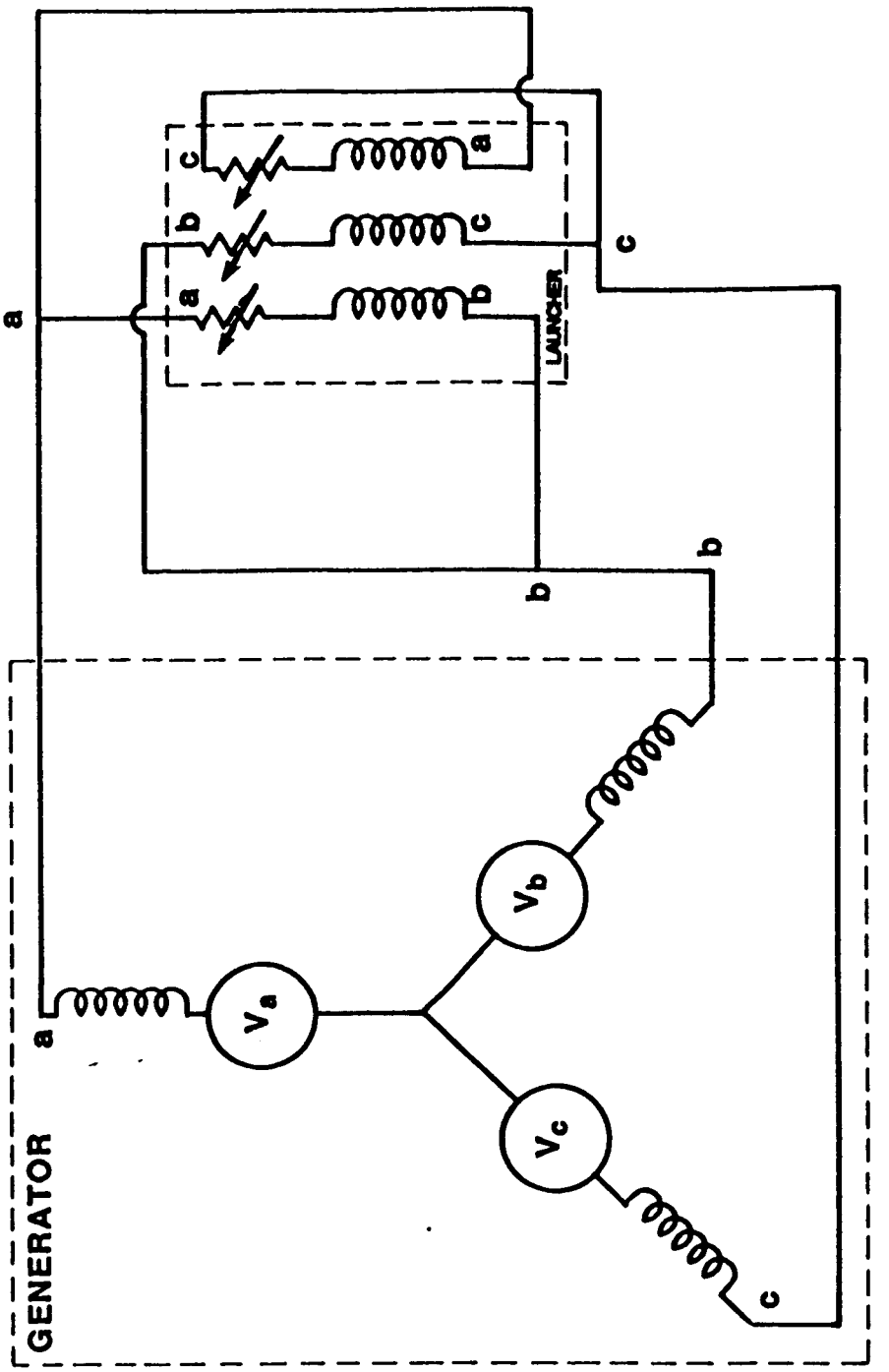

Figure A-6. Generator

The phasor diagram of the coaxial accelerator varies with the position of the projectile in the barrel, since the projectile represents a smaller fraction of the stator segment as it advances towards the muzzle. The mutual flux Φ_M induces the secondary electromotive force (emf) and current at a low phase angle ψ, due to the slip frequency. At the same time it induces the primary electromotive force which balances the applied voltage and the inductive and resistive voltage drop in the primary. In the phasor diagram (refer to fig. 14), only the stator segment containing the projectile is considered.

If the diagram is redrawn in order to take into account the fact that the whole barrel is energized, the voltage drop triangle will considerably increase,

$$(Z_{IT}I_1 = R_{IT}I_1 + j\omega(L_{TOTAL} - M)I_1)$$

while V_1 will be replaced by the phase voltage V, applied to the coaxial accelerator. In this case the primary current I_1 becomes less dependent on the load.

The circuit equations:

$$(P) \quad V = R_T I_1 + j\omega L_T I_1 - j\omega MI_1 - E_p$$

$$0 = R'_2 I'_2 + j\omega L_s - j\omega MI'_2 - E'_s$$

where

$$E_p = j\omega MI_M = E's$$

and

$$I_1 + I'_2 = I_M$$

The equivalent circuit is shown in figure A-7.

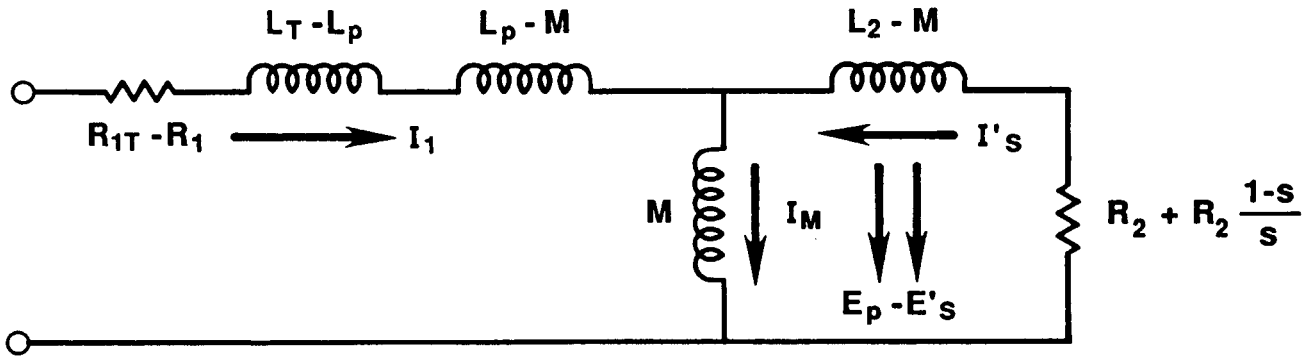

$$V = R_T I_1 + j\omega L_T I_1 - j\omega M I_1 - E_p$$

$$O = R'_2 I'_1 + j\omega L_S - j\omega M I'_2 - E_S$$

where $E_p = j\omega M I_M = E'_S$

and $I_1 + I'_2 = I_M$

Figure A-7. Simplified equivalent equation

9 MJ/PULSE AIR CORE COMPULSATOR

S. B Pratap, S. M. Manifold, W. A. Walls, M. L. Spann, and W. F. Weldon

Center for Electromechanics
The University of Texas at Austin
Austin, TX 78758-4497

Abstract

One of the most critical issues in taking electromagnetic gun technology from the laboratory to field applications is the compactness and portability of very high energy, pulsed power supplies. The air core compulsator which is under development at CEM-UT addresses these requirements. The rotor of this machine is made from fiber reinforced epoxy composites and spins at a tip speed of 500 m/s which is substantially higher than is possible with a ferromagnetic rotor. The higher tip speed greatly increases the energy density of the rotor thus reducing the size of the prime power source. The special structural features of this machine, the electrical design, and the cooling system design are discussed.

Introduction

The 9 MJ/pulse air core compulsator is being developed as a pulsed power supply for a self supporting, skid mounted, electromagnetic gun (EMG). The goal of this system is to accelerate projectiles to a muzzle energy of 9 MJ, with velocities ranging from 2.5 to 4.0 km/s. The repetition rate for this system is 20 s between shots for a total of nine shots. The pulsed power supply similar to the one described here may eventually be mounted in an armored vehicle and therefore all components must be compact and lightweight. The power density of this air core compulsator is 3.4 MW/kg and the inertial energy density is 16 kJ/kg compared to 0.17 MW/kg and 3.45 kJ/kg for compulsators using ferromagnetic materials. The other salient parameters of this machine are summarized in Table 1.

Table 1. Machine parameters

Parameter	Units	Value
Open circuit voltage	kV	8.5
Machine inductance	μH	1.0
Machine resistance	μΩ	320.0
Peak discharge current	MA	4.4
Number of poles	--	2.0
Pulse width	ms	4.0
Energy stored	MJ	166.0
Peak Power	GW	36.0
Peak rotor speed	rpm	10,000.0
Machine mass	kg	10,200.0

Two possible machine configurations were considered. The first one being a shell type rotor spinning outside the stator (fig. 1). This geometry has the advantage that the high strength fiber-epoxy composite, besides storing the required inertial energy, also provides banding for the delicate armature winding. The second geometry, which is more conventional, has the rotor spinning inside the stator (fig. 2.). This rotor has a lower energy density compared to the shell-type rotor, however the stator in this machine provides containment structure in case of a rotor failure. Therefore, after considering rotor containment the machine with the second geometry has a better overall energy density. In both these geometries the armature winding spins with the rotor, whereas the field coil is stationary.

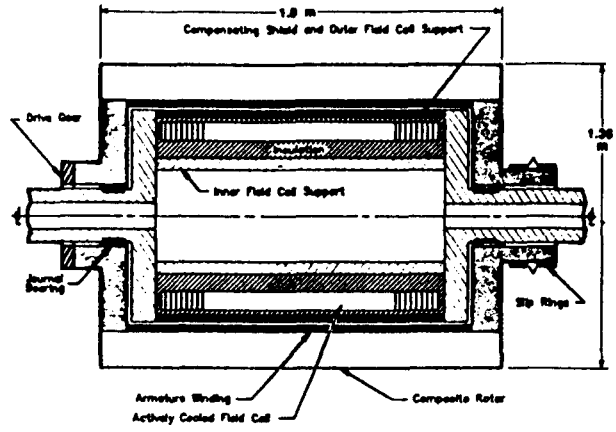

Figure 1. Air core compulsator with external rotor

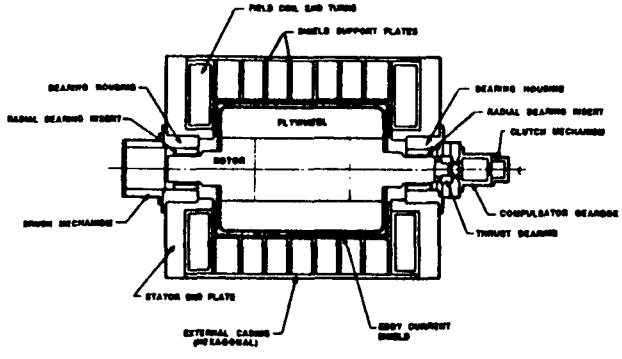

Figure 2. Air core compulsator with internal rotor

Design of the Stator

The stator is comprised of the compensating shield, the field coil, the stator housing and the end plates. The compensating shield provides passive, eddy current compensation for the armature winding and sustains the full discharge torque (26 MN-m) and pressure (62 MPa). Therefore the compensating shield needs to be highly conductive and strong. Aluminum was selected as the shield material since it is light. In order to enable the shield to withstand the mechanical loading during discharge it is banded with a high strength graphite fiber-epoxy wrapping. The discharge torque generated in the shield is transmitted to the stator housing through support plates which are placed at regular intervals along the axial length.

The field coil, which is made from aluminum conductors, provides the excitation magnetic field. Its geometry is very different from most air core machines, which use a distributed field coil. Figure 3 shows the cross section of the field coil and its location relative to the rotor. Also shown in figure 3 is the radial flux density distribution at the

radius of the armature winding. This field coil geometry has several advantages over the distributed field coil geometry, they are:

1) The shear stress distribution at peak current is uniformly distributed along the armature winding due to the nature of the radial flux density distribution.

2) It allows the stator housing to directly support the shield under the discharge loads. This would be difficult to achieve with a distributed field coil.

3) The forces generated in the field coil are more manageable since the displacement under these forces is directed radially outward, away from the rotor.

4) This geometry simplifies the fabrication and assembly of the field coil.

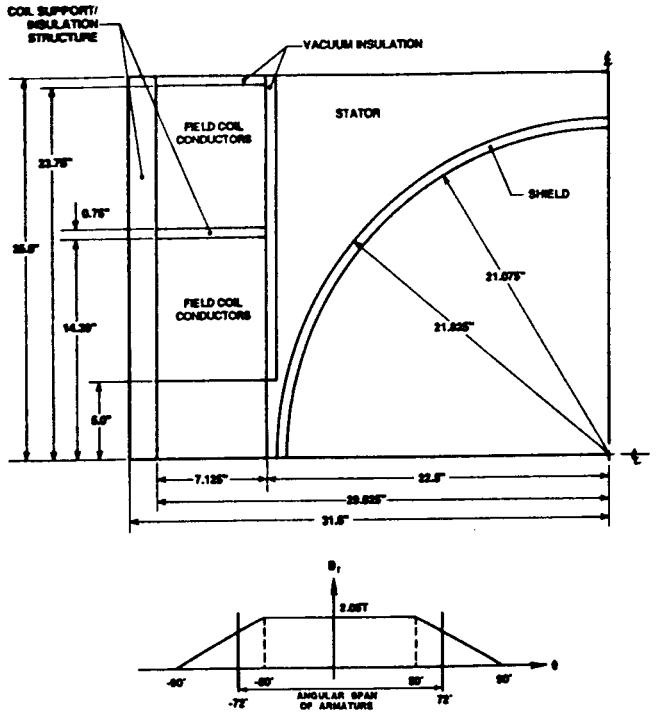

Figure 3. Field coil geometry and radial flux density distribution

The field coil provides 5 MA-T per pole excitation at a nominal current density of 3.0 kA/cm^2. In order to reduce the losses in the field coil at this current density it is cooled to 80 K with liquid nitrogen. This is especially important since the field coil operates in a self-excited mode, where the magnetic energy and the resistive losses are supplied from the rotor inertial energy.

The stator housing supports the field coils, the brush mechanism, and the bearings besides providing mechanical support to the shield. In order to make the machine lightweight the stator housing is also made with aluminum. An exploded view of the various stator components is shown in figure 4.

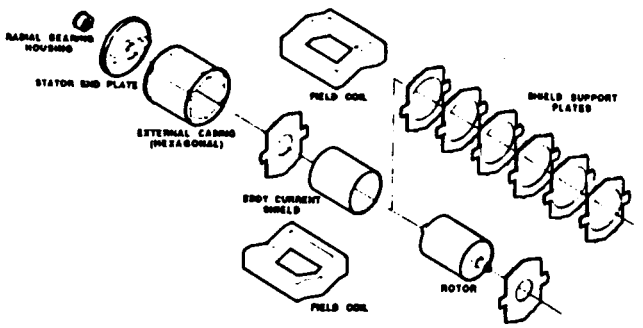

Figure 4. Isometric sketch of stator assembly

Design of the Rotor

The rotor can be divided into the following main components: the shaft, the flywheel, the armature winding and the armature overwrap. All the structural components on the rotor are made with fiber-reinforced epoxy composites. These high strength materials allow high rotational speeds and correspondingly high stresses in the rotor and also minimizes the mass of the rotor. Fiber reinforced epoxy systems have anisotropic mechanical properties with the best mechanical properties in the direction of the fibers. The structural components of the rotor are made from unidirectional fibers, oriented in a manner to fully utilize the properties of these fibers.

The shaft must have a high modulus in the flexural mode in order to ensure sub-critical operation of the machine at full speed. The shaft is therefore made of axially oriented fibers. Mechanically, graphite fibers would be an ideal choice for the shaft material, however, they are conductive. The conductivity of these fibers is about 10,000 mho/m along the fibers and about 100 to 200 mho/m transverse to the fibers. The transverse conductivity being primarily due to fiber-to-fiber contact. The result of the conductivity is that eddy current losses are incurred in these fibers since they rotate in a magnetic field of about 2.4 T oriented perpendicular to the axis of rotation. From the eddy current stand point boron fibers would be better, however, this material is very costly. Initial tests indicate that combining Kevlar® with graphite fiber will reduce the transverse conductivity to an acceptable value for use in the shaft. In order to provide strength to the shaft under centrifugal loads it is wrapped with a thin layer of azimuthally directed fibers.

The function of the flywheel is to store the required inertial energy. It is made with fibers wound azimuthally in order to enable the flywheel to withstand centrifugal loads. The secondary function of the flywheel is to provide the shaft with added strength under centrifugal loads. Kevlar® fiber is selected as the flywheel material due to its high specific strength and because it is nonconductive.

The armature winding is wound on the surface of the flywheel with the end turns completed over the axial faces. The lap wound armature winding has six conductors per pole and is made of stranded and transposed conductors. The armature conductor is 22.5 cm wide and about 1.73 cm thick and incorporates cooling passages. In order to protect the armature winding from centrifugal loads it is banded with high strength

graphite epoxy composite. This banding is discontinuous axially in order to reduce the eddy current losses. The discharge torque acting on the armature winding is transmitted to the flywheel through an epoxy bond on the surface of the flywheel. This bond exhibits a high shear strength when it is under compression. The growth of the flywheel and the armature banding is designed to maintain the bond under compression at all speeds.

The armature end turn design is complex. It must be designed so that the centrifugal loading on the end turns is symmetrical about the rotor axis to minimize imbalance and must be arranged so that the centrifugal load on the armature winding is supported uniformly along the face of the rotor rather than act cumulatively in the armature banding. The armature end turn layout for the two ends of the rotor is shown in figure 5.

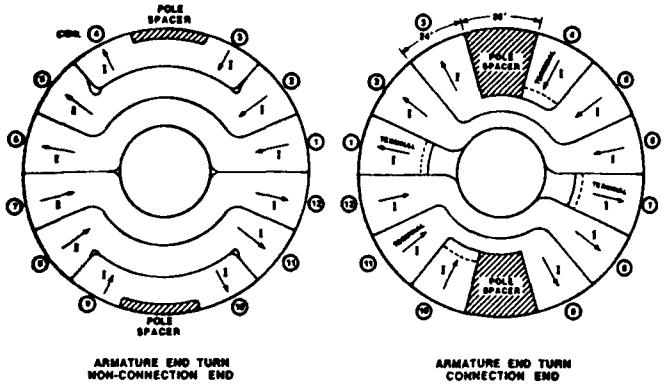

Figure 5. Armature end turn

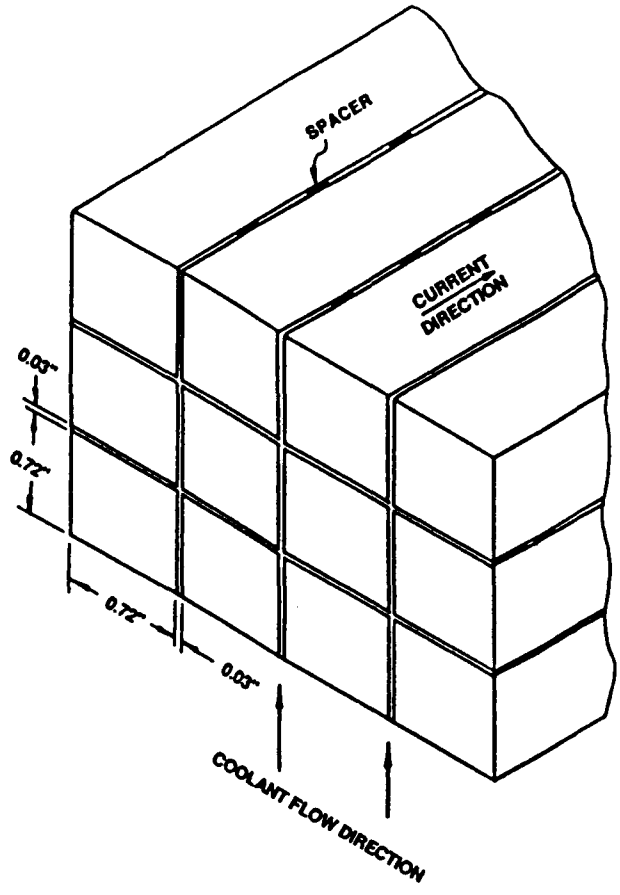

Figure 6. Field coil conductors with cooling passages

Design of the Cooling System

The two components of the machine which require active cooling are the field coil which is liquid nitrogen cooled, and the armature winding which is gaseous helium cooled. A section of the field coil conductors with the cooling passages is shown in figure 6. The cooling passages are formed by insulating spacers placed between adjacent conductors. The liquid nitrogen therefore comes in direct contact with the conductors. Two methods were investigated to accomplish the cooling. One was high pressure forced convection boiling and the second was low pressure pool boiling. The heat transfer coefficient is much higher for the forced convection case, however, the drawback is that the fluid temperature must be raised to the saturation temperature at the applied pressure before vaporization. This implies that the coil must operate at a higher temperature, therefore low pressure pool boiling was adopted. With pool boiling it is critical to exhaust the vapor effectively in order to allow the coil surface to be in contact with the liquid. Therefore, the coolant must be slightly pressurized. At present, scaled experiments are underway to determine optimum coolant passage sizes and pressures required to achieve effective pool cooling. The amount of liquid nitrogen vaporized per shot is estimated to be about 2.67 gal for the entire coil.

The cooling of the armature winding is more complicated than the cooling of the field coil since it rotates at a high tip speed on the periphery of the rotor. Liquids were eliminated as a coolant for the armature winding because of their high densities and because any phase change of the coolant in the armature winding would result in high imbalance forces on the rotor. Instead a light gas such as helium is being considered. A conceptual schematic of an armature cooling circuit is shown in figure 7. The cooling passages within the armature conductors are directed axially and the helium inlet and outlet passages are located at the center of the rotor shaft. The helium is pumped through the cooling passages by a compressor built into the shaft.

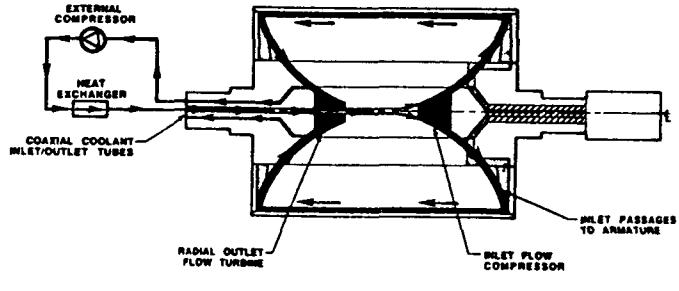

Figure 7. Armature cooling circuit--conceptual schematic

Operational Characteristics

The rotor of the compulsator is accelerated to 10,000 rpm with a gas turbine through a gearbox and clutch system. The discharge sequence is carried out

in two stages. During the first stage the inertial energy of the rotor is converted into magnetic energy of the excitation magnetic field and resistive dissipation in the field coil. During the second stage the inertial energy of the rotor is used to drive the electromagnetic accelerator. A typical rotor speed vs time curve during discharge is shown in figure 8. After the second stage the turbine re-motors the rotor to 10,000 rpm.

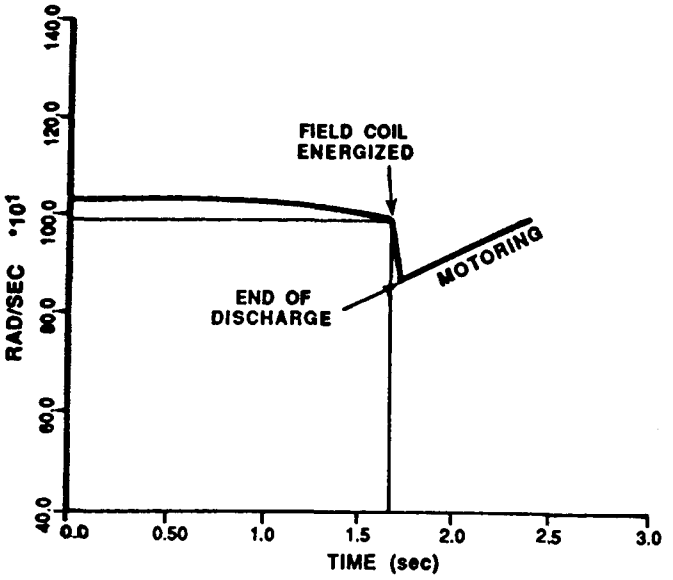

Figure 8. Machine speed during the two discharge stages

During the first stage of the discharge the field coil is energized in a self-excited mode. Figure 9 shows the circuit schematic of the self-excitation system. In order to initiate the process a current of 600 A is injected into the field coil with the aid of a battery and a switch. Thereafter the current control SCRs are triggered in succession and the armature voltage ramps the current in the field coil through the full wave rectifier. The current rises exponentially (positive exponent) to a maximum of 10 kA. At which point the second stage of the discharge is initiated. The current and voltage of the compulsator during the second stage discharge is shown in figure 10. The important performance parameters of the machine are summarized in Table 2.

Table 2. Performance Parameters

PARAMETER	UNITS	Value
Field current density	kA/cm²	2.35
Generated voltage	kV	6.80
Peak current	MA	4.00
Energy in projectile	MJ	9.00
Energy from rotor	MJ	32.63
Temperature rise in armature	°C	29.15
Temperature rise in shield	°C	10.72
Energy supplied to launcher	MJ	23.05
Pulse width	ms	4.20
Muzzle current	kA	600.00
SYSTEM EFFICIENCY	%	27.50
LAUNCHER EFFICIENCY	%	39.00

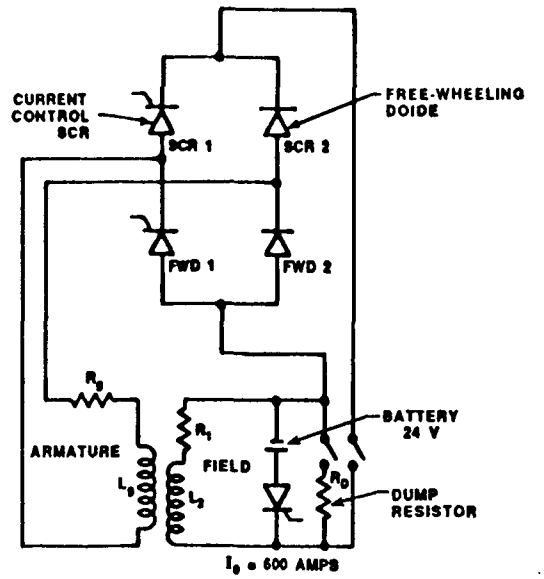

Figure 9. Excitation circuit schematic

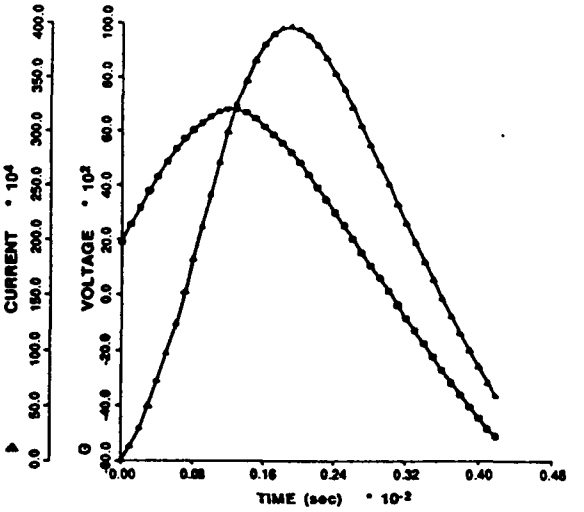

Figure 10. Compulsator voltage and current during second stage discharge

Acknowledgements

This research is supported by U.S. Army Armament Research, Development, and Engineering Center and the Defense Advanced Research Projects Agency under Contract No. DAAA21-86-C-0281.

References

[1] J. L. Allen, et al., "A Technology Plan for Electromagnetic Characteristics of Advanced Composites," RADC-TR-76-206, July 1976, A030507.

[2] J. L. Allen, et al., "Electromagnetic Properties and Effects of Advanced Composite Materials: Measurement and Modelling," RADC-TR-78-156, June 1978, A058041.

APPENDIX B

```
*****************************************************************************
*          Coaxial Inductor Design made at  20:00:37  on  09/21/87          *
*****************************************************************************
*           Exact Reproduction of Input Data File Named : INPUT             *
*****************************************************************************

**  NASA Langley HPG/I multi-rail Launcher Inductor Design ( 9/21/87 ) CIRES3.IN
5
*---------------------------------------------------------------------*
** s.g. of Al  **  Risetime  **  # of turns
        2.7,          0.48,            4
*---------------------------------------------------------------------*
** Inner cylinder(s)
   0.0000        4.801        192.0       1.1417E-06
    5.301        7.152        189.0       1.1417E-06
    7.652        9.034        186.0       1.1417E-06
    9.534        10.67        183.0       1.1417E-06
*---------------------------------------------------------------------*
** Outer cylinder(s)
    62.50        63.00        183.0       1.1417E-06
    63.50        64.00        186.0       1.1417E-06
    64.50        65.00        189.0       1.1417E-06
    65.50        66.00        192.0       1.1417E-06
*---------------------------------------------------------------------*
** End-plates
     1.000       1.1417E-06
     1.000       1.1417E-06
     1.000       1.1417E-06
     1.000       1.1417E-06
*---------------------------------------------------------------------*
```

```
Specific gravity of the conducting material =  2.7000
Current rise-time ( quarter-cycle ) = 0.48000     second
                                    =  480.00     millisecond.
Period of the driving current =  1.9200     second
                              =  1920.0     millisecond

Frequency of the driving current = 0.52083     Hertz

          Number of turns       =  4



     Cylinder number  1 :
   Inner radius =  0.00000     inches =  0.00000     cm
   Outer radius =   4.8010     inches =   12.195     cm
 Wall thickness =   4.8010     inch   =   12.195     cm
         Length =   192.00     inch   =   487.68     cm
    Resistivity =  1.14170E-06 Ohm-inch =  2.89992E-06 Ohm-cm
    Skin depth  =   4.6755     inch(es) =   11.876     cm
         Volume =  0.22783     meter**3
           Mass =   615.15     kg =   1356.2     lbs.
  dc resistance =  3.02719E-06 Ohms =   3.0272     microOhm
  ac resistance =  3.31423E-06 Ohms =   3.3142     microOhm
 Rac/Rdc ratio  =   1.095
* Inductance of space between Cylinder # 0 & # 1 =  0.0000     microHenry.
* Inductance of Cylinder # 1 =  0.2438     microHenry
* H at inner radius of cylinder is  0.00000     A/m per 1 Ampere current
* H at outer radius of cylinder is   1.3051     A/m per 1 Ampere current
* Assuming unit relative permeability:
* B at inner radius of cylinder is  0.00000     Tesla per MA current
* B at outer radius of cylinder is   1.6401     Tesla per MA current



     Cylinder number  2 :
   Inner radius =   5.3010     inches =   13.465     cm
   Outer radius =   7.1520     inches =   18.166     cm
 Wall thickness =   1.8510     inch   =   4.7015     cm
         Length =   189.00     inch   =   480.06     cm
    Resistivity =  1.14170E-06 Ohm-inch =  2.89992E-06 Ohm-cm
    Skin depth  =   4.6755     inch(es) =   11.876     cm
         Volume =  0.22428     meter**3
           Mass =   605.56     kg =   1335.0     lbs.
  dc resistance =  2.97978E-06 Ohms =   2.9798     microOhm
  ac resistance =  3.03502E-06 Ohms =   3.0350     microOhm
 Rac/Rdc ratio  =   1.019
* Inductance of space between Cylinder # 1 & # 2 =  9.5875E-02 microHenry.
* Inductance of Cylinder # 2 =  0.6287     microHenry
* H at inner radius of cylinder is   1.1820     A/m per 1 Ampere current
* H at outer radius of cylinder is   1.7522     A/m per 1 Ampere current
* Assuming unit relative permeability:
* B at inner radius of cylinder is   1.4854     Tesla per MA current
* B at outer radius of cylinder is   2.2019     Tesla per MA current



     Cylinder number  3 :
   Inner radius =   7.6520     inches =   19.436     cm
   Outer radius =   9.0340     inches =   22.946     cm
 Wall thickness =   1.3820     inch   =   3.5103     cm
         Length =   186.00     inch   =   472.44     cm
```

```
    Resistivity =  1.14170E-06 Ohm-inch =  2.89992E-06 Ohm-cm
    Skin depth  =   4.6755     inch(es) =   11.876     cm
         Volume =  0.22081     meter**3
           Mass =   596.19     kg =   1314.4     lbs.
  dc resistance =  2.93126E-06 Ohms =   2.9313     microOhm
  ac resistance =  2.97799E-06 Ohms =   2.9780     microOhm
 Rac/Rdc ratio  =   1.016
* Inductance of space between Cylinder # 2 & # 3 =  0.2574     microHenry.
* Inductance of Cylinder # 3 =  0.9719     microHenry
* H at inner radius of cylinder is   1.6377     A/m per 1 Ampere current
* H at outer radius of cylinder is   2.0808     A/m per 1 Ampere current
* Assuming unit relative permeability:
* B at inner radius of cylinder is   2.0580     Tesla per MA current
* B at outer radius of cylinder is   2.6148     Tesla per MA current


     Cylinder number  4 :
   Inner radius =   9.5340     inches =   24.216     cm
   Outer radius =   10.670     inches =   27.102     cm
 Wall thickness =   1.1360     inch   =   2.8854     cm
         Length =   183.00     inch   =   464.82     cm
    Resistivity =  1.14170E-06 Ohm-inch =  2.89992E-06 Ohm-cm
    Skin depth  =   4.6755     inch(es) =   11.876     cm
         Volume =  0.21623     meter**3
           Mass =   583.82     kg =   1287.1     lbs.
  dc resistance =  2.89759E-06 Ohms =   2.8976     microOhm
  ac resistance =  2.93888E-06 Ohms =   2.9389     microOhm
 Rac/Rdc ratio  =   1.014
* Inductance of space between Cylinder # 3 & # 4 =  0.4544     microHenry.
* Inductance of Cylinder # 4 =   1.277     microHenry
* H at inner radius of cylinder is   1.9717     A/m per 1 Ampere current
* H at outer radius of cylinder is   2.3490     A/m per 1 Ampere current
* Assuming unit relative permeability:
* B at inner radius of cylinder is   2.4777     Tesla per MA current
* B at outer radius of cylinder is   2.9518     Tesla per MA current


     Cylinder number  5 :
   Inner radius =   62.500     inches =   158.75     cm
   Outer radius =   63.000     inches =   160.02     cm
 Wall thickness =  0.50000     inch   =   1.2700     cm
         Length =   183.00     inch   =   464.82     cm
    Resistivity =  1.14170E-06 Ohm-inch =  2.89992E-06 Ohm-cm
    Skin depth  =   4.6755     inch(es) =   11.876     cm
         Volume =  0.59117     meter**3
           Mass =   1596.2     kg =   3518.9     lbs.
  dc resistance =  1.05984E-06 Ohms =   1.0598     microOhm
  ac resistance =  1.06040E-06 Ohms =   1.0604     microOhm
 Rac/Rdc ratio  =   1.001
* Inductance of space between Cylinder # 4 & # 5 =   26.29     microHenry.
* Inductance of Cylinder # 5 =  9.1428E-02 microHenry
* H at inner radius of cylinder is  0.40102     A/m per 1 Ampere current
* H at outer radius of cylinder is  0.29837     A/m per 1 Ampere current
* Assuming unit relative permeability:
* B at inner radius of cylinder is  0.50393     Tesla per MA current
* B at outer radius of cylinder is  0.37495     Tesla per MA current


     Cylinder number  6 :
   Inner radius =   63.500     inches =   161.29     cm
```

```
  Outer radius =   64.000     inches =   162.56     cm
 Wall thickness =  0.50000    inch   =   1.2700     cm
        Length =   186.00     inch   =   472.44     cm
    Resistivity =  1.14170E-06 Ohm-inch =  2.89992E-06 Ohm-cm
    Skin depth  =   4.6755    inch(es) =   11.876     cm
         Volume =  0.61044    meter**3
           Mass =   1648.2    kg =   3633.6     lbs.
  dc resistance =  1.06031E-06 Ohms =   1.0603     microOhm
  ac resistance =  1.06060E-06 Ohms =   1.0606     microOhm
 Rac/Rdc ratio  =   1.000
* Inductance of space between Cylinder # 5 & # 6 =  6.6683E-02 microHenry.
* Inductance of Cylinder # 6 =  4.6984E-02 microHenry
* H at inner radius of cylinder is  0.29602     A/m per 1 Ampere current
* H at outer radius of cylinder is  0.19581     A/m per 1 Ampere current
* Assuming unit relative permeability:
* B at inner radius of cylinder is  0.37200     Tesla per MA current
* B at outer radius of cylinder is  0.24606     Tesla per MA current


    Cylinder number  7 :
  Inner radius =   64.500     inches =   163.83     cm
  Outer radius =   65.000     inches =   165.10     cm
 Wall thickness =  0.50000    inch   =   1.2700     cm
        Length =   189.00     inch   =   480.06     cm
    Resistivity =  1.14170E-06 Ohm-inch =  2.89992E-06 Ohm-cm
    Skin depth  =   4.6755    inch(es) =   11.876     cm
         Volume =  0.63001    meter**3
           Mass =   1701.0    kg =   3750.1     lbs.
  dc resistance =  1.06078E-06 Ohms =   1.0608     microOhm
  ac resistance =  1.06088E-06 Ohms =   1.0609     microOhm
 Rac/Rdc ratio  =   1.000
* Inductance of space between Cylinder # 6 & # 7 =  2.9650E-02 microHenry.
* Inductance of Cylinder # 7 =  1.7328E-02 microHenry
* H at inner radius of cylinder is  0.19429     A/m per 1 Ampere current
* H at outer radius of cylinder is  9.63991E-02 A/m per 1 Ampere current
* Assuming unit relative permeability:
* B at inner radius of cylinder is  0.24415     Tesla per MA current
* B at outer radius of cylinder is  0.12113     Tesla per MA current


    Cylinder number  8 :
  Inner radius =   65.500     inches =   166.37     cm
  Outer radius =   66.000     inches =   167.64     cm
 Wall thickness =  0.50000    inch   =   1.2700     cm
        Length =   192.00     inch   =   487.68     cm
    Resistivity =  1.14170E-06 Ohm-inch =  2.89992E-06 Ohm-cm
    Skin depth  =   4.6755    inch(es) =   11.876     cm
         Volume =  0.64990    meter**3
           Mass =   1754.7    kg =   3868.5     lbs.
  dc resistance =  1.06123E-06 Ohms =   1.0612     microOhm
  ac resistance =  1.06124E-06 Ohms =   1.0612     microOhm
 Rac/Rdc ratio  =   1.000
* Inductance of space between Cylinder # 7 & # 8 =  7.4157E-03 microHenry.
* Inductance of Cylinder # 8 =  2.4818E-03 microHenry
* H at inner radius of cylinder is  9.56632E-02 A/m per 1 Ampere current
* H at outer radius of cylinder is  0.00000     A/m per 1 Ampere current
* Assuming unit relative permeability:
* B at inner radius of cylinder is  0.12021     Tesla per MA current
* B at outer radius of cylinder is  0.00000     Tesla per MA current
```

```
 End Plate number  1 :
   Inner radius =   10.670     inches =   27.102     cm
   Outer radius =   62.500     inches =   158.75     cm
Plate thickness =   1.0000     inch   =   2.5400     cm
    Resistivity =  1.14170E-06 Ohm-inch =  2.89992E-06 OHM-cm
    Skin depth  =   4.6755     inch(es) =   11.876     cm
         Volume =  0.19523     meter**3
           Mass =   527.14     kg =   1162.1     lbs.
  dc resistance =  3.21209E-07 Ohms =  0.32120     microOhm
  ac resistance =  3.23957E-07 Ohms =  0.32395     microOhm
 Rac/Rdc ratio  =   1.0086


 End Plate number  2 :
   Inner radius =   9.0340     inches =   22.946     cm
   Outer radius =   63.500     inches =   161.29     cm
Plate thickness =   1.0000     inch   =   2.5400     cm
    Resistivity =  1.14170E-06 Ohm-inch =  2.89992E-06 OHM-cm
    Skin depth  =   4.6755     inch(es) =   11.876     cm
         Volume =  0.20338     meter**3
           Mass =   549.14     kg =   1210.6     lbs.
  dc resistance =  3.54337E-07 Ohms =  0.35433     microOhm
  ac resistance =  3.55886E-07 Ohms =  0.35588     microOhm
 Rac/Rdc ratio  =   1.0044


 End Plate number  3 :
   Inner radius =   7.1520     inches =   18.166     cm
   Outer radius =   64.500     inches =   163.83     cm
Plate thickness =   1.0000     inch   =   2.5400     cm
    Resistivity =  1.14170E-06 Ohm-inch =  2.89992E-06 OHM-cm
    Skin depth  =   4.6755     inch(es) =   11.876     cm
         Volume =  0.21154     meter**3
           Mass =   571.16     kg =   1259.2     lbs.
  dc resistance =  3.99624E-07 Ohms =  0.39962     microOhm
  ac resistance =  4.00256E-07 Ohms =  0.40025     microOhm
 Rac/Rdc ratio  =   1.0016


 End Plate number  4 :
   Inner radius =   4.8010     inches =   12.195     cm
   Outer radius =   65.500     inches =   166.37     cm
Plate thickness =   1.0000     inch   =   2.5400     cm
    Resistivity =  1.14170E-06 Ohm-inch =  2.89992E-06 OHM-cm
    Skin depth  =   4.6755     inch(es) =   11.876     cm
         Volume =  0.21968     meter**3
           Mass =   593.14     kg =   1307.6     lbs.
  dc resistance =  4.74842E-07 Ohms =  0.47484     microOhm
  ac resistance =  4.74930E-07 Ohms =  0.47493     microOhm
 Rac/Rdc ratio  =   1.0002


* Inner radius of innermost inner cylinder =  0.0000     " =  0.0000     cm
* Outer radius of outermost inner cylinder =   10.67     " =   27.10     cm
* Inner radius of innermost outer cylinder =   62.50     " =   158.7     cm
* Outer radius of outermost outer cylinder =   66.00     " =   167.6     cm


 * Length of air enclosed by innermost turn = 181. inches = 4.5974 meters
```

```
   Outer radius =   64.000     inches =   162.56     cm
 Wall thickness =  0.50000     inch   =   1.2700     cm
         Length =   186.00     inch   =   472.44     cm
    Resistivity =  1.14170E-06 Ohm-inch =  2.89992E-06 Ohm-cm
    Skin depth  =   4.6755     inch(es) =   11.876     cm
         Volume =  0.61044     meter**3
           Mass =   1648.2     kg =   3633.6     lbs.
  dc resistance =  1.06031E-06 Ohms =   1.0603     microOhm
  ac resistance =  1.06060E-06 Ohms =   1.0606     microOhm
 Rac/Rdc ratio  =   1.000
* Inductance of space between Cylinder # 5 & # 6 =  6.6683E-02 microHenry.
* Inductance of Cylinder # 6 =  4.6984E-02 microHenry
* H at inner radius of cylinder is  0.29602     A/m per 1 Ampere current
* H at outer radius of cylinder is  0.19581     A/m per 1 Ampere current
* Assuming unit relative permeability:
* B at inner radius of cylinder is  0.37200     Tesla per MA current
* B at outer radius of cylinder is  0.24606     Tesla per MA current


    Cylinder number  7 :
   Inner radius =   64.500     inches =   163.83     cm
   Outer radius =   65.000     inches =   165.10     cm
 Wall thickness =  0.50000     inch   =   1.2700     cm
         Length =   189.00     inch   =   480.06     cm
    Resistivity =  1.14170E-06 Ohm-inch =  2.89992E-06 Ohm-cm
    Skin depth  =   4.6755     inch(es) =   11.876     cm
         Volume =  0.63001     meter**3
           Mass =   1701.0     kg =   3750.1     lbs.
  dc resistance =  1.06078E-06 Ohms =   1.0608     microOhm
  ac resistance =  1.06088E-06 Ohms =   1.0609     microOhm
 Rac/Rdc ratio  =   1.000
* Inductance of space between Cylinder # 6 & # 7 =  2.9650E-02 microHenry.
* Inductance of Cylinder # 7 =  1.7328E-02 microHenry
* H at inner radius of cylinder is  0.19429     A/m per 1 Ampere current
* H at outer radius of cylinder is  9.63991E-02 A/m per 1 Ampere current
* Assuming unit relative permeability:
* B at inner radius of cylinder is  0.24415     Tesla per MA current
* B at outer radius of cylinder is  0.12113     Tesla per MA current


    Cylinder number  8 :
   Inner radius =   65.500     inches =   166.37     cm
   Outer radius =   66.000     inches =   167.64     cm
 Wall thickness =  0.50000     inch   =   1.2700     cm
         Length =   192.00     inch   =   487.68     cm
    Resistivity =  1.14170E-06 Ohm-inch =  2.89992E-06 Ohm-cm
    Skin depth  =   4.6755     inch(es) =   11.876     cm
         Volume =  0.64990     meter**3
           Mass =   1754.7     kg =   3868.5     lbs.
  dc resistance =  1.06123E-06 Ohms =   1.0612     microOhm
  ac resistance =  1.06124E-06 Ohms =   1.0612     microOhm
 Rac/Rdc ratio  =   1.000
* Inductance of space between Cylinder # 7 & # 8 =  7.4157E-03 microHenry.
* Inductance of Cylinder # 8 =  2.4818E-03 microHenry
* H at inner radius of cylinder is  9.56632E-02 A/m per 1 Ampere current
* H at outer radius of cylinder is  0.00000     A/m per 1 Ampere current
* Assuming unit relative permeability:
* B at inner radius of cylinder is  0.12021     Tesla per MA current
* B at outer radius of cylinder is  0.00000     Tesla per MA current
```

```
 End Plate number  1 :
   Inner radius =   10.670     inches =   27.102     cm
   Outer radius =   62.500     inches =   158.75     cm
Plate thickness =   1.0000     inch   =   2.5400     cm
    Resistivity =  1.14170E-06 Ohm-inch =  2.89992E-06 OHM-cm
    Skin depth  =   4.6755     inch(es) =   11.876     cm
         Volume =  0.19523     meter**3
           Mass =   527.14     kg =   1162.1     lbs.
  dc resistance =  3.21209E-07 Ohms =  0.32120     microOhm
  ac resistance =  3.23957E-07 Ohms =  0.32395     microOhm
 Rac/Rdc ratio  =   1.0086


 End Plate number  2 :
   Inner radius =   9.0340     inches =   22.946     cm
   Outer radius =   63.500     inches =   161.29     cm
Plate thickness =   1.0000     inch   =   2.5400     cm
    Resistivity =  1.14170E-06 Ohm-inch =  2.89992E-06 OHM-cm
    Skin depth  =   4.6755     inch(es) =   11.876     cm
         Volume =  0.20338     meter**3
           Mass =   549.14     kg =   1210.6     lbs.
  dc resistance =  3.54337E-07 Ohms =  0.35433     microOhm
  ac resistance =  3.55886E-07 Ohms =  0.35588     microOhm
 Rac/Rdc ratio  =   1.0044


 End Plate number  3 :
   Inner radius =   7.1520     inches =   18.166     cm
   Outer radius =   64.500     inches =   163.83     cm
Plate thickness =   1.0000     inch   =   2.5400     cm
    Resistivity =  1.14170E-06 Ohm-inch =  2.89992E-06 OHM-cm
    Skin depth  =   4.6755     inch(es) =   11.876     cm
         Volume =  0.21154     meter**3
           Mass =   571.16     kg =   1259.2     lbs.
  dc resistance =  3.99624E-07 Ohms =  0.39962     microOhm
  ac resistance =  4.00256E-07 Ohms =  0.40025     microOhm
 Rac/Rdc ratio  =   1.0016


 End Plate number  4 :
   Inner radius =   4.8010     inches =   12.195     cm
   Outer radius =   65.500     inches =   166.37     cm
Plate thickness =   1.0000     inch   =   2.5400     cm
    Resistivity =  1.14170E-06 Ohm-inch =  2.89992E-06 OHM-cm
    Skin depth  =   4.6755     inch(es) =   11.876     cm
         Volume =  0.21968     meter**3
           Mass =   593.14     kg =   1307.6     lbs.
  dc resistance =  4.74842E-07 Ohms =  0.47484     microOhm
  ac resistance =  4.74930E-07 Ohms =  0.47493     microOhm
 Rac/Rdc ratio  =   1.0002


* Inner radius of innermost inner cylinder =  0.0000     " =  0.0000     cm
* Outer radius of outermost inner cylinder =   10.67     " =   27.10     cm
* Inner radius of innermost outer cylinder =   62.50     " =   158.7     cm
* Outer radius of outermost outer cylinder =   66.00     " =   167.6     cm


 * Length of air enclosed by innermost turn = 181. inches = 4.5974 meters
```

```
 * Total thickness of the end-plates at each end of the inductor.
 *           (including insulations) = 5.5 inches = 13.97 cm
 * The overall length of the inductor = 192. inches = 16. feet.
 *                                    = 16. feet = 4.8768 meters


***** Total dc resistance =  1.91780E-05 Ohms =   19.178     microOhmS
***** Total ac resistance =  1.96193E-05 Ohms =   19.619     microOhms
***** Total ac/dc ratio   =   1.0230


** External inductance =  2.7205E-05 Henry =  27.21     microHenry
** Internal inductance =  4.0214E-06 Henry =  4.021     microHenry
***** Total inductance =  3.1227E-05 Henry =  31.23     microHenry

** Internal inductance is  12.88 % OF TOTAL.

 * Ltotal/Rdc ratio =   1.628
 * Ltotal/Rac ratio =   1.592


 * Lext/Rdc ratio =   1.419
 * Lext/Rac ratio =   1.387


Total volume of conductor =   5.0304     m**3
Total mass of the inductor =   13582.     kilograms =   29943.     pounds.
```

NASA Langley Multi-HPG-powered DES Railgun Computer Model

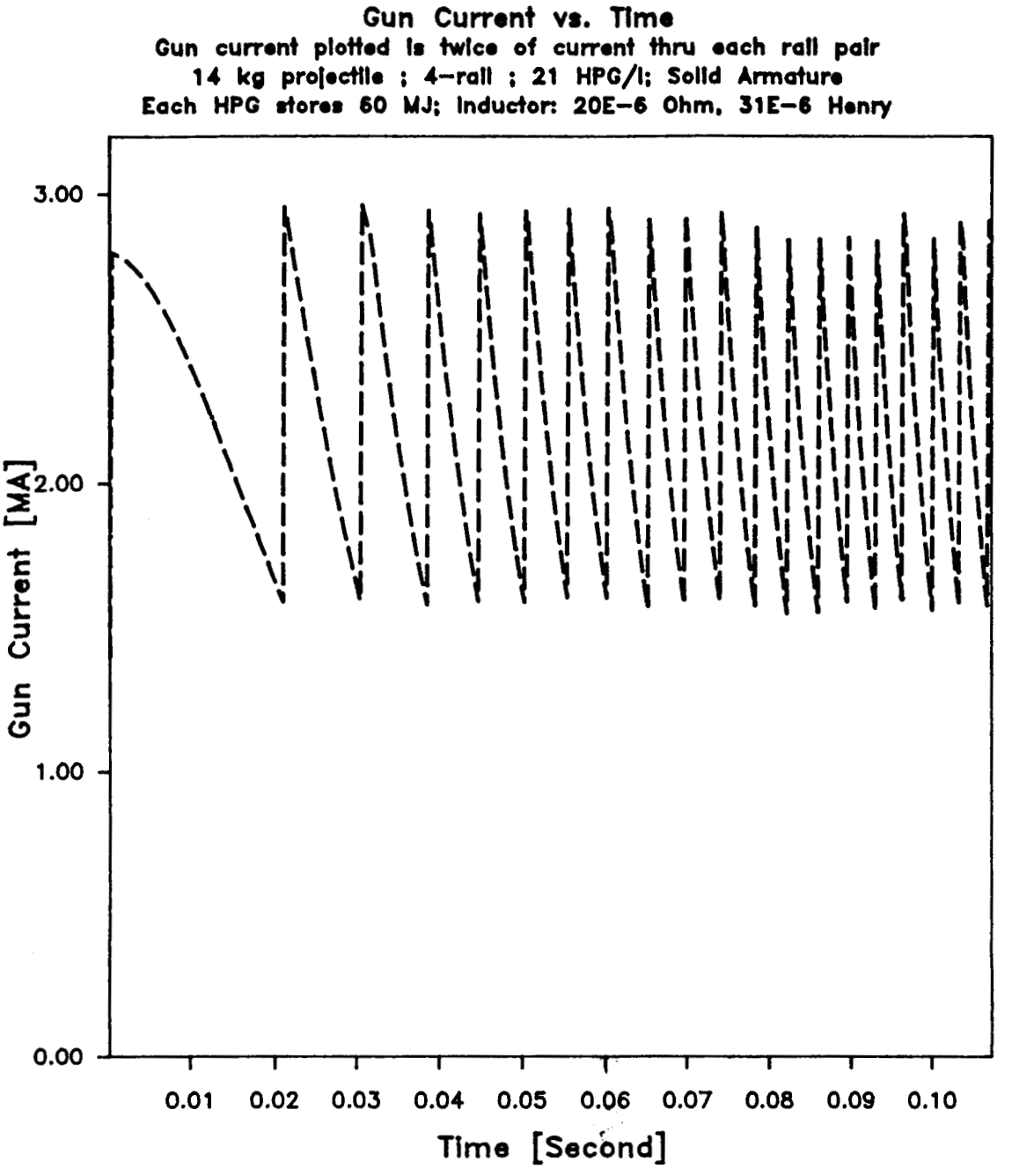

NASA Langley Multi-HPG-powered DES Railgun Computer Model

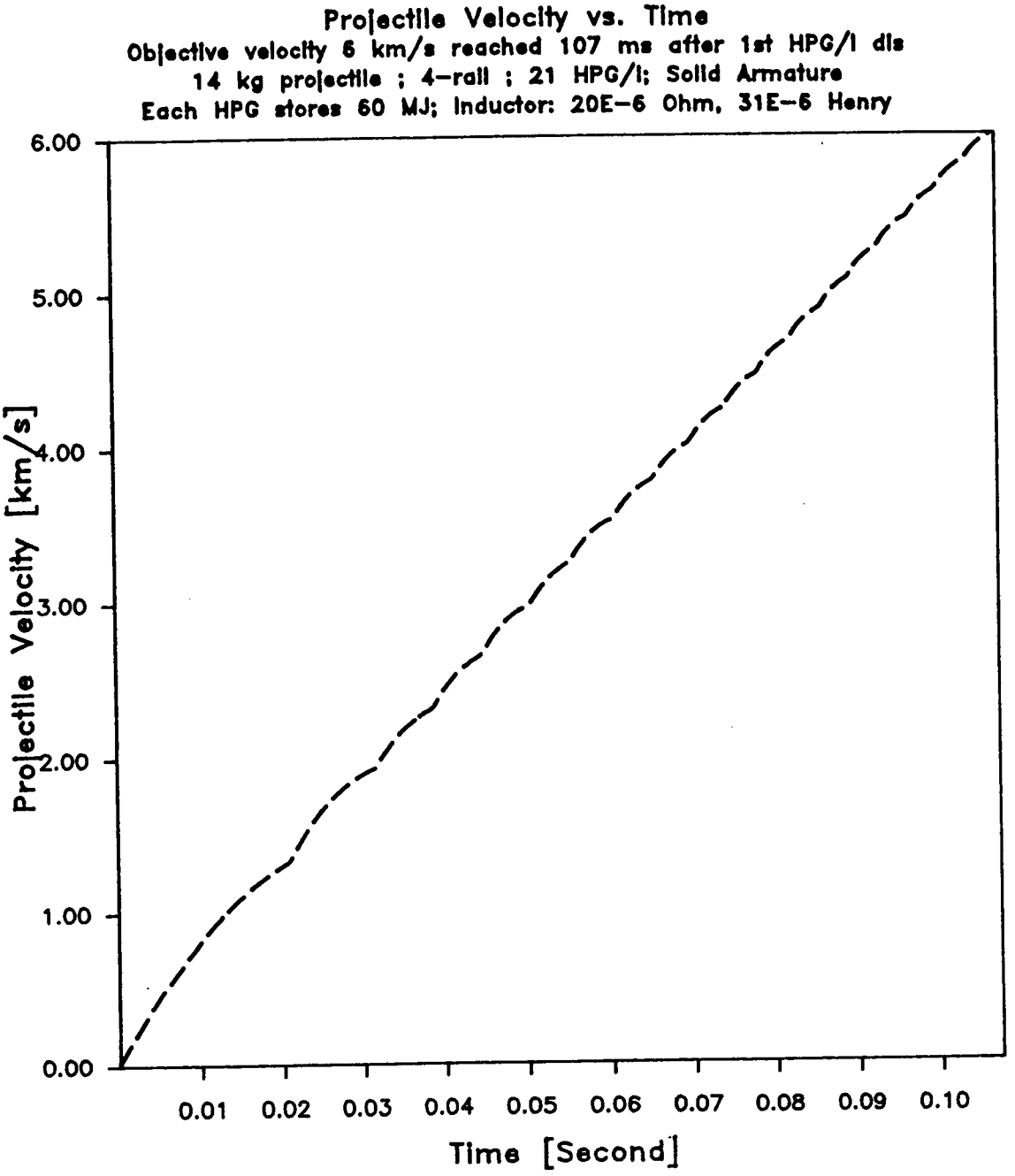

NASA Langley Multi-HPG-powered DES Railgun Computer Model

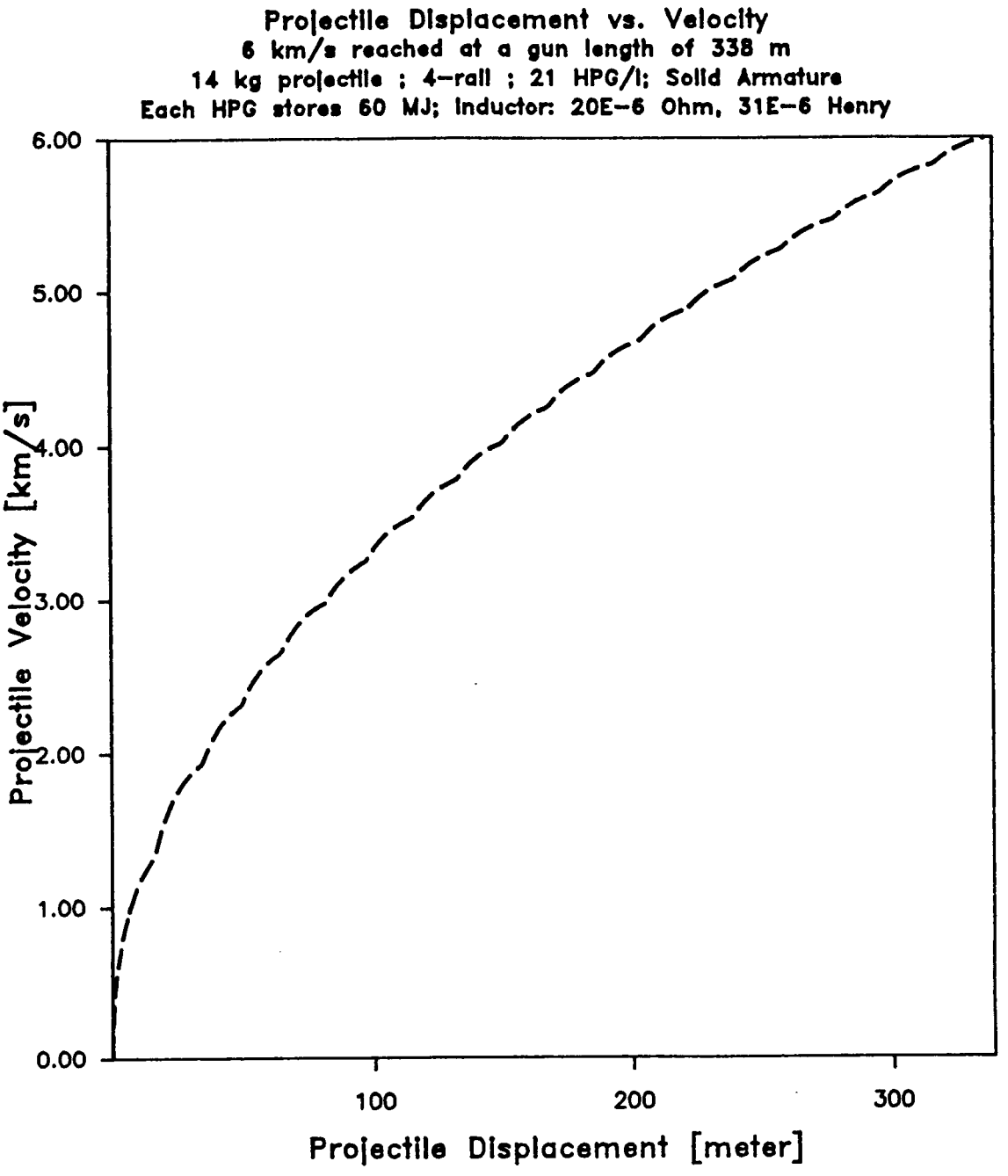

APPENDIX C

Pressure Transducers

In addition to acceleration data, air foil surface pressure can be obtained in a similar manner. This measurement, in the past, has been difficult to obtain because of the bulk of the transducer. Conversion times required for interpretation of analog signals is long compared to the flight. A digital method, using a bus compatable pressure transducer can be formed by following the general solution and data acquisition method of the gravity switches, the exception being that the actual pressure is to be measured with the use of a tactile membrane (1 side metal coated) using the pressure to set a group of switches (just as the keyboard strike of a pocket calculator). This device is also bus compatible and word oriented, using the pressure from a tube and port located in the aircraft surface to set the switches which becomes data, stored in the on-board memory. By taking the above physical layout, we can easily rearrange the database and use a computer aided manufacturing system (CAM) system to precisely draw each of the elements. Figure C-1 illustrates a pressure switch, developed as a microscale transducer that is sensitive to 8 pressure levels. Increased resolution and range can be obtained by adding devices with different pressure pad areas.

The pressure switch portion of this device fits between the bus and gate drivers similar to the board and bus lay out of that of the G-switch. The formulas governing the forces associated with the pressure switches are as follows:

$$S = P/A$$

$$F = M/A$$

A Mylar® dome formed with 0.005 in. thick material with a dome formed with a 0.030 in. height and a 0.125 in. diameter would have a force set pressure of 100 psi. Also a dome with a height of 0.008 in. and a diameter of 0.008 in. would have a force set pressure of 4,000 psi. By changing the size of the domes to actuate at particular pressures of interest, 100 and 4,000 psia, in eight steps could be selected from table C-1.

Compound pressure gauges that measure pressures above and below a wing, can be constructed by this method. An illustration of a circuit that forms this sensor as a board structure is shown in figure C-2.

Sensors can be placed on both sides of the PC Board with tubing connecting the sensor to the surface pressure port.

Heating Rates

Heating rates are best measured by high melting, small mass thermocouples. Calorimetry methods can be used to determine the heating rates. The slow sample and hold devices, and the time required for an analog to digital (A/D) conversion, can be used to advantage when measuring heating rates. A block diagram of a calorimeter is shown in figures C-3a and b.

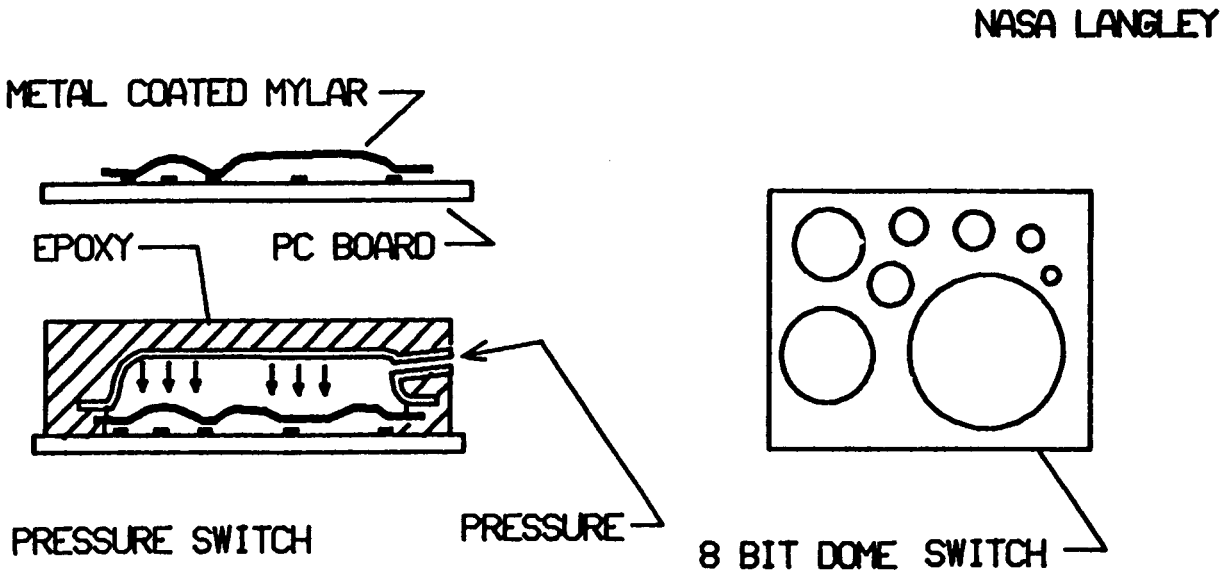

Figure C-1. Pressure switch

Table C-1. Gravity meter design parameters

G-load	8 k	9 k	10 k	11 k	12 k	13 k	14 k	15 k
Length	0.54	0.48	0.42	0.36	0.30	0.24	0.18	0.12
Moment	0.27	0.24	0.21	0.18	0.15	0.12	0.09	0.06
Width	0.02	0.02	0.02	0.02	0.02	0.02	0.02	0.02
Thickness	0.015	0.015	0.015	0.015	0.015	0.015	0.015	0.015

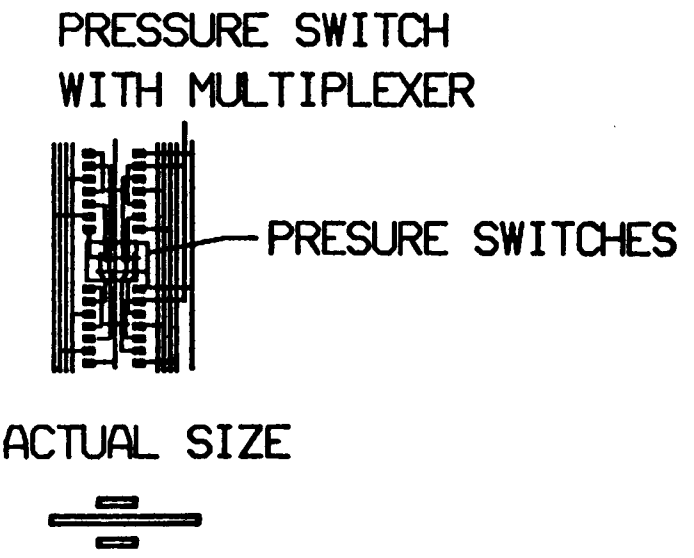

Figure C-2. PC board layout of pressure switch

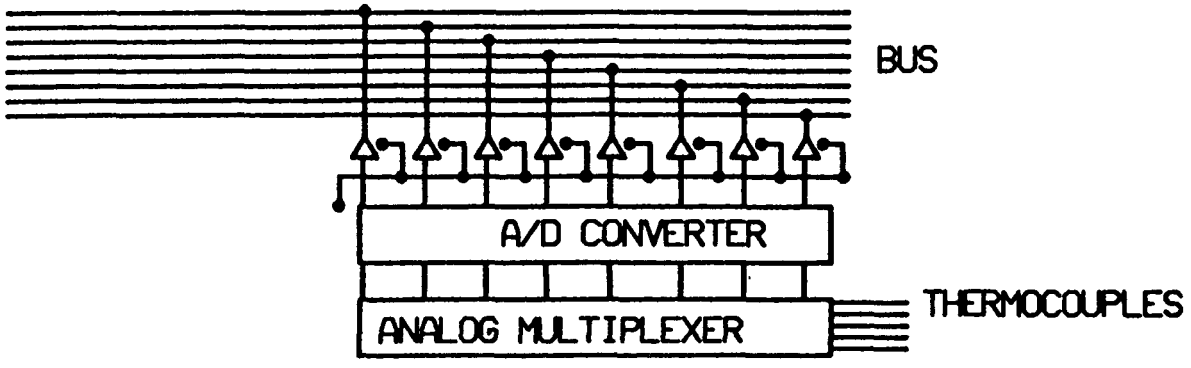

Figure C-3a. Calorimeter diagram

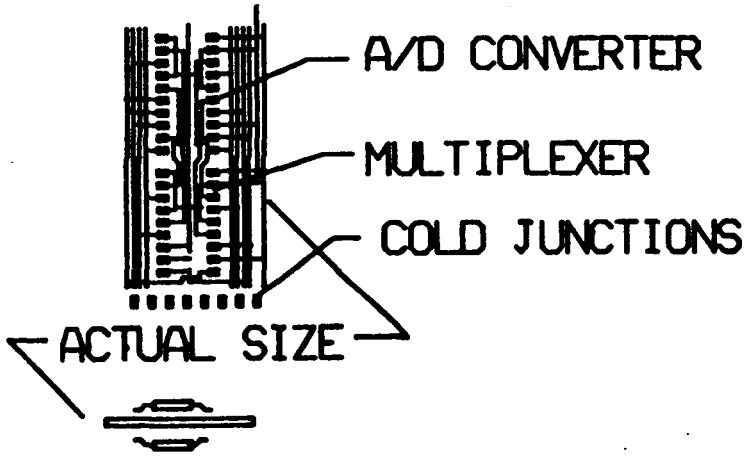

Figure C-3b. Calorimeter PC board layout

Because the A/D conversion and settling time are a part of the solution, the data, as it becomes available, can be placed on the multiplexed bus by skipping many clock cycles until the data is available to write to memory.

Spectral Response

A parameter of interest for hypersonic flight and reentry, is spectral response to study the radiative properties of nitrogen, oxygen, carbon dioxide and a mixture of these gases. A spectrometer can be constructed by using a quartz window (quartz sputtered on glass would be more efficient) with an array of thin film evaporated pass filters covering an array of nine photodetectors, (fig. C-4). These photo devices should have a response in the range of 0.15 to 1.25 μm. To be consistent, an arrangement of the form of the acquisition bus is proposed. An 8 bit x 10 part intensity spectrometer, is proposed and when enabled, will read into memory the complete spectrum of ten relative intensities in 150 ns. Should more than 8-bit accuracy be needed, there is the opportunity to parallel another device, taking over where the first device ran off scale. In this manner, the same device types (by simply adding more) will cover ranges to suit mission requirements. Resolution can be accomplished by making multiple passes.

Electromagnetic Flux

By modifying the circuit treatments described above, a device to measure electric fields up to 1 T could be added to the array of sensors, (fig. C-5). It will be important to measure and record the field during the launch to provide a quality audit of the launch system and also provide information for more robust launch systems.

As with spectral response, again the concern is with wide range, and also high resolution. The solution is again, a combination of wide and narrow, fast sensors.

Three Axis Gyro

Another device that would have utility on-board the model would be a three axis gyro. In the past, attitude and position of aircraft have been determined by rotating flywheels, powered first by vacuum, and later by electric motors. A recent breakthrough in instrumentation is the ring laser for motion detection. These devices can be built as small as 10 cubic cm for one axis. The hypersonic model size would accommodate a device of this type, however, the support electronics must also be accommodated. A simplistic approach is borrowed from early aeronautics (ball and needle).

Attitude sensing in the model, along with other sensors, would produce Euler angles while providing a first step towards computer controlled flight in the tunnel.

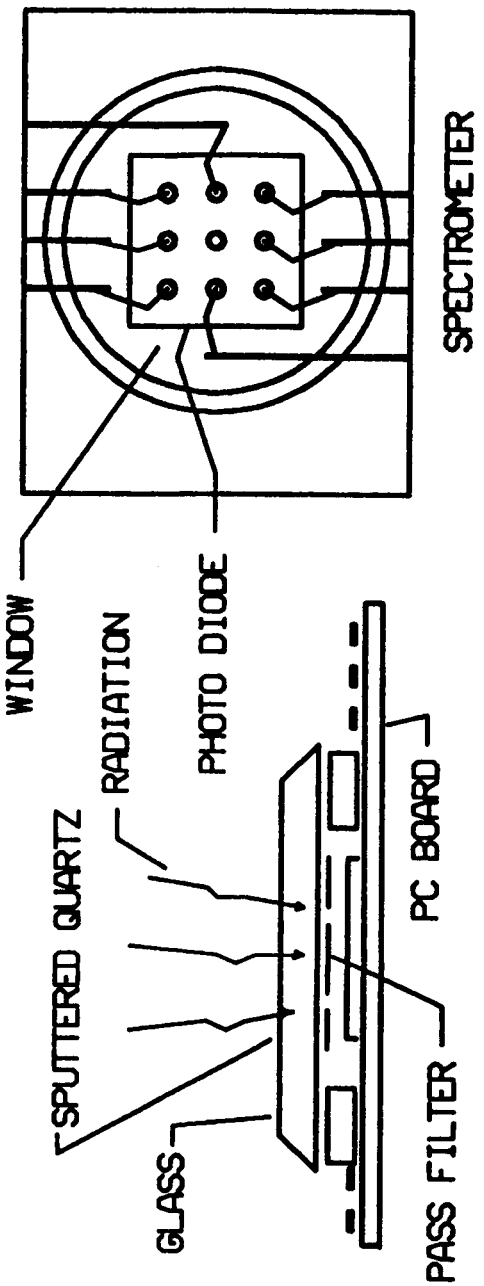

Figure C-4. Spectral response sensor

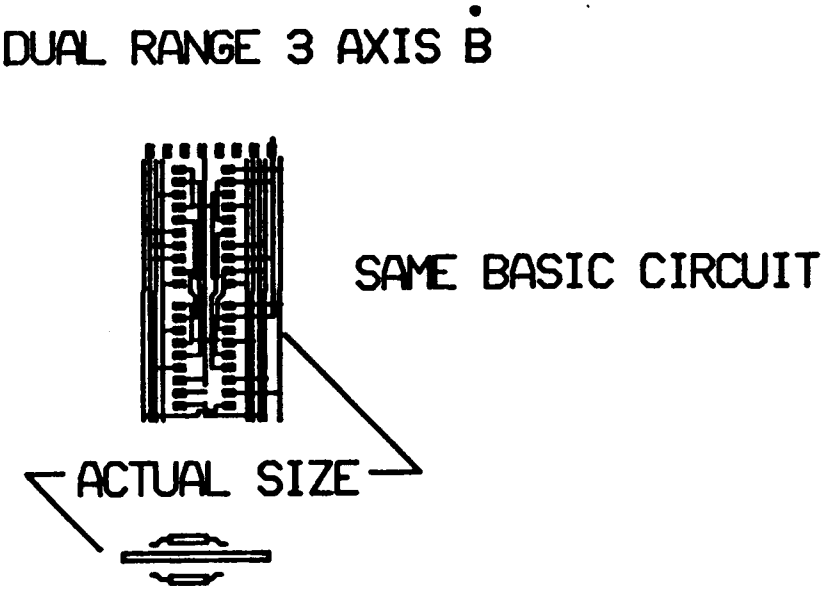

Figure C-5. Electromagnetic flux sensor

Although the model is to be accelerated to 10 km/s, the flight is for now, unpowered, and is in a slowdown mode that is affected by the density of the atmosphere and the drag of the model. The gravity that is experienced from inside the model will be in a direction parallel to a line that passes through the center mass and goes in the direction of the nose, depending on the angle the model left the sabot; i.e. 40° nose high, gravity would be 40° lower than the nose. For the case where a model is rolling on launch, the detection of the gravity vector would still be the same providing the sensors are mounted in the center of mass.

An instrument could be composed and fabricated using the same techniques as described above, that would indicate the aircraft's attitude during flight. This device would be almost insensitive to the deceleration gravity loads caused by increase drag due to reentry conditions. Bearings and pendulums are out of the question because of the interference they would contribute in this difficult environment. It is equivalent to a carpenter's level, not influenced by the decelerating forces in other axes. Figure C-6 illustrates the concept.

The switch pad is fabricated by drawing (plotting) a nickel polymer grid over a concave portion of the substrate. This system will detect the attitude of the model with respect to G direction over an angle determined by the radius of the curvature of the cave. To simplify, this device measures in one axis only. Information about the 90° axis can be obtained by using an identical unit, mounted 90° angle to the first unit (on top), normal to the expected gravity vector. By analyzing the data of both sensors, a Euler analysis can be made. The data acquisition rate is also 25 ns with 8 part accuracy of the chosen angles.

This device will not replace the 3-axis ring laser gyro, but may prove useful in this particular application after refinement. These sensors can be drawn by CAM as one more part of a collage that forms the instrument package.

The physical size of each of the instruments are described full size in figure C-7. Because some of the sensors are position sensitive (gyro, calorimeter, spectrometer), these devices are to be cut from the main PCBoard after CAM and positioned in the model during investment casting (assuming the model is filled epoxy, not steel).

Packaged as a stick, (figs. C-8a and b), the combination of sensors is shown below as a combined database ready for plotting. The circuit is cast as a stick of silica filled epoxy with transceiver, batteries, and antenna to fit the smallest models.

Wing Flexure

To study every aspect possible in the brief flights, the structural shapes of flying bodies under stress may be of interest. Because the flight bodies undergo very high stresses, it may be possible to study these flying bodies in real time under highly stressed condition (wings flapping). To link the parametric data with the stressed shape of the body, a specially constructed strain gauge (fig. C-9a) that placed data on the bus would be able to determine the flexure of the wings and

control structures of the airplane. This can be accomplished by a variation of the above designs.

This sensor can be embedded in the model (fig. C-9b) to determine the frame shape during flight, on a real time basis. By a combination of sensors, molded into a model, more flight data would be available from each flight.

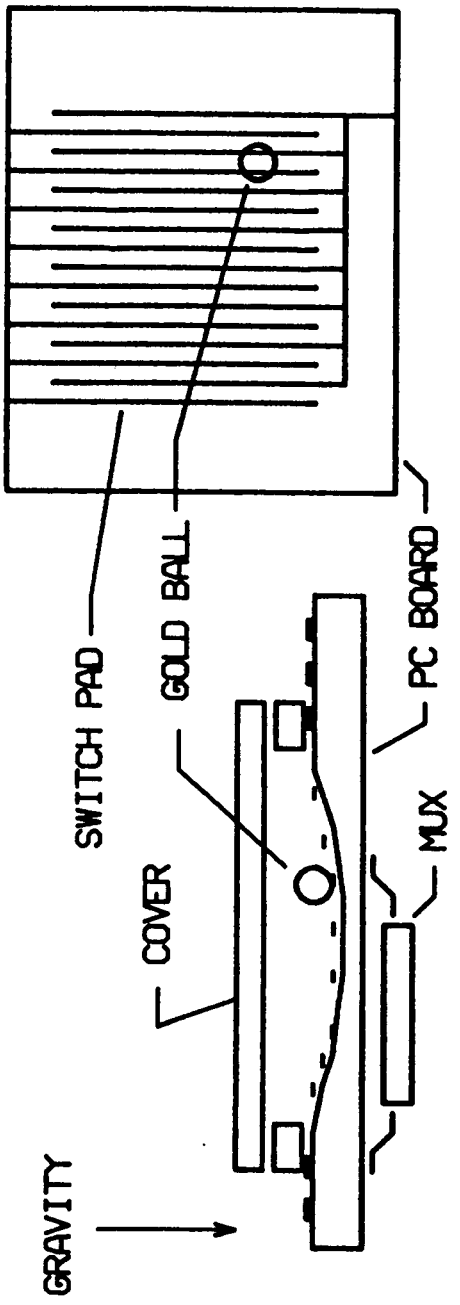

Figure C-6. Attitude sensor

Figure C-7. Full scale sensors

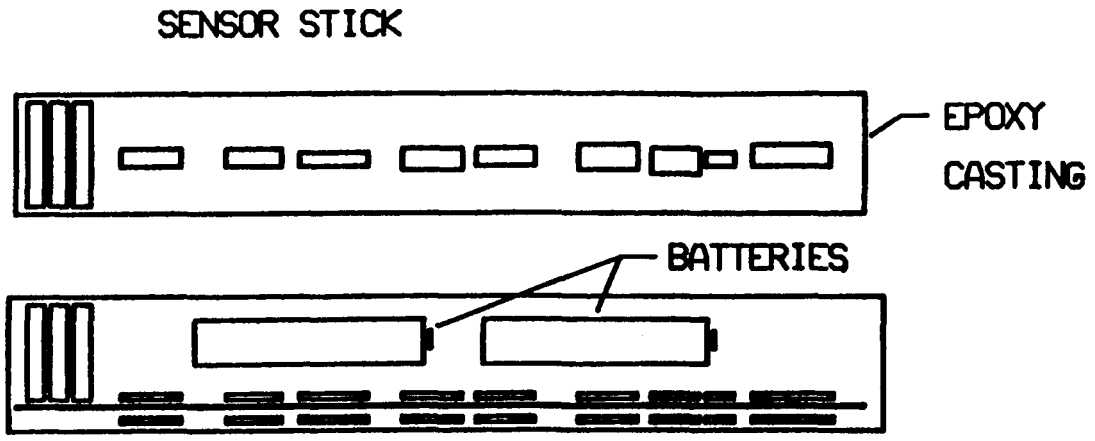

Figure C-8a. Composite instrument board layout

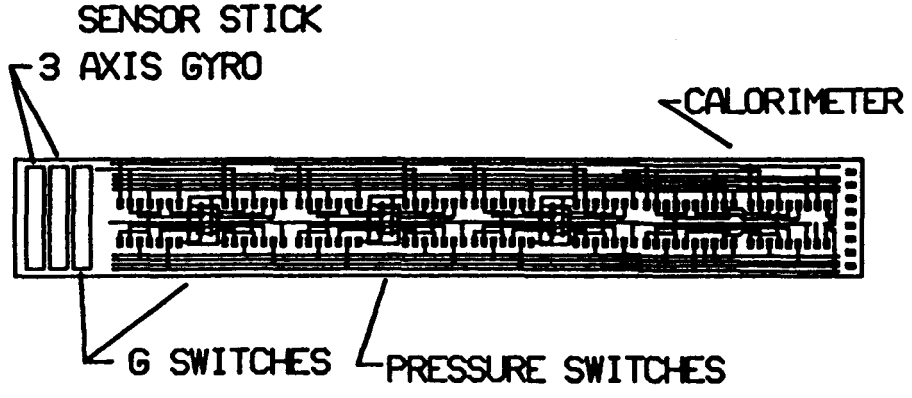

Figure C-8b. Instrument package potted as a still

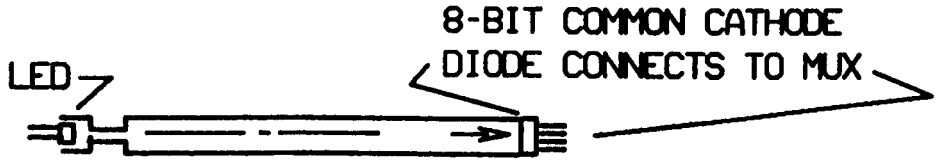

Figure C-9a. Wing flex sensor

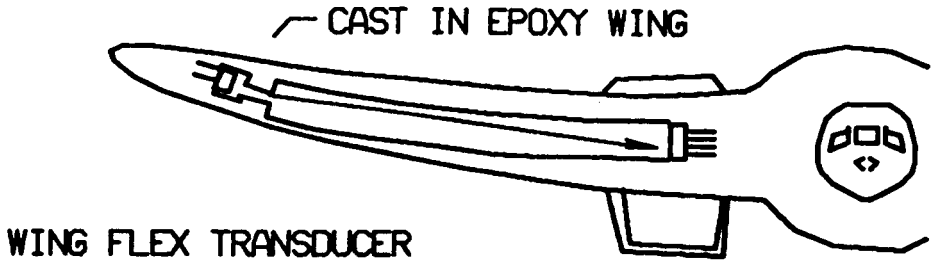

Figure C-9b. Wing flex sensor mounted in model